523-0762559-00111M

FINAL DEVELOPMENT REPORT
for
UHF Solid-State RF Preselector Study

COLLINS RADIO COMPANY
CEDAR RAPIDS, IOWA

Prepared for Department of the Navy
Naval Electronic Systems Command
Washington, D. C. 20360

January 3, 1970

Russell W. Hanson

Steve F. Russell

David B. Hallock

Front-End Design Group, Telecommunications Department

DOCUMENT INFORMATION

CITATION: Hanson, Russell W., Steve F. Russell, and David B. Hallock, UHF RF Preselector Study: Final Development Report, Collins Radio Company, Cedar Rapids, January 3, 1970. (149 Pages) Department of the Navy, Naval Electronics Systems Command, Contract No. N00039-69-C-2602, Project Serial No. 62105N XF 52545 001.

ABSTRACT: A theoretical analysis of superheterodyne design principles is presented with emphasis on noise figure, selectivity trade-off, spurious response, and image phasing mixers. Magnetically tunable filters were examined on a theoretical and practical basis. Problems associated with uhf microminiaturization are discussed. Examination of varactor tuning techniques, and a consideration of large signal effects are presented. Distributed and active inductors and their relative advantages and disadvantages are presented. Distortion and low-noise performance of FET and switching mixers are presented with comparisons of dynamic range.

A theoretical analysis is presented relating the best method of resonator distribution when considering image, noise figure, and cross modulation specifications. Methods of UHF preselection are discussed including capacitance-tuned resonators, switched bandpass filters, and the parametric up-converter. The relative capabilities of amplifiers and discrete inductors as components for microminiature UHF preselector design are presented. Block diagram and component trade-offs are presented, which in turn lead to a recommended design. Also specified are component areas where further investigation is deemed necessary.

KEY WORDS: Preselectors, Receivers, UHF Amplifiers, Mixers, Noise Figure, Image Suppression, Dynamic Range, Varactor Tuning, (Tuned Amplifiers, Ultrahigh Frequency), (Radio Receivers, Tuned Amplifiers), Radio Frequency Amplifiers, Radio Frequency Filters, Tuning Devices, Varactor Diodes, UHF Coils, Field Effect Transistors, Crystal Mixers, Ring-Diode Mixers, Microelectronics.

PUBLISHER SOURCE: Ft. Belvoir Defense Technical Information Center, 03 JAN 1970.
http://www.worldcat.org/title/uhf-rf-preselector-study/oclc/227663219

523-0762559-00111M

FINAL DEVELOPMENT REPORT

FOR

UHF RF PRESELECTOR STUDY

COLLINS RADIO COMPANY

CEDAR RAPIDS, IOWA

FINAL DEVELOPMENT REPORT

FOR

UHF RF PRESELECTOR STUDY

This report covers the period
15 September 1969 to 3 January 1970

COLLINS RADIO COMPANY
CEDAR RAPIDS, IOWA

DEPARTMENT OF THE NAVY
NAVAL ELECTRONICS SYSTEMS COMMAND

CONTRACT NO N00039-69-C-2602
PROJECT SERIAL NO 62105N XF 52545 001

3 January 1970

ABSTRACT

A theoretical analysis is presented relating the best method of resonator distribution when considering image, noise figure, and cross modulation specifications.

Methods of uhf preselection are discussed including capacitance-tuned resonators, switched bandpass filters, and the parametric up-converter.

The relative capabilities of amplifiers and discrete inductors as components for microminiature uhf preselector design are presented.

Block diagram and component trade-offs are presented, which in turn lead to a recommended design. Also specified are component areas where further investigation is deemed necessary.

TABLE OF CONTENTS

TABLE OF CONTENTS (CONT)

LIST OF ILLUSTRATIONS

LIST OF ILLUSTRATIONS (CONT)

PART I

1. PURPOSE

This study has as its objective the exploratory development and design of circuits and techniques that will advance the state-of-the-art in the application of microelectronic principles to the development of uhf front ends capable of extreme miniaturization while preserving useful performance characteristics.

2. GENERAL FACTUAL DATA

2.1 Identification of Technical Personnel

The individuals contributing to this contract from 15 September 1969 through 3 January 1970 and the man-hours worked are as follows:

D. B. Hallock -- 318
R. W. Hanson -- 612
S. F. Russell -- 543
R. L. Craiglow -- 66
D. J. Mooty -- 96
L. C. Rasmussen -- 66

2.2 References

1. The Semiconductor Data Book, Fourth Edition, Motorola, Inc., Phoenix, Ariz., 1969.

2. Blackwell, L. and Kotzebue, K., Semiconductor Diode Parametric Amplifiers, Englewood Cliffs, N. J., Prentice-Hall, 1961.

3. Manley, J. M. and Rowe, H. E., "Some General Properties of Nonlinear Elements - Part I, General Energy Relations," Proc IRE, vol 44, pp 904-913, July 1956.

4. The Microwave Engineers' Handbook and Buyers Guide, Dedham, Mass., Horizon House, p 90, 1969.

5. Reference Data for Radio Engineers, Fourth Edition, New York, International Telephone and Telegraph Corp., pp 639-640, 1956.

6. Harrison, W. H., "A Miniature High-Q Bandpass Filter Emplying Dielectric Resonators," IEEE Transactions on Microwave Theory and Techniques, vol MTT-16, no 4, pp 210-218, April 1969.

7. "MIC Parametric Amplifier," The Microwave Journal, p 84, Sept 1969.

8. Lane, R. Q., "The Comparative Performance of FET and Bipolar Transistors at VHF," IEEE Journal of Solid-State Circuits, vol SC-1, no 1, pp 35-39, Sept 1966.

9. "Applications of PIN Diodes," Hewlett-Packard Application Note 922, Palo Alto, Calif.

10. Electronics International, "Planting Bears Fruit," Electronics, p 226, Sept 15, 1969.

11. Miller, A., "Silicon-on-Sapphire Approach Affords Freedom and Flexibility," Electronics, pp 171-176, February 20, 1967.

12. Zuleeg, R., "Silicon-on-Sapphire Transistors Point Way to Microwave IC's," Electronics, pp 106-108, Mar 20, 1967.

13. Bronwell, A. B. and Beam, R. E., Theory and Application of Microwaves, New York, McGraw-Hill, pp 371-373, 1947.

14. Terman, F. E., Radio Engineers Handbook, New York, McGraw-Hill, p 47, 1943.

15. Daly, D. A., Knight, S. P., Caulton, M., and Ekholdt, R., "Lumped Elements in Microwave Integrated Circuit," IEEE Transactions on Microwave Theory and Techniques, vol MTT-15, no 12, pp 713-721, Dec 1967.

16. Keister, F. Z., "An Evaluation of Materials and Processes for Integrated Microwave Circuits," IEEE Journal of Solid-State Circuits, vol SC-3, no 2, pp 131-137, June 1968.

17. Rand, A. "Inductor Size vs Q: A Dimensional Analysis," IEEE Transactions on Component Parts, pp 31-35, March 1963.

18. Terman, F. E., Electronic and Radio Engineering, Fourth Edition, New York, McGraw-Hill, pp 11-12, 1955.

19. Cohn, S. B., "Dissipation Loss in Multiple-Coupled Resonator Filters," Proc IRE, pp 1342-1348, August, 1959.

20. Taub, J. J., "Design of Minimum Loss Bandpass Filters," Microwave Journal, pp 67-76, Nov 1963.

21. Taub, J. J., "The Minimum Volume of an Equal-Element Bandpass Filter," IEEE Transactions on Microwave Theory and Techniques, pp 264, 265, April 1968.

22. Zverev, A. I. and Blinchikoff, H. J., "Realization of a Filter with Helical Components," IEEE Transactions on Component Parts, pp 99-110, Sept 1961.

23. Cline, J. F., Cohn, S. B., Martin, J. A., Schiffman, B. M., and Sherk, P. M., "Design Data for Antenna - Multicoupler Systems," Technical Report no AFCRC-TR-59-350, Air Force Cambridge Research Center, Contract AF 19(604)-2247, Sept 1959.

24. Grove, A. S., Deal, B. E., Snow, E. H., and Sah, C. T., "Investigation of Thermally Oxidized Silicon Surfaces Using Metal-Oxide-Semiconductor Structures," Solid-State Electronics, vol 8, pp 145-163, 1965.

25. Friis, H. T., "Noise Figures of Radio Receivers," IRE Proceedings, pp 419-422, July 1944.

26. Strickholm, G., "Designing Varactor-Tuned Circuits," Electronic Industries, pp 72-74, Aug 1965.

27. Caulton, M. and Poole, W., "Designing Lumped Elements into Microwave Amplifiers, Electronics, pp 100-110, April 14, 1969.

2.3 Formulae

Pertinent formulae are contained within the appropriate detailed factual data sections.

2.4 Illustrations

Pertinent illustrations are contained within the appropriate detailed factual data sections.

2.5 Measurement Procedures

Any unusual measurement procedures are explained in the appropriate detailed factual data sections.

3. DETAIL FACTUAL DATA

3.1 Preselector Design Concepts

3.1.1 Distribution of Filtering

Basic design concepts relating to the determination of the best method of distributing the resonators used for filtering are presented when image and cross-modulation specifications are considered.

Filtering is incorporated into the signal path of a receiver to perform three distinct functions as follows:

a. Adjacent channel rejection or the attenuation of nearby signals and noise.
b. Image rejection or the attenuation of the if image frequency prior to the mixer.
c. Cross-modulation rejection or the attenuation of strong off-channel signals before they overload a stage and cause cross modulation and/or desensitization of that stage.

Any one filter may serve several or all of these functions simultaneously. The question arises as to how the filtering should be distributed within a receiver such as shown in figure 1-1. The desired adjacent channel rejection can be accomplished in the smallest volume at the if. This filter also generally provides all the cross-modulation rejection for all succeeding stages. To avoid the necessity of additional cross-modulation rejection filters, the adjacent channel rejection filter should be placed as close to the mixer as

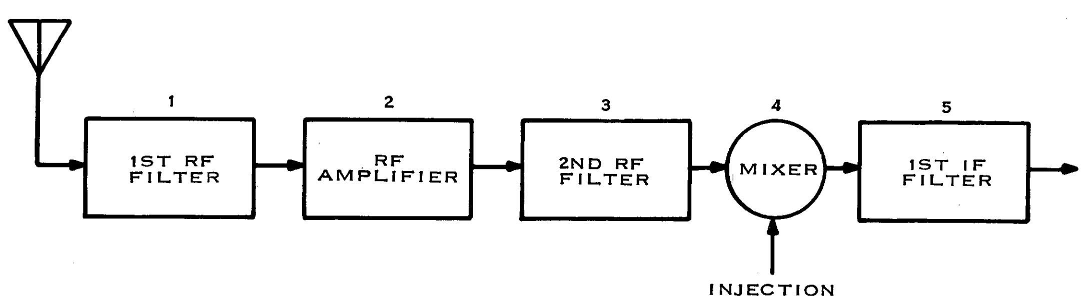

Figure 1-1. Receiver block diagram.

possible without degrading the noise figure of the receiver appreciably. The filtering for image rejection must, of course, precede the mixer. If this filtering is moved ahead of the rf amplifier, the in-band filter loss will degrade the noise figure more than if this filtering is provided after the rf amplifier, so this filtering function should follow the rf amplifier. Since the passband loss of the first rf filter degrades the overall noise figure in a linear manner, the only filtering that should be done at that point is for the purpose of cross-modulation protection of the rf amplifier.

3.1.1.1 Receiver Noise Temperature

It was shown that the first rf filter should only protect the rf amplifier from cross-modulating signals. It remains, therefore, for the second rf filter to provide the additional image rejection required above that supplied by the first filter and to provide cross-modulation rejection for the mixer. The volume of both rf filters depends on the required attenuations and the passband loss allowed in these filters. The passband loss in these filters must be kept low in order to meet the noise figure specifications. The combined volume of the two filters will be minimized for a certain in-band loss assignment for the two filters ($1/G_1$ and $1/G_3$) such that the noise figure is just met. It is shown in part III, section 1 that the receiver noise temperature, T_E, is related to the noise factor, F_E, by

$$T_E = 290\,(F_E - 1)$$

By combining the equations of part III, section 1, we can obtain

$$T_E = T_A\left(\frac{1}{G_1} - 1\right) + \frac{T_2}{G_1} + \frac{T_A\left(\frac{1}{G_3} - 1\right)}{G_1 G_2} + \frac{1}{G_1 G_2 G_3} T_R$$

where G_1, G_2 and G_3 are the available power gains of the first rf filter, rf amplifier, and second rf filter respectively; T_A is the ambient temperature of the filters; T_2 is the noise temperature of the rf amplifier; and T_R is the noise temperature of that portion of the receiver from the mixer to the output. In general, T_A, T_2, T_R, and G_2 will be known, and T_E will be given in the specifications. This leaves only G_1 and G_3 as unknowns. Solving for G_1 in terms of G_3 gives

$$G_1 = \frac{(T_A + T_2) - T_A/G_2 + (T_A + T_R)/G_2 G_3}{T_A + T_E}$$

Using this equation, values of G_3 may be assumed and the corresponding values of G_1 can be calculated to meet the required noise temperature. Note, however, that both G_1 and G_3 must be greater than zero and less than unity since a passive filter cannot have a negative power gain or a power gain greater than unity.

3.1.1.2 First RF Filter Design

It was established earlier that the first rf filter should serve primarily to protect the rf amplifier against cross modulation. From systems considerations, the strongest expected cross-modulating signal power, P_c, would usually be known. This strong interfering signal, for example, often comes from simultaneous operation of a receiver and transmitter in a communication center. It would, of course, be desirable to provide cross-modulation rejection even when the interfering signal is in the adjacent channel. This is not normally practical because of size and cost limitations. In lieu of this, it is desirable to provide protection

as close to the desired signal frequency as possible. How close in to the desired signal this protection is required may or may not be specified. If it is not, one can provide as close-in protection as possible with a minimum volume filter that will meet the image rejection requirement.

Let the power drive level into the rf amplifier at the commencement of cross-modulation distortion be P_{c2}. The cross-modulation rejection of the first rf filter must be

$$\alpha_{c_1} + L_1 = 10 \log_{10} (P_c/P_{c2})$$

where α_{c1} is the relative attenuation of the filter in db at the cross-modulation frequency and L_1 is the passband filter loss in db. The minimum volume filter, which will provide the required rejection, is a minimum-volume Cohn filter discussed in part III, section 2. The number of filter sections is independent of how close in the protection is required and is given by

$$N_{v1} = \frac{p}{p+1} \cdot \frac{\alpha_{c_1} + L_1 + 6}{8.686}$$

p is defined in section 2 and is called the law of variation.

when α_{c_1} lies in the stopband where the logarithmic attenuation is linearly increasing. The nearest integer, N_1, to N_{v1} should be used as the number of stages or resonators in the first rf filter.

A complete analytical minimization of filter volume presents mathematical difficulties. Once the passband attenuations of the first and second rf filters, L_1 and L_3, have been assumed, then the minimum volume may be arrived at analytically. The losses L_1 and L_3 are related to the available stage gains and stage noise temperatures as shown in section 3.1.2 where, by definition,

$$L_1 = -10 \log_{10} G_1$$

$$L_3 = -10 \log_{10} G_3$$

The procedure then is to assume several allowable sets of L_1 and L_3 and calculate the total volume of the resulting minimum volume filters. Of these filters, the set with the minimum total volume is the desired minimum volume filter, and the filters should be designed for the corresponding passband losses L_1 and L_3.

The cross-modulation bandwidth, BW_c, is calculated from the cross-modulation center frequency separation, f_c, by

$$BW_c = \frac{\Delta f_c \, (2f_o + \Delta f_c)}{f_o + \Delta f_c}$$

where the Δf_c is taken on the high side of the center frequency since this results in the largest value (worst case) of BW_c.

For an assumed L_1, the unloaded Q of the filter section is given in part III, section 2 as

$$Q_1 = \frac{4.343\, N_1}{L_1\, BW_c/f_o} \cdot 10^{(\alpha_{c_1} + L_1 + 6)/(20N_1)}$$

The first rf filter volume is given in part III, section 2 as

$$V_1 = N_1 C Q_1^{\,p}$$

where V_1 is the volume, and C and p are constants depending on the type of resonators used in the filter. The volumes of filters using N_1 as nearest integers above and below N_{v1} should be calculated to obtain the minimum volume integer resonator filter.

The skirt selectivity, α_{x_1}, of this filter at a bandwidth BW_x may be written in terms of L_1, α_{c1}, and BW_c as previously shown, or

$$\alpha_{x_1} = \alpha_{c_1} + 20\, N_1 \log (BW_x/BW_c)$$

This equation will be useful later even when BW_c is not specified explicitly.

3.1.1.3 Second RF Filter Design

The second rf filter must supply cross-modulation rejection and image rejection for the mixer stage. Some protection is already provided by the first rf filter. Let α_i be the total image rejection required (in db). The additional image rejection required of the second rf filter is the total rejection less the rejection provided by the first rf filter as given in the preceding equation or

$$\alpha_{i_2} = \alpha_i - \alpha_{c_1} + 20\, N_1 \log (BW_i/BW_c)$$

The cross-modulation rejection should be such that the mixer just starts into cross-modulation distortion at the same time that the rf amplifier starts into cross-modulation distortion. In the absence of filtering the signal on the mixer at this point would be G_2P_{c2} where G_2 is the numeric actual power gain of the rf amplifier. If the overload driving power into the mixer is P_{c4}, then the required cross-modulation rejection of the second rf filter in db is

$$\alpha_{c_3} + L_3 = 10 \log(G_2 P_{c2}/P_{c4})$$

In the absence of a specified cross-modulation bandwidth, the second rf filter may be designed to provide the desired cross-modulation rejection with an unspecified BW_c, and then choose BW_c so that the required image rejection is obtained. The optimum number of filter resonators is found from

$$N_{v3} = \frac{p}{p+1} \cdot \frac{\alpha_{c_3} + L_3 + 6}{8.686}$$

where the actual number of filter resonators, N_3, is chosen to be the nearest integer to N_{v3}. The attenuation of this filter at a bandwidth BW_x is again given by

$$\alpha_{x3} = \alpha_{c3} + 20\, N_3 \log (BW_x / BW_c)$$

In particular, we obtain the total image rejection by combining α_{x1} and α_{x3} with $BW_x = BW_i$ of

$$\alpha_i = \alpha_{c1} + \alpha_{c3} + 20\,(N_1 + N_3) \log (BW_i / BW_c)$$

Solving this for the cross-modulation frequency bandwidth gives

$$BW_c = BW_i / (10)^{\frac{\alpha_i - \alpha_{c1} - \alpha_{c3}}{20\,(N_I + N_3)}}$$

With this cross-modulation bandwidth, the detailed design of the filters may proceed by assuming various losses for L_1 and L_3 and calculating the Q's and volumes by using equations in part III, section 2. The resulting overall filter design is one that just meets the image rejection and noise figure specifications and also provides cross-modulation protection as close to the center frequency as possible for the resulting volume. The filter may, however, provide a greater BW_c than might be desired or a larger filter volume than might be practical.

In the more realistic case where BW_c is specified, we are confronted with the problem of designing a minimum volume filter that will provide an image rejection of α_{i3} at a bandwidth BW_i and a cross-modulation rejection $\alpha_{c3} + L_3$ at a bandwidth of BW_c. First, a minimum volume filter should be made to meet the image rejection specification and the resulting design checked to see if it meets the cross-modulation specification and vice versa. If either of these approaches succeeds, the minimum volume second rf filter has been found. If not, the problem should be attacked as a minimum volume filter providing a given in-band loss and providing a required attenuation at two bandwidths as shown in part III, section 3. The optimum number of resonators is given by

$$N_{v2} = \frac{\alpha_{i3} - \alpha_{c3}}{20 \log_{10} (BW_i / BW_c)}$$

The volume of filters designed with integer values of resonators either side of N_{v2} should be checked to find the number of integer resonators that give the minimum volume filter. This procedure in the design of the first and second rf filters is repeated several times with different sets of L_1 and L_3 to obtain the final minimum volume filter that meets the noise figure, image rejection, and cross-modulation rejection specifications.

3.1.2 UHF Preselection

It is the purpose of this section to examine some of the various methods by which uhf preselection may be obtained. These methods are capacitance-tuned resonators, switched bandpass filters, and the parametric up-converter.

3.1.2.1 Capacitor-Tuned Resonators

3.1.2.1.1 Tuning Range and Circuit Quality Factor

Voltage-controlled capacitor elements may be used to electrically tune the preselector over a band of frequencies. In the present discussion we are interested in examining the resonator characteristics that are most important to the design of the complete filter. Also, it is important to present these parameters in a form most appropriate to actual design application.

The necessary equations will be developed from several equivalent circuits that have been selected on the basis of being simple yet applicable to current filter designs. This selection is not entirely obvious and many alternate selections would probably yield equivalent results. When other factors were equal, the selection of a specific circuit was made from a consideration of the most commonly used uhf filter components.

In the derivation it has been assumed that the individual circuit elements have Q's greater than 10. This was done to simplify the equations, but it also is an economical approximation to make because any useful filter design will require Q in excess of 10.

The general form of the resonator circuit employing voltage-controlled capacitor tuning is shown in figure 1-2. If the resonator is represented by a driving point impedance, the node-to-node equivalent circuit can be represented by three parallel circuit functions, which are the voltage-controlled tuning capacitor, the net inductive reactance, and a nodal capacity used to account for node-to-node capacity not included in the tuning capacitor.

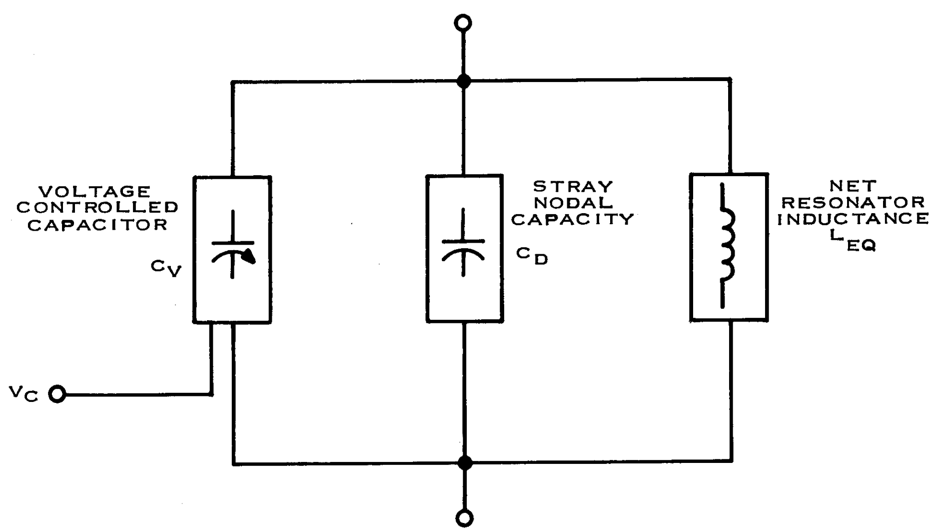

Figure 1-2. Basic voltage controlled resonator circuit.

Before discussing the complete resonator circuit, we should take a look at a common equivalent circuit that is used to illustrate the basic properties of a voltage-controlled capacitor. Figure 1-3 illustrates the equivalent circuit for a typical tuning capacitor. The maximum and minimum tuning capacity and capacitor Q are the most important characteristics of the tuning capacitor. When examining the capacitor Q it is important to emphasize the fact that this Q must be evaluated as the capacitor is tuned; that is, the Q is evaluated as the total value of capacity changes and as the frequency band is tuned. This occurs when the tuning capacitor is a varactor. The varactor capacity and series resistance are essentially constant with frequency for a fixed bias, but when the varactor is used in a tuned circuit the series resistance is a function of bias voltage and thus a function of frequency.

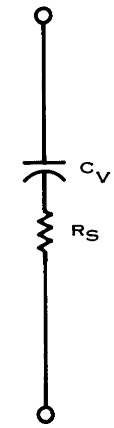

Figure 1-3. Typical tuning capacitor.

This frequency dependence can be analyzed by considering the circuit of figure 1-3. The nodal, Q, of this circuit is expressed as the ratio of reactance level to resistance as

$$Q \triangleq \frac{X_C}{R} \qquad Q_V \triangleq \frac{1}{\omega C_V R_S}$$

Where Q_V represents the variable capacitor Q. To examine the frequency dependence of Q_V we can evaluate the Q at two separate frequencies and take the ratio of the Q's.

$$Q_1 = \left(\frac{1}{\omega\, C_V R_S}\right)\Bigg|_{\omega_1} \qquad Q_2 = \left(\frac{1}{\omega\, C_V R_S}\right)\Bigg|_{\omega_2}$$

$$\frac{Q_1}{Q_2} = \frac{(\omega\, C_V R_S)\big|_{\omega_2}}{(\omega\, C_V R_S)\big|_{\omega_1}} = \left(\frac{F_2}{F_1}\right)\cdot\left(\frac{C_2}{C_1}\right)\cdot\left(\frac{R_2}{R_1}\right)$$

If the value of Q_1/Q_2 is examined as the frequency ratio is changed, but while the C and R values are held constant, we get

$$C_1 = C_2 \qquad R_1 = R_2 \qquad Q_1 = Q_2\left(\frac{F_2}{F_1}\right)$$

which shows that the Q for a single fixed capacitor is linearly dependent on frequency, a fact that is almost trivial to state, but nevertheless is helpful in illustrating the true nature of frequency dependence of Q in a tuning capacitor.

Consider now the circuit of figure 1-4 where the voltage-controlled capacitor is used to tune a simple inductor. The Q of the resonator can be expressed as

$$Q_T = \frac{1}{\omega C_V R_S} \quad \text{or} \quad Q_T = \frac{\omega L_{EQ}}{R_S} \qquad Q_V > 10$$

When the resonator is tuned over a band of frequencies the total Q of the resonator can be expressed as a function of frequency ratio and total circuit Q at the maximum resonating frequency as

$$Q_{T\ MAX} = \left(\frac{1}{\omega C_V R_S}\right)\Bigg|_{\omega\ MAX}$$

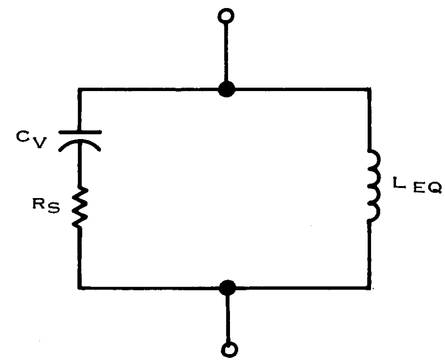

Figure 1-4. Simple inductor resonator with voltage controlled capacitor tuning.

$$Q_T = \left(\frac{1}{\omega C_V R_S}\right)\Bigg|_{\omega_O} \qquad Q_V > 10 \qquad \frac{Q_T}{Q_{T\ MAX}} = \frac{\left(\omega C_V R_S\right)\big|_{\omega MAX}}{\left(\omega C_V R_S\right)\big|_{\omega_O}}$$

Also from resonance conditions,

$$\omega_O^{\,2} = \frac{1}{C_V L} \qquad \omega^2_{MAX} = \frac{1}{C_{V\ MIN} L} \qquad \frac{C_{V\ MIN}}{C_V} = \left(\frac{F_O}{F_{MAX}}\right)^2$$

From an examination of the empirical data on various types of voltage-controlled capacitors it has been concluded that a good approximation to the Q-frequency dependence is a relationship expressed as follows:

$$\frac{Q_V}{Q_{V\ MAX}} = \left(\frac{X_{CV}}{X_{CV\ MIN}}\right)^A$$

where A is an exponent that depends on the specific capacitor characteristic but generally $1 \leq A \leq 5$. The meaning of "A" will be explained in more detail for specific circuits in later sections. For the lumped circuit presently being discussed, the normalized total Q is equal to the normalized tuning capacitor Q so that

$$\frac{Q_T}{Q_{V\ MAX}} = \left(\frac{X_{CV}}{X_{CV\ MIN}}\right)^A = \left(\frac{F_O}{F_{MAX}}\right)^A$$

If we assume that the series resistance R_S is independent of frequency, then A = 1 and we can write the equation for Q_T as

$$Q_T = Q_{T\ MAX} \left(\frac{F_O}{F_{MAX}}\right)$$

which is linearly dependent on frequency.

From the discussion so far we can conclude that the resonator Q-frequency dependence was the same as the tuning capacitor frequency dependence when R_S is assumed constant with frequency. Before considering more general resonator circuit models, we first will consider a general approach to specifying the nodal Q of a general driving point impedance.

In a simple RLC resonant circuit the fundamental definition of circuit Q, namely the ratio of reactance level to series resistance, gives a Q-value that is useful in determining the filter selectivity using this particular circuit. This fundamental concept no longer applies, however, when the resonator is composed of a complex RLC circuit. For this reason the concept of nodal Q using the equal slope criteria will be introduced.

Nodal Q is conceptualized, as shown in figure 1-5, by the decomposition of a complex admittance, R(S) into a simple RLC network for one specific frequency. At any frequency, F, the admittance Y(S) is separated into its real and imaginary parts such that

$$R_{EQ} = \frac{1}{\text{RE } Y(S)} \text{ and (net reactance of } C_{EQ} \text{ and } L_{EQ}) = \frac{1}{\text{IM } Y(S)}$$

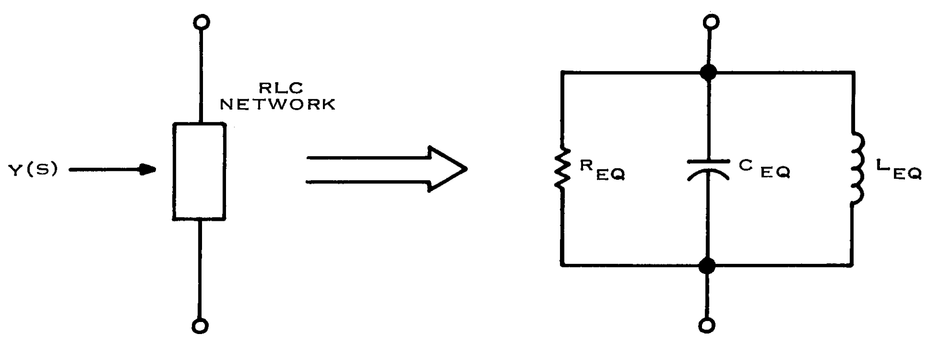

$$Y(S)$$
$$\text{RE } Y(S) = 1/R_{EQ}$$
$$\text{IM } Y(S) = B(S)$$
$$\frac{DB(S)}{DS} = C(S)$$

$$Y(S) = 1/R_{EQ} + SC_{EQ} + 1/S\,L_{EQ}$$
$$\text{RE } Y(S) = 1/R_{EQ}$$
$$\text{IM } Y(S) = S\,C_{EQ} + 1/S\,L_{EQ}$$
$$\frac{DB(S)}{DS} = C_{EQ} - \frac{1}{S\,L_{EQ}}$$

SOLVE TWO EQUATIONS

$$B(S) = S\,C_{EQ} + 1/S\,L_{EQ}$$
$$C(S) = C_{EQ} - 1/S^2\,L_{EQ}$$

Figure 1-5. Decomposition of Y(S) by the equal slope criteria.

Because Y(S) is a complex function of S, it is possible to find an infinite combination of values of C_{EQ} and L_{EQ} that characterizes the magnitude of IM Y(S) at any single frequency. Probably the most logical selection of C_{EQ} and L_{EQ} would be the combination that gives a selectivity at resonance equal to that of the single RLC resonator. Upon examining the reactance curve for any arbitrary admittance Y(S), we see that a simple RLC circuit with the same slope at F will give the same nodal Q at F and this separation criteria is called the equal slope criteria.

The equivalence relationships for equal slopes are shown in figure 1-5. Using these equations the nodal Q of the Y(S) network can be written as

$$Q_T = \frac{R_{EQ}}{\omega L_{EQ}} \quad \text{or} \quad Q_T = R_{EQ}\, \omega_O\, C_{EQ}$$

The specification of nodal Q and the equal slope concept are useful in filter designs because the selectivity calculation near resonance obtained with nodal Q is directly applicable to filter selectivity calculations using 3-db bandwidths. For the resonators analyzed in the following sections, the unloaded Q's will be computed using the equal slope criteria unless otherwise noted.

It should be emphasized that the equal slope criteria gives a value of Q that is good only at the specific resonance for which it is evaluated. When the Q is evaluated by the 3-db method, a small error is introduced because the Q was obtained from two frequencies. The equal slope Q can be thought of as an "instantaneous" Q; that is, the Q is exact only for a vanishingly small bandwidth. This problem is of little consequence for most practical resonator designs.

It would be possible to formulate a general approach to the analysis of resonator circuits for uhf filters and become completely engrossed in the mathematical details of such an analysis. This approach has been abandoned in favor of the analysis of a few specific circuit models most generally used for uhf applications, and the study will address itself to the examination of the basic parameters involved in filter design.

A study of the commonly used resonator configurations in the uhf band has resulted in the generic listing of circuits as shown in figure 1-6. The list proceeds from the simplest approximation to the most useful approximations in such a manner as to include the most important circuit refinements first. The equations applicable to the performance of the circuits will be derived using circuits 4B and 4C. The performance of the basic circuits can then be obtained through simplification of the more general equations.

Figures 1-7 and 1-8 represent the circuit models from which the basic design equations are formulated. The circuit elements are defined as follows:

a. Lumped Inductor Resonator of Figure 1-7(A).

   1. C_V - is a capacitor that accounts for the variable capacity element across the node. The change in C_V must reflect the total capacity change needed to tune an entire band. C_V can be characterized by maximum and minimum values and a unique frequency function.

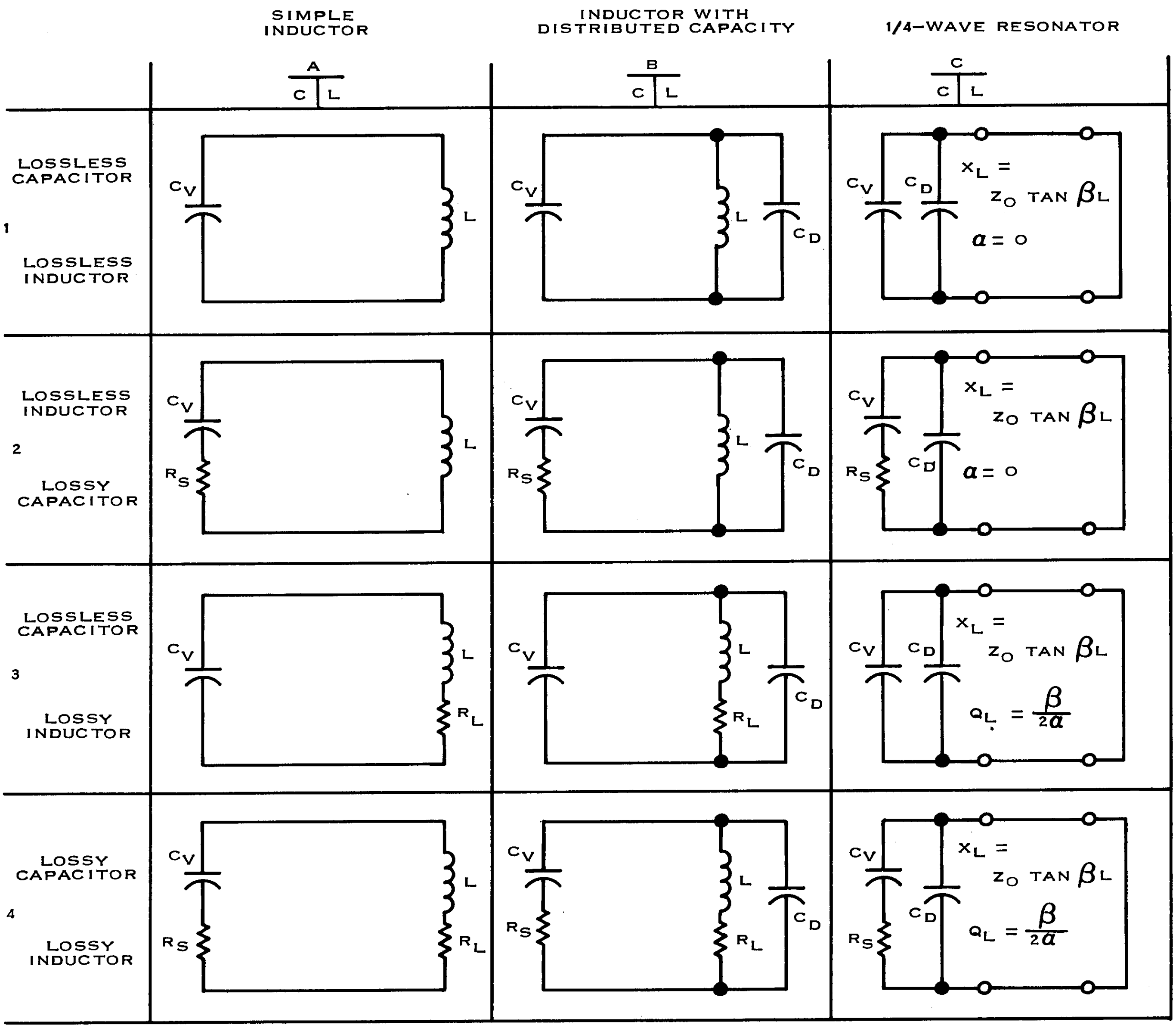

Figure 1-6. Generic class of capacitor tuned uhf resonators.

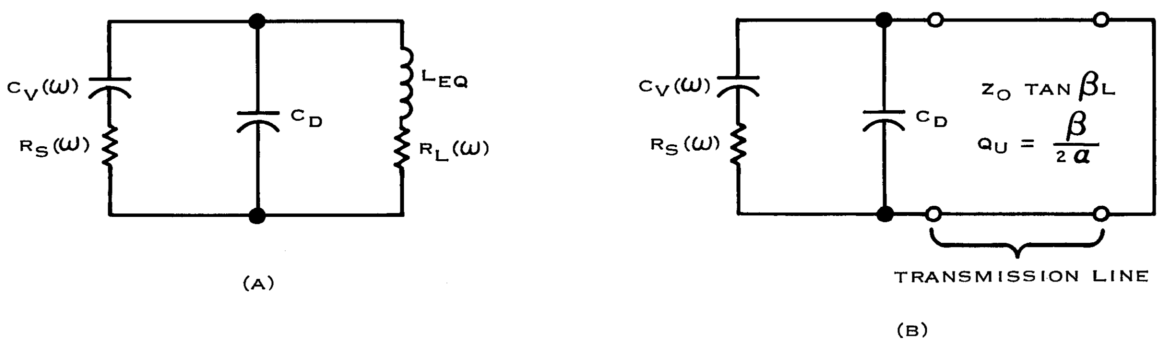

Figure 1-7. Design equation circuit models.

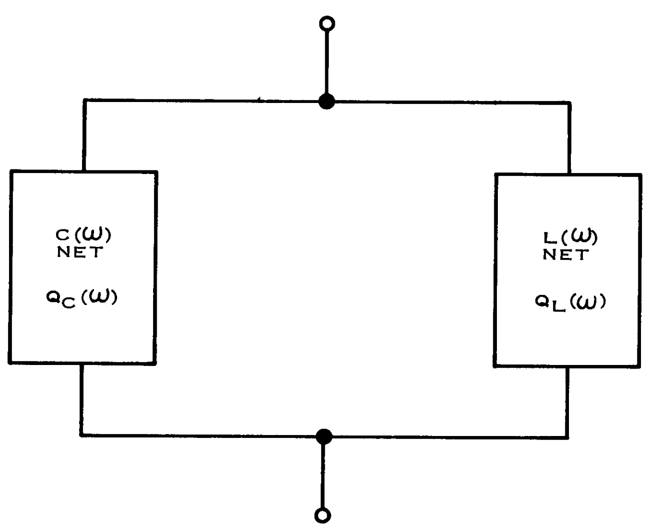

Figure 1-8. Reactance separation circuit for total Q computation.

2. R_S - is a series resistor used to account for the loss associated with C_V. In general R_S is a function of frequency because the loss of most tuning capacity elements is a function of frequency. A series R was chosen because it most reasonably models the actual loss element in a typical uhf tuning capacitor.
3. C_D - is a capacitor in addition to C_V, which is not actually a part of the tuning capacity but is used to account for nodal capacity not directly attributed to C_V. C_D includes stray nodal capacity, maximum frequency trimmer capacity, and the parasitic capacity of the lumped inductor.
4. L_{EQ} - is the net nodal inductive component, which is the equivalent inductance required to tune C_V and C_D. L_{EQ} is assumed purely inductive except for resistive loss. Any parasitic capacity associated with an actually lumped inductor has been accounted for in C_D.
5. R_L - is a series resistor used to account for the losses associated with L_{EQ}. The series model was chosen because it most nearly characterizes inductor loss at uhf frequencies where skin loss is the most significant contributor and R_L is a function of frequency.

b. Transmission Line Resonator of Figure 1-7(C).

1. C_V, R_S, and C_D assume the same functions and definitions as in the lumped resonator case.
2. C_{EQ} - is an equivalent capacitor associated with the transmission line, which is obtained from application of the equal slope criteria. C_{EQ} is a function of frequency.
3. L_{EQ} - is an equivalent inductor associated with the transmission line, which is obtained from application of the equal slope criteria. L_{EQ} is a function of frequency.
4. R_L - is a series loss resistor that accounts for the losses associated with the transmission line. R_L is also a function of frequency, which to a first approximation is attributable to skin loss.

An extensive discussion of the assumptions made to obtain these circuit models would not be practical, but a brief mention of the more important ones will give insight into the effectiveness of the chosen models.

a. The losses in C_D have not been specified explicitly because for most practical applications the losses associated with stray capacity and trimmer capacity are much higher than the losses in C_V. If this assumption is not accurate for a specific application, the losses in C_D can be implicitly accounted for, to a first approximation, in R_S.
b. A more detailed model of the losses in C_V would include a shunt R across C_V as well as the series loss R_S. This shunt loss has been neglected in the present model because the low impedance levels encountered at uhf frequencies make the loss contribution negligible compared to R_S.
c. Series inductance in C_V has been neglected to simplify the model. In actual circuits there is always a series inductive contribution to C_V, but in well-designed miniature circuits this effect is small. If the designer wishes to account for this series inductance, it is possible to modify the tuning curve function to include series inductance.
d. The losses associated with the transmission line are assumed to be conductor losses only. These conductor losses are due to skin and proximity effects. This assumption is made possible by the very low loss dielectric materials available for construction. For microstrip inductors the use of alumina or sapphire as substrates and for helical inductors the use of rexolite or Polyphenylene-oxide (PPO) as coil forms have made the dielectric contribution to total loss quite small.

In the majority of filter designs the electrical characteristics of a resonator can be described in terms of its tuning range and quality factor. Again, it is possible to approach the problem in a variety of ways. The approach used here is an example of what might be compiled. Most likely each design attempted will require modification of the following approach to better suit the specific application.

The first topic will be the analysis of the resonator properities affecting tuning range. For the resonator circuits of figure 1-7, this analysis produces the following five interdependent parameters needed to specify tuning range:

a. The filter tuning ratio of maximum and minimum frequencies

$$\frac{F_{MIN}}{F_{MAX}} \triangleq \overline{F}_T$$

b. The total variable capacity change from maximum to minimum frequency

$$\frac{C_{V\ MAX}}{C_{V\ MIN}} \triangleq \overline{C}_V$$

c. The ratio of parasitic nodal capacity to the minimum tuning capacity

$$\frac{C_D}{C_{V\ MIN}} \triangleq \overline{C}_D$$

d. The ratio of quarter-wave frequency or pole frequency to maximum filter frequency

For transmission line resonator

$$\frac{F_{1/4}}{F_{MAX}} = \overline{F}$$

For lumped inductor resonator

$$\frac{F_P}{F_{MAX}} = \overline{F}$$

e. For transmission line resonators the value of the characteristic impedance Z_O.

Table 1-1 summarizes the interdependent design equations for resonator tuning. These equations are derived in more detail in part III, sections 4 and 5.

TABLE 1-1. RESONATOR TUNING INTERDEPENDENT DESIGN EQUATIONS.

PARAMETER	LUMPED INDUCTOR RESONATOR	TRANSMISSION LINE RESONATOR
$\overline{F}_T \triangleq$	$\frac{F_{MIN}}{F_{MAX}}$	$\frac{F_{MIN}}{F_{MAX}}$
$\overline{C}_V \triangleq$	$\frac{C_{V\ MAX}}{C_{V\ MIN}}$	$\frac{C_{V\ MAX}}{C_{V\ MIN}}$
$\overline{C}_D \triangleq$	$\frac{C_D}{C_{V\ MIN}}$	$\frac{C_D}{C_{V\ MIN}}$
$\overline{C}_T \triangleq$	$\frac{\overline{C}_V + \overline{C}_D}{1 + \overline{C}_D}$	$\frac{\overline{C}_V + \overline{C}_D}{1 + \overline{C}_D}$
$\overline{F} \triangleq$	$\frac{F_P}{F_{MAX}}$	$\frac{F_{1/4}}{F_{MAX}}$
$\overline{C}_T =$	$\left(\frac{F_{MAX}}{F_{MIN}}\right)^2$	$\frac{F_{MAX}}{F_{MIN}} \frac{\text{TAN}\ \pi/2\ F_{MAX}/F_{1/4}}{\text{TAN}\ \pi/2\ F_{MIN}/F_{1/4}}$
$\overline{C}_D =$	$\frac{\overline{C}_T - \overline{C}_V}{1 - \overline{C}_T}$	$\frac{\overline{C}_T - \overline{C}_V}{1 - \overline{C}_T}$
$\overline{C}_V =$	$\overline{C}_T + \overline{C}_D\ (\overline{C}_T - 1)$	$\overline{C}_T + \overline{C}_D\ (\overline{C}_T - 1)$
$\overline{C}_V =$	$\frac{(F_{MAX}/F_{MIN})^2 - (F_{MAX}/F_P)^2}{1 - (F_{MAX}/F_P)^2}$	--
$L_{EQ} =$	$\frac{1}{\omega^2_{MAX}\ C_{T\ MIN}}$	--
$L_{EQ}\ C_{V\ MIN} =$	$\left(\frac{1}{\omega^2_{MAX}} - \frac{1}{\omega^2_P}\right)$	--
$C_I =$	-	$1 + \overline{C}_D$
$Z_O\ C_{V\ MIN} =$	-	$1/\omega_{MAX}\ C_I\ \text{TAN}\ \pi/2\ F_{MAX}/F_{1/4}$

With the design equations presented in the table it is possible to formulate a general design approach to resonators characterized by the circuits of figure 1-7.

If one attempts to apply the equations in a general manner to all resonator problems, the results are too complicated to be presented in graphic form. This problem led to the conclusion that if a typical design approach were illustrated it would characterize the important resonator tuning properties. The equations chosen to best describe resonator tuning are listed below:

a. $\overline{F}_T = F_{MIN}/F_{MAX}$

b. $\overline{C}_D = \dfrac{C_D}{C_{V\ MIN}}$

c. $\overline{C}_V = \overline{C}_T + \overline{C}_D\ (\overline{C}_T - 1)$

d. $$\overline{C}_V = \frac{\left(\frac{F_{MAX}}{F_{MIN}}\right)^2 - \left(\frac{F_{MAX}}{F_P}\right)^2}{1 - \left(\frac{F_{MAX}}{F_P}\right)^2}$$

e. $$\overline{C}_V = \frac{F_{MAX}}{F_{MIN}} \left(\frac{\mathrm{TAN}\,\pi/2\ \frac{F_{MAX}}{F_{1/4}}}{\mathrm{TAN}\,\pi/2\ \frac{F_{MIN}}{F_{1/4}}} \right) + \overline{C}_D \left(\frac{F_{MAX}}{F_{MIN}}\ \frac{\mathrm{TAN}\,\pi/2\ \frac{F_{MAX}}{F_{1/4}}}{\mathrm{TAN}\,\pi/2\ \frac{F_{MIN}}{F_{1/4}}} - 1 \right)$$

f. $$L_{EQ} = \frac{1}{\omega^2_{MAX}\ C_{V\ MIN}\ (1 + \overline{C}_D)}$$

g. $$Z_O\ C_{V\ MIN} = \frac{1}{\omega_{MAX}\ (1 + \overline{C}_D)\ \mathrm{TAN}\,\pi/2\ \frac{F_{MAX}}{F_{1/4}}}$$

These design equations were applied directly to the uhf filter design problem. The graphs of figures 1-9 through 1-13 were generated to serve as uhf filter design aids and to illustrate the magnitude of the effects of variable changes in the design equations.

When approaching a filter design problem, the designer usually knows the range of frequencies to be covered. This gives a knowledge of F_{MAX}, F_{MIN} and $\overline{F}_T$. Secondly, an attempt to minimize stray nodal capacity is made by careful physical layout. The design equations

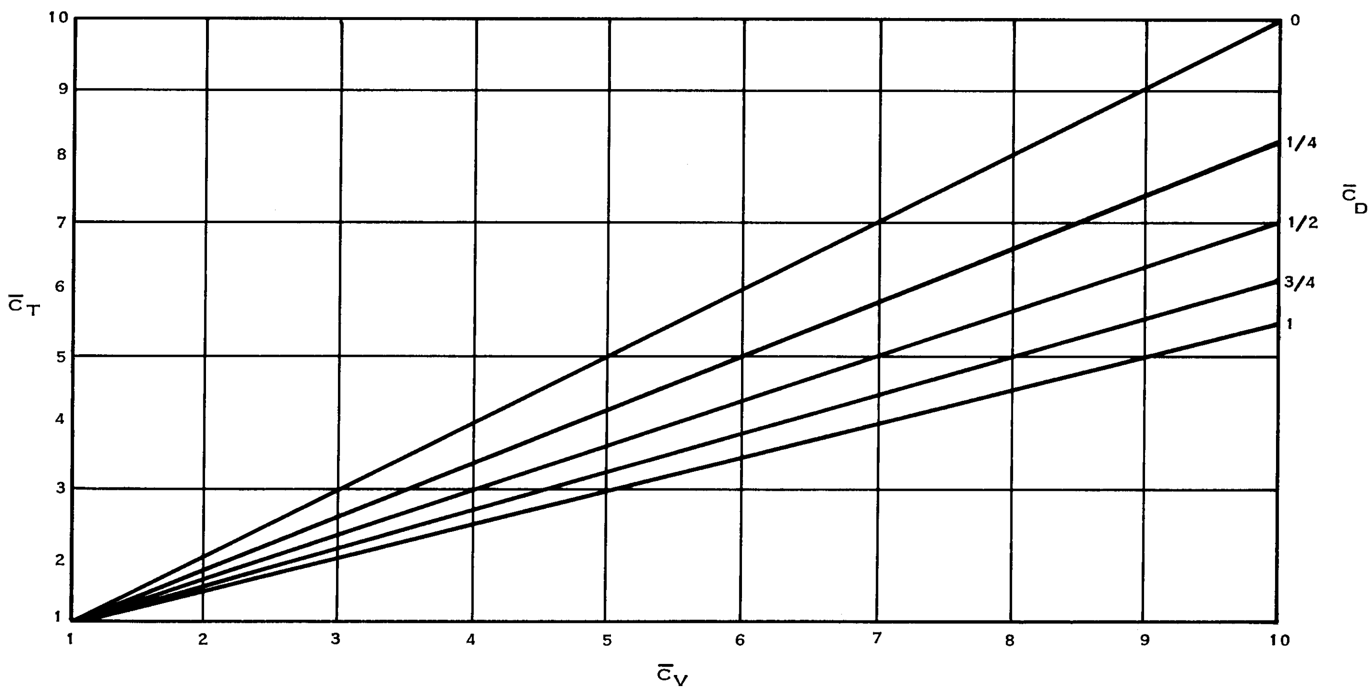

Figure 1-9. $\bar{C}_V$, $\bar{C}_T$ relationship.

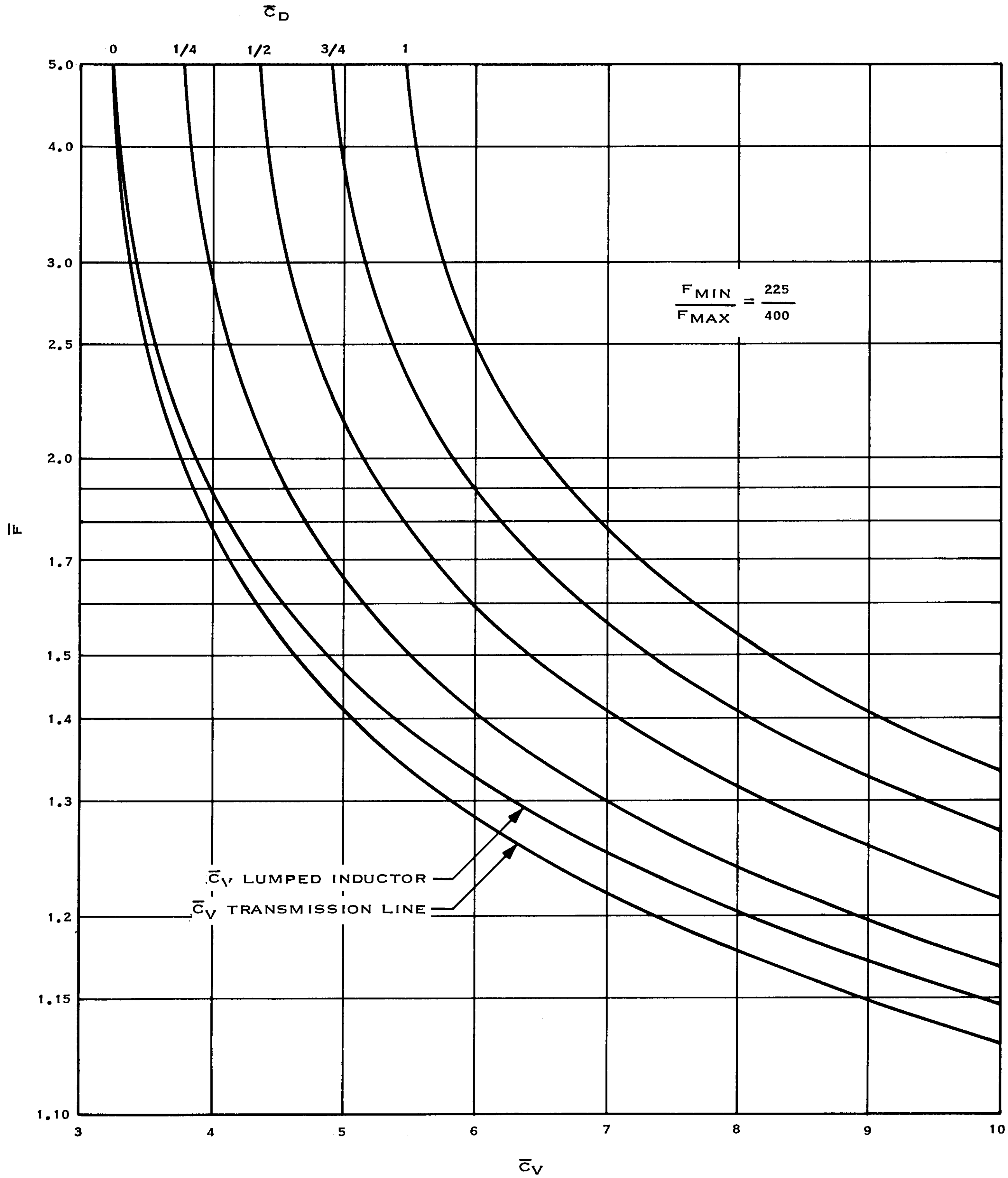

Figure 1-10. Pole and quarter-wave frequencies versus tuning ratio.

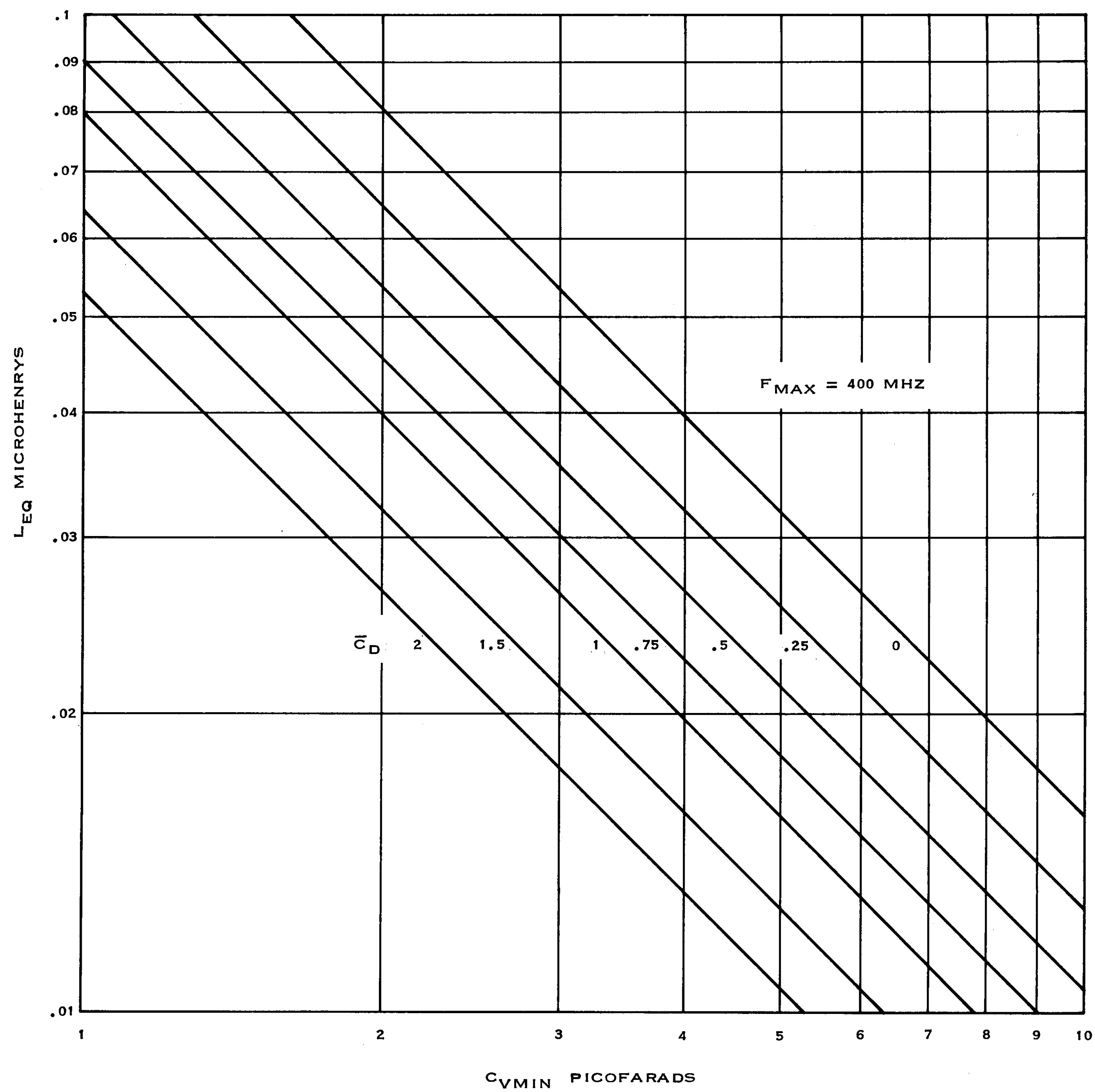

Figure 1-11. Reactance values.

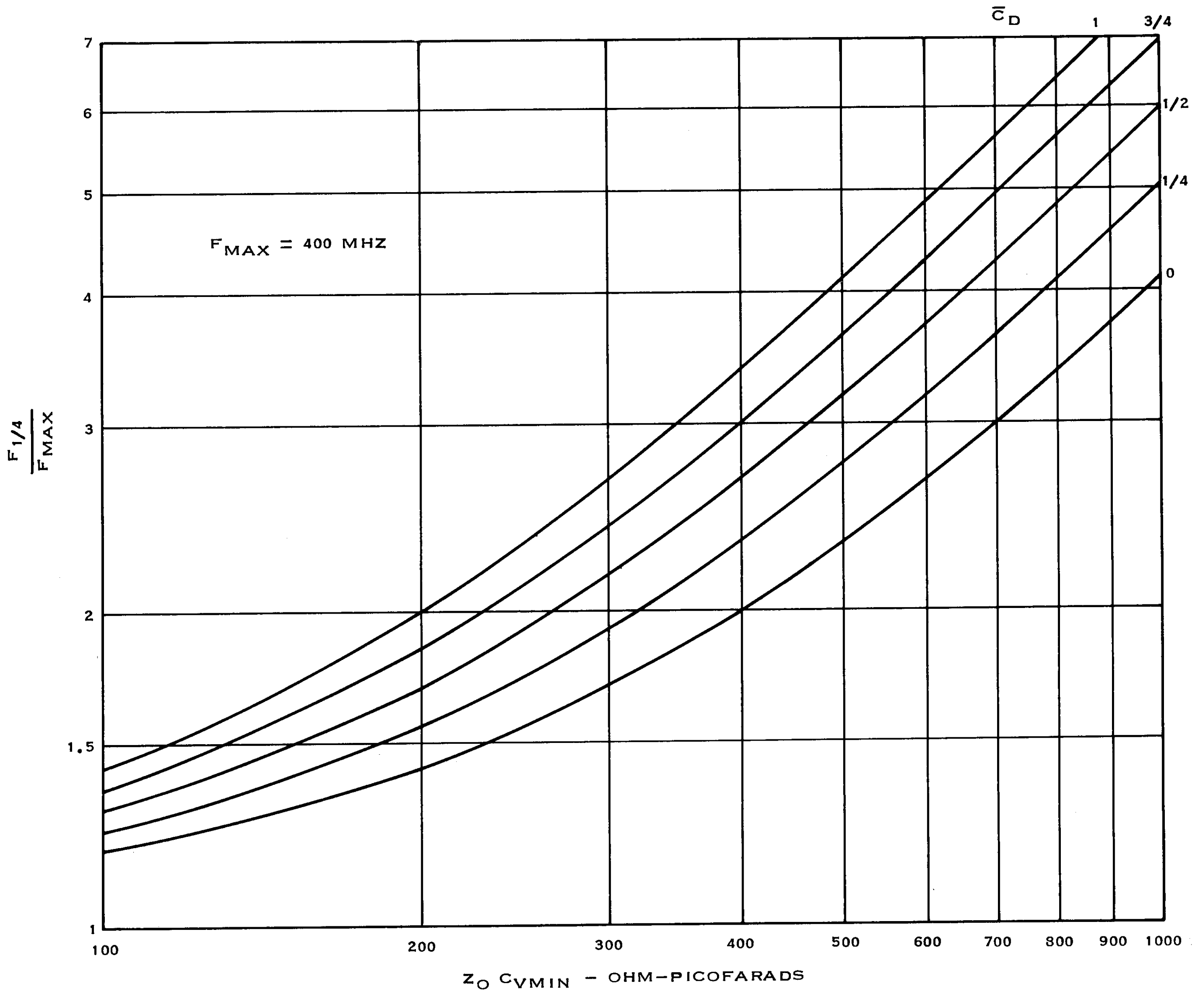

Figure 1-12. Z_O - minimum tuning capacity product.

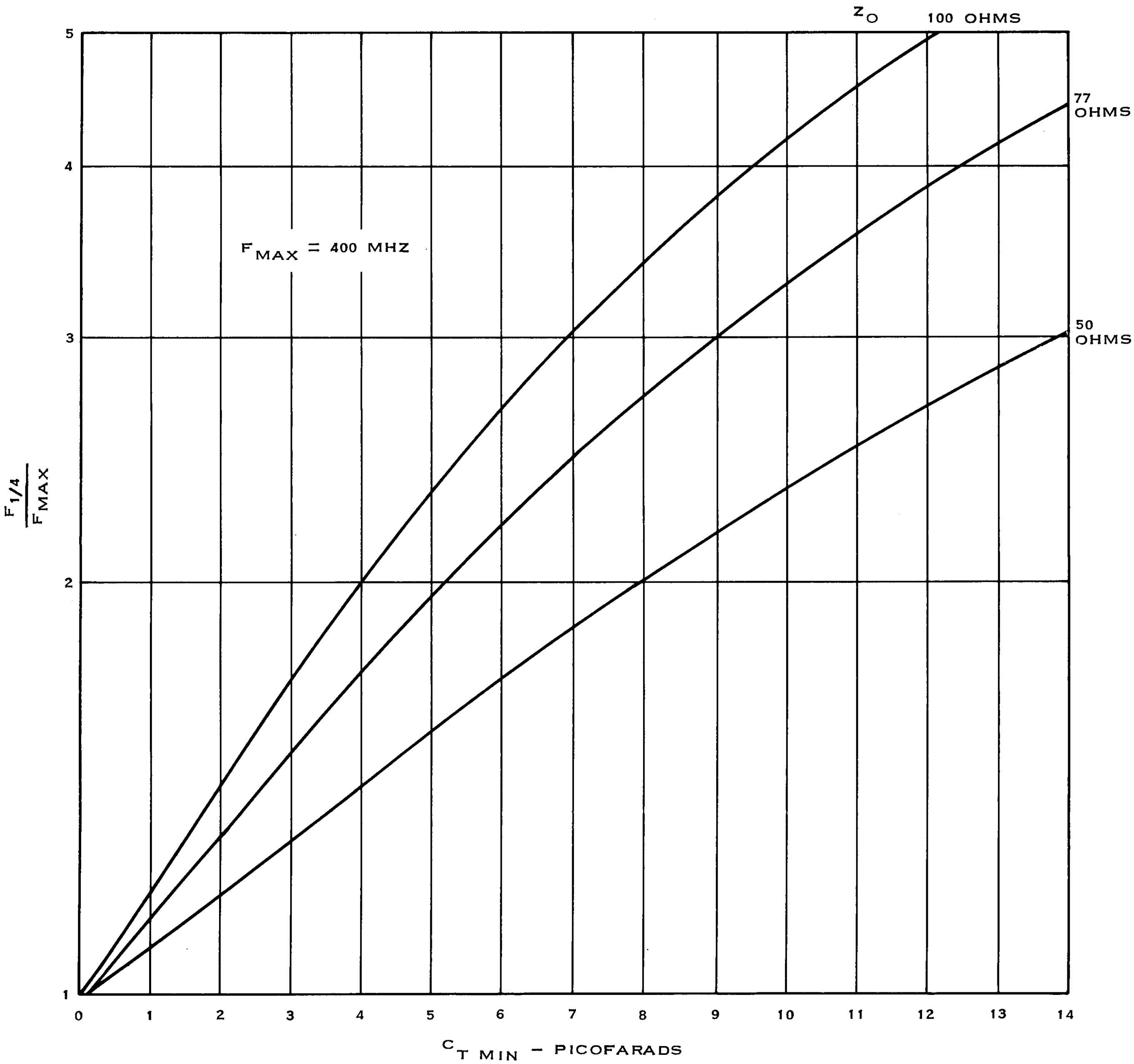

Figure 1-13. $C_{T\ MIN}$ for typical Z_O values.

will illustrate why this is generally desirable. Thirdly, a trimmer capacitor is incorporated to make the resonator tune exactly to the highest frequency F_{MAX} for best tracking. With a rough idea of stray capacity and available values of trimmer capacity the designer has reasonable limits on the value of total stray nodal capacity C_D (trimmer capacity is included as stray because it does not actually participate in the resonator tuning scheme). With these known quantities it is reasonable to pick an approximate value of $C_D/C_{V\ MIN}$ and let the trimmer capacitor compensate until that exact value of $\bar{C}_D$ can be realized. This provides justification for the assumed knowledge of F_{MAX}, F_{MIN}, $\bar{F}_T$ and $\bar{C}_D$.

Figure 1-9 illustrates the effect of $\bar{C}_D$ on the tuning capacity element represented by $\bar{C}_V$. The curves show that $\bar{C}_V$ can be minimized for any required $\bar{C}_T$ while selecting as small a value of $\bar{C}$ as is physically realizable. These curves are used to obtain $\bar{C}_{V\ MIN}$ from $\bar{C}_{T\ MIN}$.

Figure 1-10 shows how $\bar{C}_V$ and $\bar{F}$ are related and what the effect of $\bar{C}_D$ is on this relationship. These design curves show the effect of quarter-wave frequency on the tuning capacitor tuning ratio $\bar{C}_V$. Note that the generation of this curve depended upon a knowledge of $\bar{F}_T$ (for uhf $\bar{F}_T$ = 225/400). The curve for $\bar{C}_V$ of the lumped inductor is independent of $\bar{C}_D$ so that one curve incorporates all values of stray capacity. This occurs because $F = F_P/F_{MAX}$ accounts for all the stray nodal C. For the transmission line resonator five values of $\bar{C}_D$ are used to represent the tuning relationship. It is interesting to note how similiar the lumped inductor curve and the transmission line curve for $\bar{C}_D = 0$ are in shape. This supports the analogy between F_P and $F_{1/4}$.

Figure 1-11 simply gives the resonance curve of L_{EG} and $C_{V\ MIN}$ at varying values of $\bar{C}_D$ for F_{MAX} = 400 mhz.

Figure 1-12 is a design aid for determining the relationship between Z_O, $C_{V\ MIN}$, and $F_{1/4}$ when designing transmission line resonators. The effect of $\bar{C}_D$ on these relationships is represented by the family of curves. F_{MAX} is known.

Figure 1-13 also represents the Z_O, $C_{V\ MIN}$, and $F_{1/4}$ dependencies but for these curves $\bar{C}_D = 0$ and $C_{V\ MIN}$ is replaced by $C_{T\ MIN}$. This curve was included to provide a design aid for three specific but commonly used values of Z_O. Note the value $Z_O = 77\,\Omega$ is included because this is the characteristic impedance for maximum Q in a coaxial resonator.

Figure 1-14 shows the relationship between F_P, L_{EQ}, and $C_{V\ MIN}$. This curve is helpful in computing F_P for Q-calculations and is generally used with figure 1-11 for design calculations.

In any of the design curves presented it is possible to equate $C_{V\ MIN} = C_{T\ MIN}$ when $\bar{C}_D = 0$. This is useful when the design parameters have already been formulated to account for stray nodal capacity C_D.

3.1.2.1.1.1 Tuning Range Summary

The equations summarized in table 1-1 can be used to generate design curves applicable to a given filter requirement as was done in figures 1-9 through 1-13. The curves become most useful when filter designs are repeatedly done for the same band of frequencies. Computer programs were written to provide the data for plotting the curves.

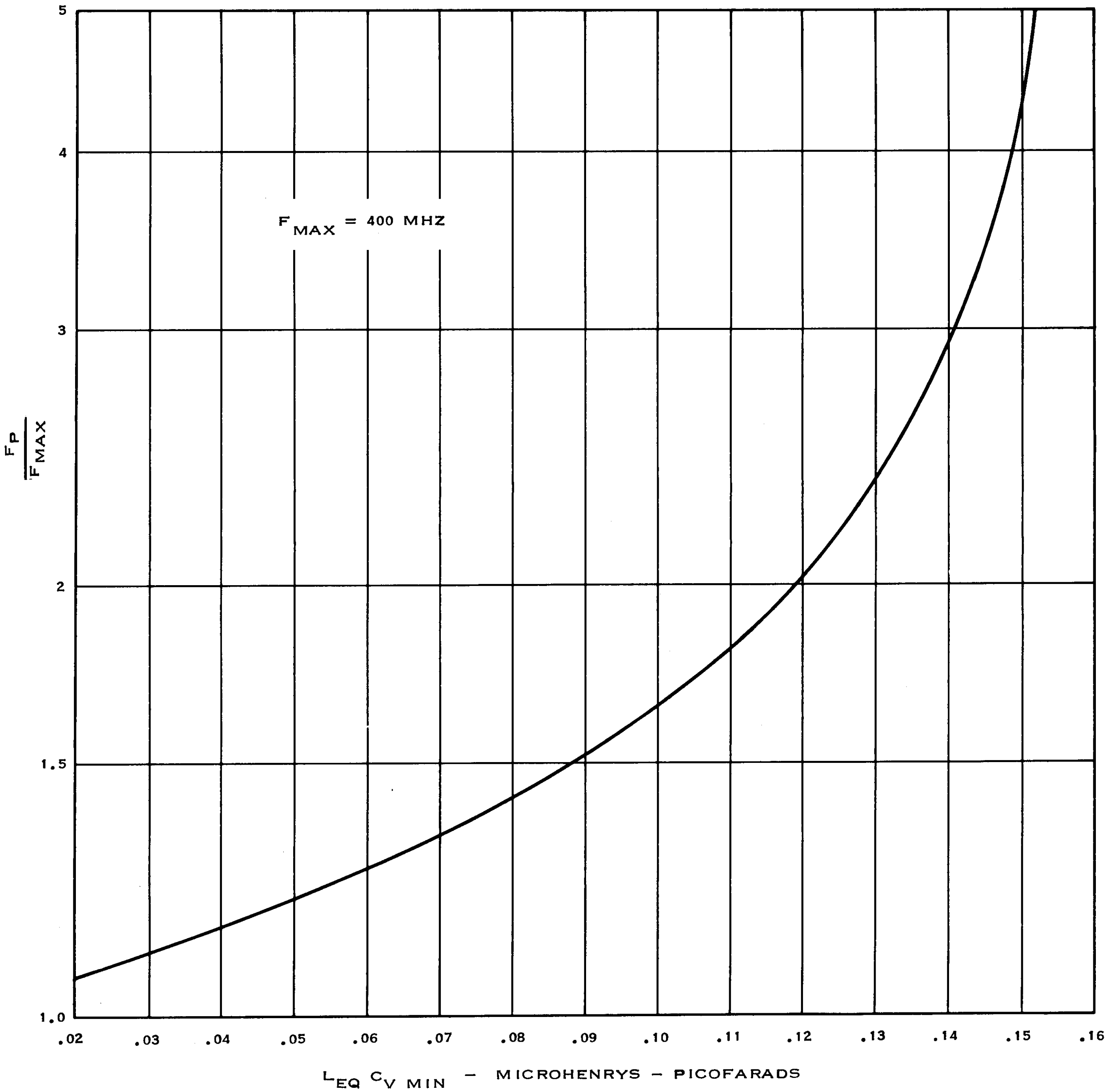

Figure 1-14. Equivalent inductance-minimum tuning capacity product.

3.1.2.1.1.2 Tuning Range Examples

A uhf filter is to be constructed using lumped inductor and transmission line resonators. The resonator must tune 225-400 mhz. Figure 1-10 shows the minimum value of $\bar{C}_V$ to accomplish this tuning range to be 3.25. Larger $\bar{C}_V$ are also usable depending on other circuit requirements. We now decide a varactor will be used to tune the resonator and from manufacturers' specifications of varactors for uhf applications we select a varactor with the following characteristics:

a. Maximum tuning range consistent with distortion specifications = 7.0.
b. Minimum varactor capacity $C_{V\,MIN} = 2.0$ pf.

On the basis of available trimmer capacitors and physical layout it is estimated the total nodal stray capacity will be $C_D \cong 1.0$ pf; then $\bar{C}_D = 1/2$.

First, we design a resonator using a lumped inductor; from figure 1-9 $\bar{C}_V = 4.22$ for

$\bar{C}_T = \left(\frac{400}{225}\right)^2 = 3.16$; from figure 1-10 the absolute minimum pole frequency F_P is

$$F_P = (400)\ 1.74 = 696\text{mhz};$$

from figure 1-11 the required inductance L_{EQ} is

$$L_{EQ} = .053\ \mu h;$$

and we summarize the results as

$$2\text{ pf} \le C_V \le 8.44\text{ pf}$$

$$225\text{ mhz} \le F_O \le 400\text{ mhz}$$

$$C_D = 1\text{ pf}$$

$$F_P = 500\text{ mhz}$$

$$L_{EQ} = .053\,\mu h$$

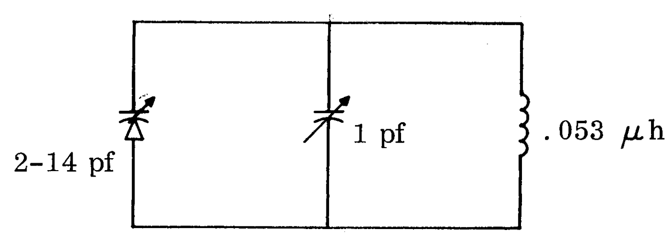

Secondly, we design a resonator employing a transmission line inductor but still using the same varactor and physical layout;

$$\bar{C}_V = 7.0$$

$$C_{V\ MIN} = 2.0\ pf$$

$$C_{V\ MAX} = 14.0\ pf$$

$$C_D = 1\ pf$$

$$\bar{C}_D = 1/2$$

from figure 1-10 $\bar{F} = 1.41$

$$F_{1/4} = (1.41)(400) = 564\ mhz;$$

from figure 1-12 $Z_O\ C_{V\ MIN} = 130$ ohm-pf

$$Z_O = 130/2 = 65\ ohms.$$

The resonator could also be designed on the basis of maximum Q. Refer to figure 1-13 where $Z_O = 77$ ohms. The curve shows the available $C_{T\ MIN}$ and $F_{1/4}$ values.

$$C_{T\ MIN} = C_{V\ MIN} + C_D = 3\ pf$$

$$F_{1/4} = (400)(1.5) = 600\ mhz.$$

$$Z_O = 77\ ohms$$

From figure 1-10 at $\bar{C}_D = 1/2$ and $\bar{F} = 1.5$ we obtain $\bar{C}_V = 6.4$ and the final maximum Q values are:

$$2\ PF \leq C_V \leq 12.8\ pf$$

$$C_D = 1\ pf$$

$$F_{1/4} = 600\ mhz.$$

$$Z_O = 77\ ohms$$

$$225\ mhz \leq F_O \leq 400\ mhz.$$

The designer might wish to minimize tuning range to improve distortion and this can also be done. Referring to figure 1-10, $\overline{C}_D = 1/2 \quad \overline{F} = 4.0 \quad \overline{C}_V = 4.42$

From figure 1-12

$$Z_O \, C_{V\ MIN} = 640$$

$$Z_O = 640/2 = 320 \text{ ohms}$$

and the final minimum tuning range values are

$$2 \text{ pf} \leq C_V \leq 8.84 \text{ pf}$$

$$C_D = 1 \text{ pf}$$

$$F_{1/4} = 1600 \text{ mhz}$$

$$Z_O = 320 \text{ ohms}$$

$$225 \text{ mhz} \leq F_O \leq 400 \text{ mhz.}$$

3.1.2.1.2 Q-Frequency Dependence for Lumped Inductor Resonators

The design equations for resonator tuning characteristics will be useful in analyzing the quality factor, Q, of the various resonator circuits. Figures 1-7 and 1-8 are the example circuit models to be used in obtaining equations which describe the Q of the resonator as it is tuned over a band of frequencies. The total nodal Q of a resonator can be computed by consideration of the net Q's associated with the inductive and capacitive components respectively. This is accomplished by separation of each nodal circuit into net capacitive and inductive parts with their associated Q's as represented by figure 1-8. Generally the Q's, L's, and C's are functions of frequency but this presents no great problem in the analysis. After the separated circuits are obtained it is then a simple matter to compute the total nodal Q as the parallel combination of the two parts by summing the decrements, or equivalently:

$$1/Q_T \triangleq 1/Q_C + 1/Q_L$$

This approach is always valid when the equal slope criteria is applied.

The total nodal Q for a lumped inductor resonator can be derived in terms of F_{MAX}, F_P, F_O, $Q_{V\ MAX}$, a and b. The equations, normalized for ease of design, are derived in detail in part III, section 6. These equations are

$$Q_T/Q_{V\ MAX} \triangleq \frac{1}{\left(\frac{F_{MAX}}{F_O}\right)^b \frac{Q_{V\ MAX}}{Q_{L\ MAX}} + \left(\frac{F_{MAX}}{F_O}\right)^a \frac{1 - \left[(F_O/F_P)^2\right]^2}{1 - (F_{MAX}/F_P)^2}}$$

and

$$Q_T/Q_{T\ MAX} \triangleq \frac{\frac{Q_{V\ MAX}}{Q_{L\ MAX}} + 1 - \left(F_{MAX}/F_P\right)^2}{\left(\frac{F_{MAX}}{F_O}\right)^b \frac{Q_{V\ MAX}}{Q_{L\ MAX}} + \left(\frac{F_{MAX}}{F_O}\right)^a \frac{\left[1 - (F_O/F_P)^2\right]^2}{1 - (F_{MAX}/F_P)^2}}$$

These equations are not easily analyzed and presented for the general case but a specific design example will illustrate the typical results to be expected.

The equations were programmed for solution by computer and a catalog of design tables was generated. The complete listing is too large to be included in the report but a specific example can be given. The example is illustrated using figure 1-6, circuit 4B.

Consider a lumped inductor with losses attributable to skin loss only and a tuning capacitor with series resistance independent of frequency. Also it is assumed the individual element Q's are greater than 10. The varactor exponent for this example is a = 1.0 and the inductor exponent for skin loss is b = 0.5. The normalized Q as a function of normalized frequency is shown in figure 1-15 where $\frac{Q_{V\ MAX}}{Q_{L\ MAX}} = 1$ and F_P/F_{MAX} are the parameters. The curves

illustrate the effect of F_P on the total Q change over a band. In most cases it is desirable to minimize the percentage change in Q which requires as large an F_P as is practical. The value of a curve such as the typical one presented is in the ability to predict the resonator Q's effect on the filter's requirements, such as stopband attenuation, over the entire tuning range. For example, suppose we have the following resonator fabricated:

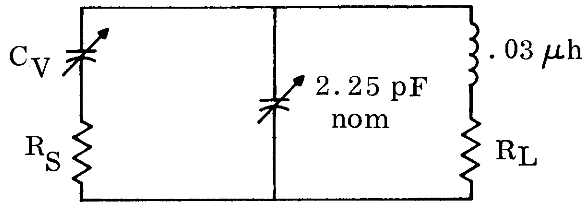

$L_{EQ}\, C_{V\ MIN} = .09\ \mu\text{h-pf}$ $\qquad$ $F_{MAX} = 400$ mhz

$\bar{C}_D = .75$ $\qquad$ $F_{MIN} = 225$ mhz

$C_{V\ MIN} = 3$ pf $\qquad$ $Q_{V\ MAX} = 100$

$Q_{L\ MAX} = 100$

From figure 1-14, $F_P/F_{MAX} = 1.52$

$F_P = 608$ mhz

From figure 1-10, the curve for lumped inductors

$\bar{C}_V = 4.75$

$3_{PF} \leq C_V \leq 14.25$ PF

The total circuit Q change can be estimated from figure 1-15 is where $F_P/F_{MAX} = 1.5$ and

$$\frac{Q_{V\ MAX}}{Q_{L\ MAX}} = 1.0$$

$$Q_T = \frac{1}{\frac{1}{100} + \frac{1}{100}} = 50$$

The curve may be used to generate the following tabulation:

F_O MHZ	Q_T
400	50.0
350	39.5
300	31.0
260	25.5
225	20.2

This tabulation illustrates the large change in Q as a resonator is tuned across a band of frequencies. This large change is primarily due to the large value of C_D, hence the small ratio of F_P/F_{MAX}.

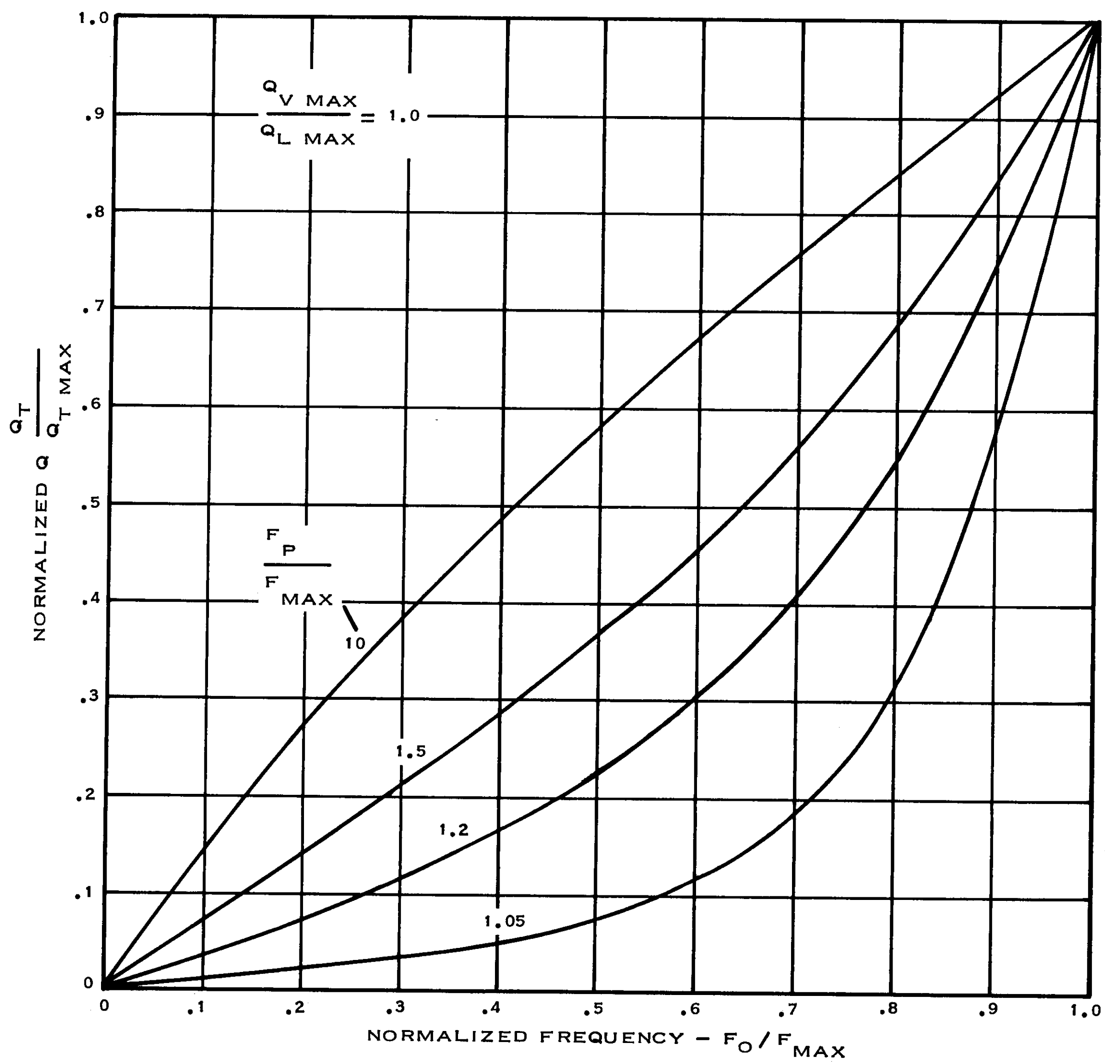

Figure 1-15. Normalized Q versus normalized frequency for lumped inductor.

The following tabulation illustrates the improvement in Q-change if the circuit is modified so $F_P/F_{MAX} = 10.0$:

F_O MHZ	Q_T
400	50.0
350	45.0
300	40.0
260	36.0
225	32.0

The Q at the lowest frequency is improved about 60 percent. This illustrates the need to keep the stray nodal capacity as small as possible, hence to keep the pole frequency as large as possible.

3.1.2.1.3 Q-Frequency Dependence for Transmission Line Resonators.

The total nodal Q for a transmission line inductor must be obtained by applying the equal slope criteria to the circuit of figure 1-7(b). The problem is complicated by the addition of C_D but the solution can still be obtained in a manner similar to that for lumped inductors. The following design equations are derived in detail in part III, section 7.

The first result obtained from the equal slope criteria is the solution for the equivalent inductive and capacitive reactances X_{LEQ} and X_{CEQ}. These reactances normalized by Z_O, as well as the tuning reactance curve, are presented in figures 1-16 through 1-18. These curves are useful in presenting the idea of representing the transmission line circuit by its equal slope lumped equivalent. The following equations are repeated for convenience:

$$X_{LEQ} \triangleq Z_O \frac{\text{TAN } \theta_O}{1/2 + \theta_O/\text{SIN } 2\ \theta_O} \triangleq \frac{X_{CT}}{1/2 + \theta_O/\text{SIN } 2\ \theta_O}$$

$$X_{CEQ} \triangleq -Z_O \frac{\text{TAN } \theta_O}{1/2 - \theta_O/\text{SIN } 2\ \theta_O} \triangleq \frac{-X_{CT}}{1/2 - \theta_O/\text{SIN } 2\ \theta_O}$$

$$X_{CT} \triangleq Z_O \text{ TAN } \theta_O \qquad\qquad \theta \triangleq \pi/2\left(F_O/F_{1/4}\right)$$

With these equations it is possible to compute the equivalent circuit for a transmission line resonator based on the equal slope criteria. For example, suppose a transmission line resonator has a $Z_O = 77$ ohms and $F_{1/4} = 800$ MHz, and it is desired to find the equivalent circuit at $F_O = 266$ MHz.

Then: $$\theta_O = \frac{\pi}{2} F_O/F_{1/4} \longrightarrow 30° \text{ at } 266 \text{ MHZ.}$$

From figure 1-16, the total capacitive reactance required to tune the line is

$$-\frac{X_{CT}}{Z_O} = .58 \qquad\qquad X_{CT} = -77\ (.58) = -44.6 \text{ ohms}$$

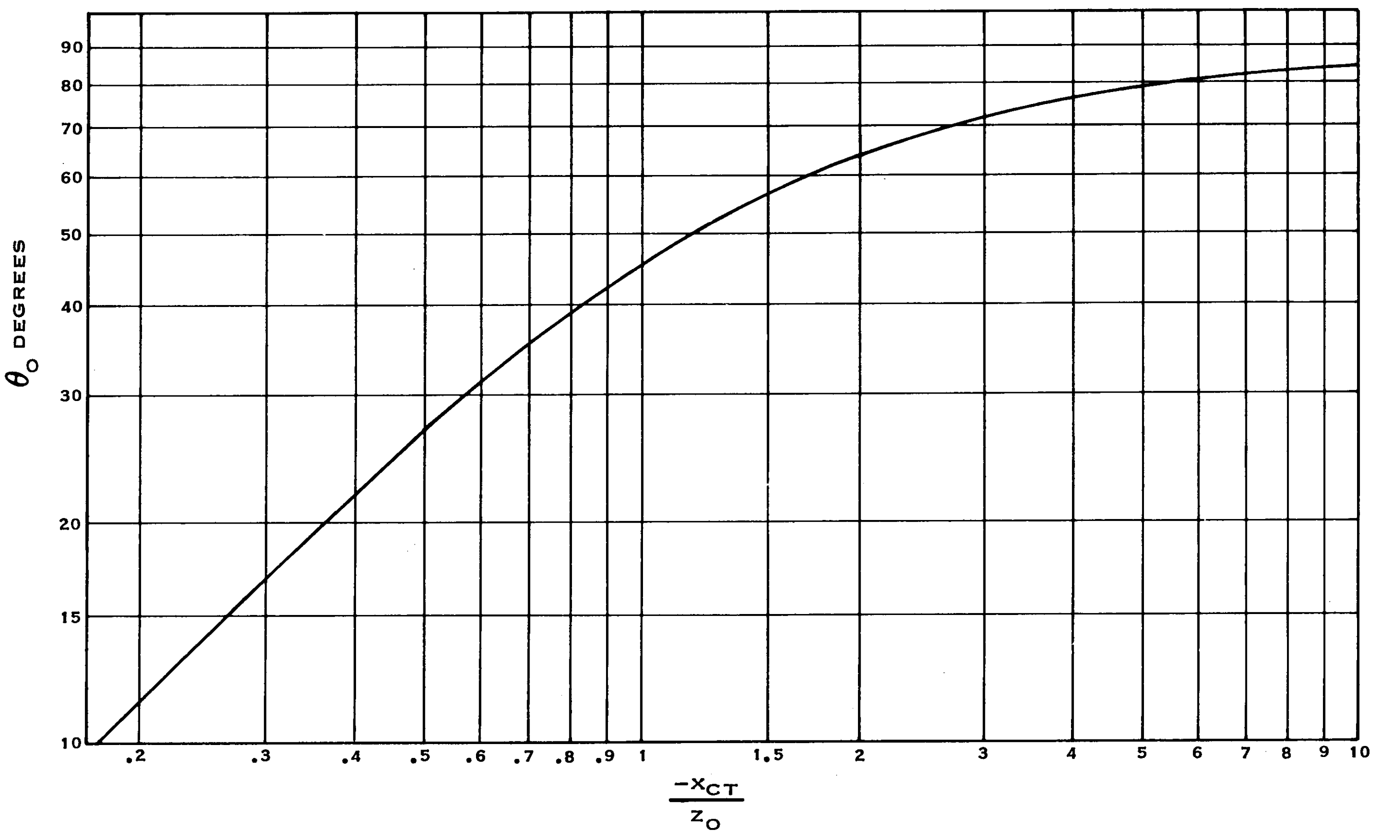

Figure 1-16. Transmission line tuning curve.

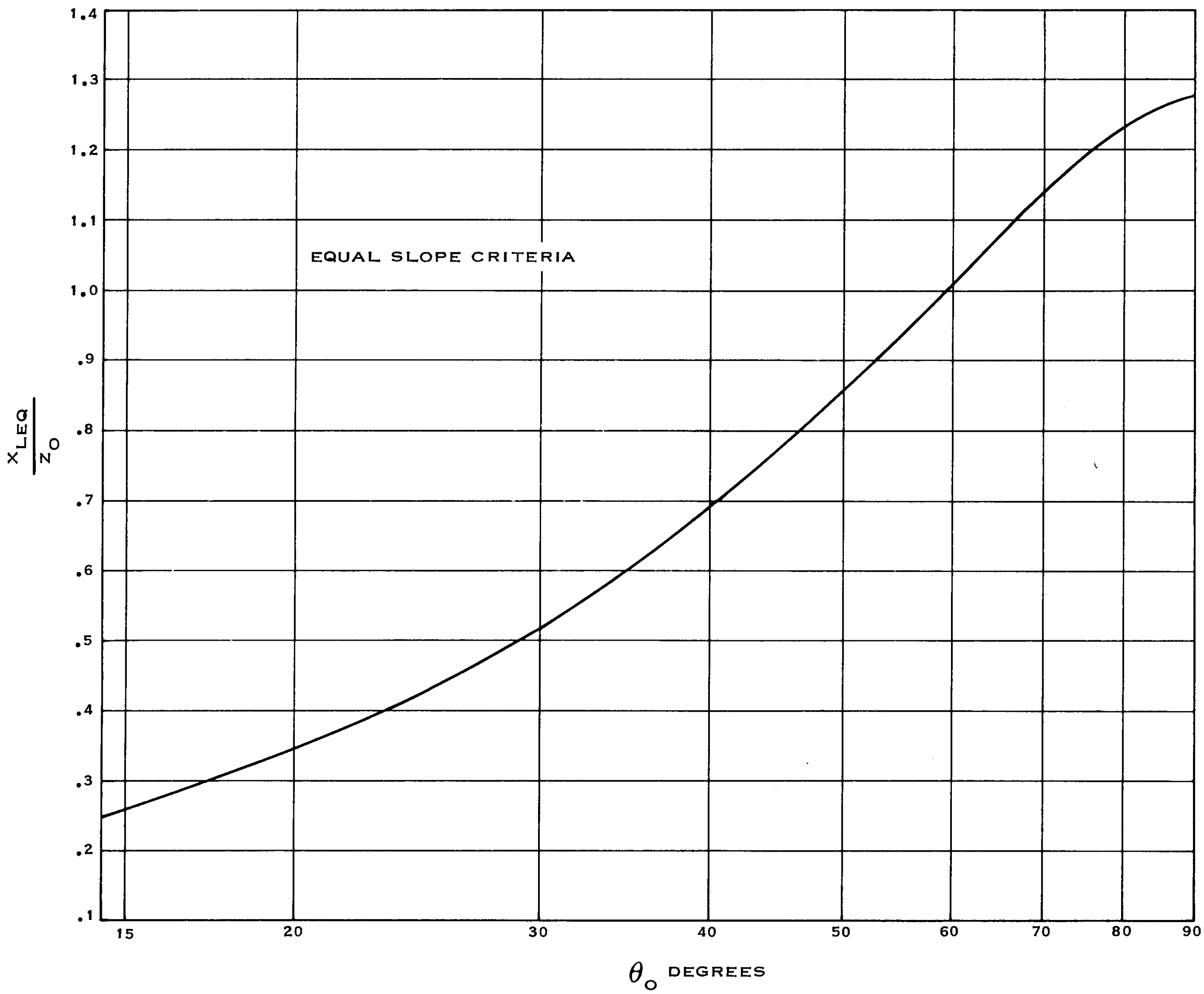

Figure 1-17. Normalized equivalent inductive reactance.

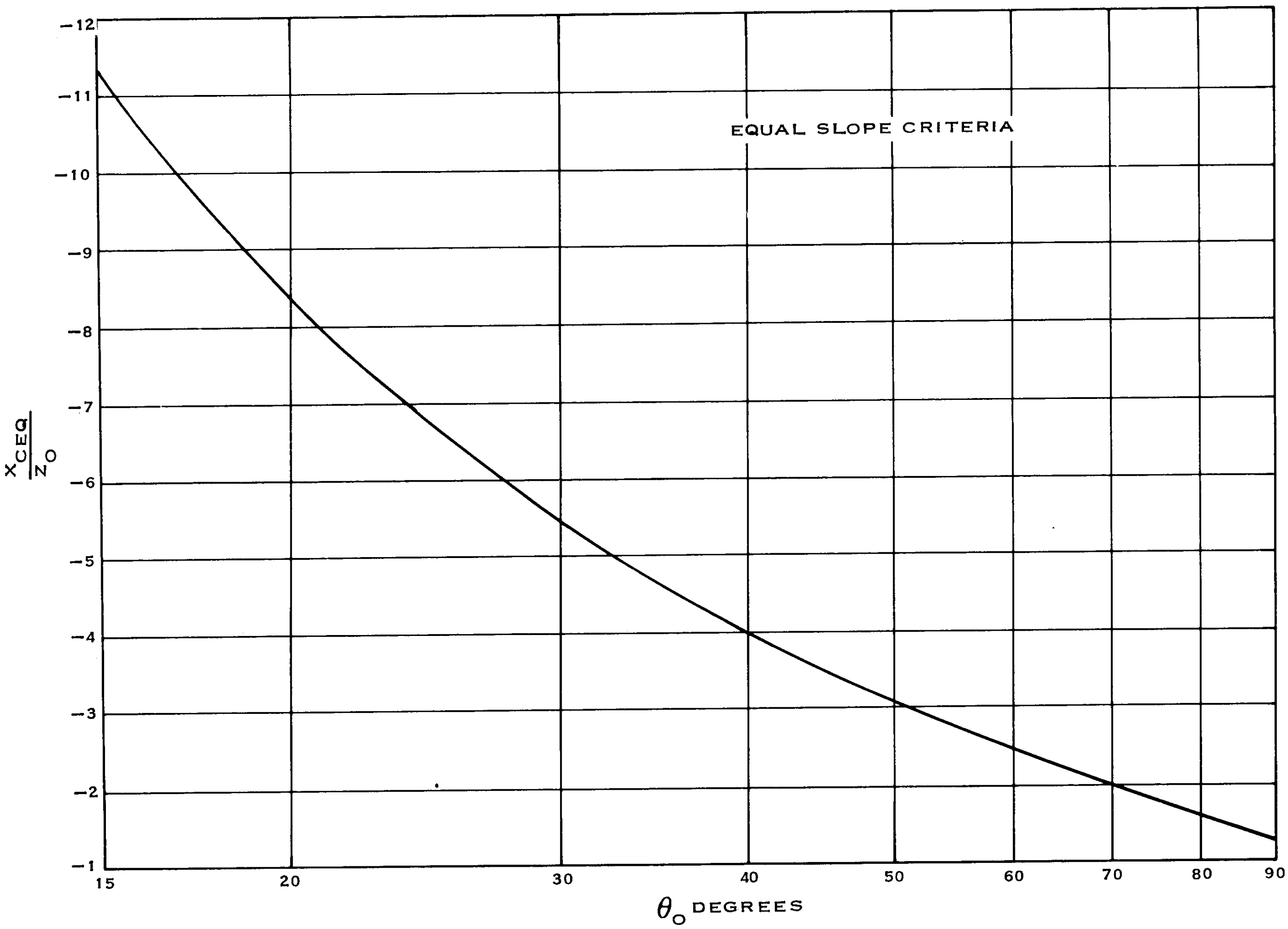

Figure 1-18. Normalized equivalent capacitive reactance.

The transmission line provides the following equivalent circuit values:

From figure 1-17

$$X_{LEQ} = 77\ (.52) = 40 \text{ ohms}$$

From figure 1-18

$$X_{CEQ} = 77\ (-5.5) = -423 \text{ ohms}$$

The parallel combination of X_{CT}, X_{LEQ}, and X_{CEQ} resonates at 266 mhz. These variables are then used with figure 1-7(c) to obtain the total nodal Q-equations for the transmission line resonator:

$$Q_T = Q_{V\ MAX} \frac{1}{\left(\frac{F_{MAX}}{F_O}\right)^{1/2} \frac{Q_{V\ MAX}}{Q_{L\ MAX}} + \left(\frac{\mathrm{TAN}\ \theta_{MAX}}{\mathrm{TAN}\ \theta_O}\right)^a \frac{1 - \omega_O C_D Z_O \mathrm{TAN}\ \theta_O}{(1/2 + \theta_O/\mathrm{SIN}\ 2\ \theta_O)}}$$

Normalized Q_T is

$$Q_T/Q_{T\ MAX} = \frac{\frac{Q_{V\ MAX}}{Q_{L\ MAX}} + \frac{1 - \omega_{MAX} C_D Z_O \mathrm{TAN}\ \theta_{MAX}}{1/2 + \theta_{MAX}/\mathrm{SIN}\ 2\ \theta_{MAX}}}{\left(\frac{F_{MAX}}{F_O}\right)^{1/2} \frac{Q_{V\ MAX}}{Q_{L\ MAX}} + \left(\frac{\mathrm{TAN}\ \theta_{MAX}}{\mathrm{TAN}\ \theta_O}\right)^a \frac{1 - \omega_O C_D Z_O \mathrm{TAN}\ \theta_O}{(1/2 + \theta_O/\mathrm{SIN}\ 2\ \theta_O)}}$$

with

$$\theta_O = \pi/2\left(F_O/F_{1/4}\right) = \pi/2\left(F_O/F_{MAX}\right)\left(\theta_{MAX}\right)$$

$$\theta\ \mathrm{MAX} = \pi/2\left(F_{MAX}/F_{1/4}\right)$$

The normalized Q-equation is simplified if the stray capacity can be ignored, that is, $C_D \cong O$.

When $C_D \equiv O$ the equation becomes

$$Q_T/Q_{T\ MAX} = \frac{\frac{Q_{V\ MAX}}{Q_{L\ MAX}} + \left(1/2 + \theta_{MAX}/\mathrm{SIN}\ 2\ \theta_{MAX}\right)^{-1}}{\left(\frac{F_{MAX}}{F_O}\right)^{1/2} \frac{Q_{V\ MAX}}{Q_{L\ MAX}} + \left(\frac{\mathrm{TAN}\ \theta_{MAX}}{\mathrm{TAN}\ \theta_O}\right)^a \left(1/2 + \theta_O/\mathrm{SIN}\ 2\ \theta_O\right)^{-1}}$$

To illustrate typical results, the assumption $C_D = O$ was made and a computer program was written to obtain a tabular listing of normalized Q as a function of normalized frequency. Again it was assumed the varactor exponent a = 1.0 and the inductor exponent for skin loss b = 0.5. Normalized Q as a function of normalized frequency is shown in figure 1-19, where

$\frac{Q_{V\ MAX}}{Q_{L\ MAX}} = 1.0$ and $\frac{F_{1/4}}{F_{MAX}}$ are the parameters.

The curves illustrate the large percentage change in Q when the 1/4-wave frequency is close to F_{MAX}. Note that when $\frac{F_{1/4}}{F_{MAX}} = 2.0$ the Q-dependence is very nearly linear with frequency, and the resonator Q behaves very much like the simple lumped inductor model presented at the beginning of the section.

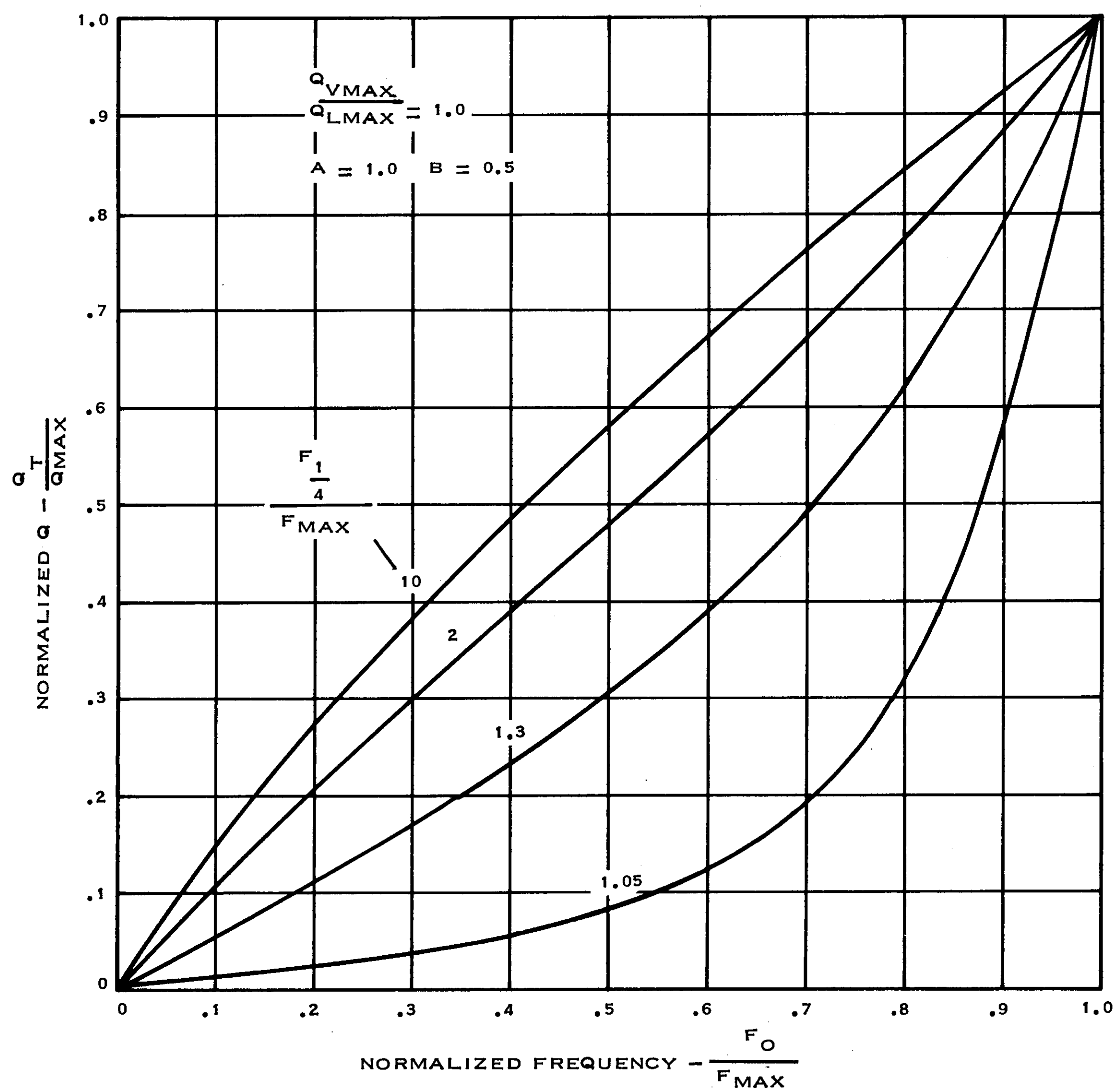

Figure 1-19. Normalized Q versus normalized frequency for transmission line.

The last area to be discussed is the phenomena of Q-enhancement. The Q obtained from the equal slope method is very much dependent on how close to quarter-wave frequency the operating frequency is. In fact, for line lengths between 30° and 90° the Q-enhancement must be accounted for in design applications. In part III, section 7, the equation for total capacitance Q was obtained:

$$Q_C/Q_{V\ MAX} = \left(\frac{\mathrm{TAN}\ \theta_O}{\mathrm{TAN}\ \theta_{MAX}}\right)^a \left(1/2 + \theta_O/\mathrm{SIN}\ 2\ \theta_O\right) \text{ for } C_D \equiv O$$

For a lossless transmission line tuned by a capacitor with fixed R_S the total resonator Q simplifies to the equation

$$Q_T = Q_V \left(1/2 + \theta_O/\mathrm{SIN}\ 2\ \theta_O\right)$$

Figure 1-20 has been included for convenience in computing total resonator Q-enhancement. For example, a tuning capacitor with a Q of 100 is connected across a lossless transmission line. The line length at resonance (where $Q_V = 100$) is 40°. The total resonator Q due to Q-enhancement is:

$$Q_T = 100/.83 \cong 120$$

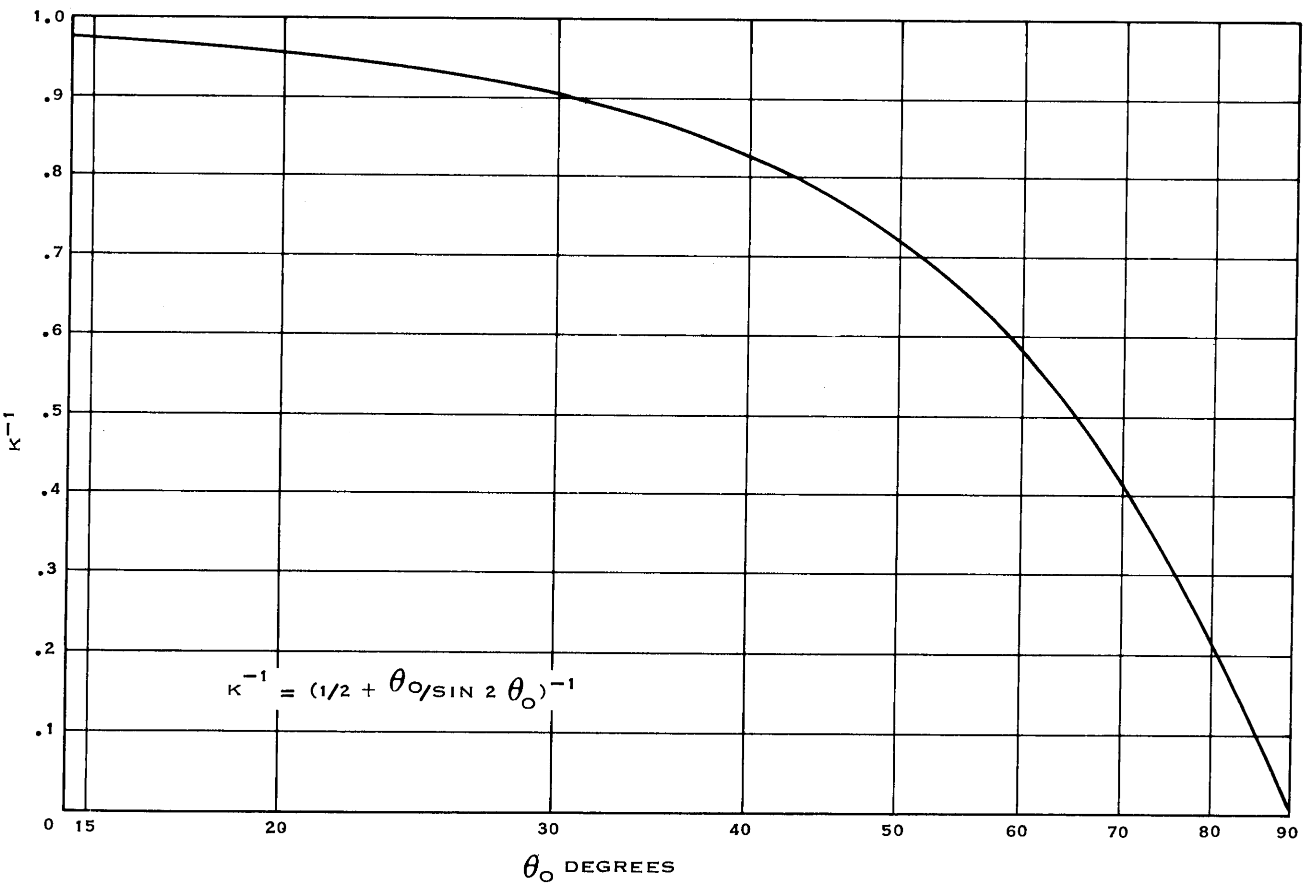

Figure 1-20. Tuning capacitor Q-enhancement factor.

This concept provides an easy method for computing the maximum resonator Q from the sum of Q_C and Q_L,

$$Q_C = Q_{V\ MAX}\ (1/2 + \theta_O / \text{SIN } 2\ \theta_O)$$

$$Q_L = Q_{1/4}\left(\frac{F_O}{F_{1/4}}\right)^{1/2}$$

$$Q_{T\ MAX} = \left(\frac{1}{1/Q_C + 1/Q_L}\right)\Bigg|_{\omega_O = \omega_{MAX}}$$

Example: Suppose we have the following resonator fabricated

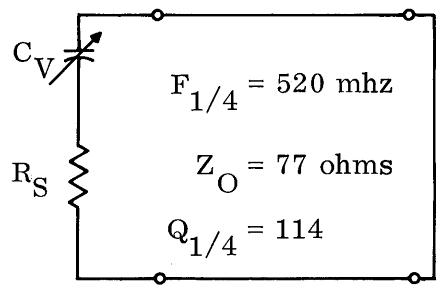

$$F_{MAX} = 400 \text{ MHZ}$$

$$Q_{V\ MAX} = 43.5$$

The total circuit Q can be computed from summing Q_C and Q_L

$$Q_{L\ MAX} = 114\ \left(\frac{400}{520}\right)^{1/2} = 100$$

$$Q_{C\ MAX} = 43.5/.435 = 100$$

$$\theta_O = 90° \frac{400}{520} = 69.3°$$

$$Q_{T\ MAX} = 50$$

assuming a = 1.0 and b = 0.5 we can obtain Q as a function of frequency from figure 1-19 where $F_{1/4}/F_{MAX} = 1.3$.

The following tabulation shows the Q-variation for the graph values.

F_O MHZ	Q_T
400	50
350	37.2
300	27.5
260	21.7
225	17.8

The relatively large change in Q_T is caused by the small $F_{1/4}/F_{MAX}$ ratio. Actually, the Q-enchancement effect makes the change in Q much more pronounced. The net effect is that the attractiveness of the larger Q obtained from Q-enhancement is offset by the larger change in total Q as the resonator is tuned.

Q-enhancement is most attractive for a fixed frequency filtering application, but when the filter must be tuned over a large percentage frequency range the enhancement effect seriously degrades the total-Q change over frequency. When designing resonators for uhf applications, it is desirable to keep the quarter-wave frequency above 800 mhz to minimize both $\overline{C}_V$ and total Q-change.

3.1.2.1.4 Q-Frequency Dependence for Varactor-Tuned UHF Resonators.

The varactor diode is a commonly used voltage controlled capacitor method. For this reason, a separate section has been included to discuss the merits of varactor tuning at uhf. High quality uhf varactors currently being manufactured for tuner applications are characterized at 400 mhz by the variables listed in table 1-2.

TABLE 1-2. TYPICAL VARIABLES IN PRESENT UHF VARACTORS.

PARAMETER	RANGE OF VALUES
$C_{V\ MIN}$	1.2 to 22 pF
$\overline{C}_V$	1 to 3
$Q_{V\ MAX}$	300 to 1600
Breakdown voltage	20 to 80 volts

In tuner applications requiring reasonably good distortion performance the tuning ratio $\bar{C}_V$ is reduced to 1.5 because of the low voltage limit imposed by distortion performance. This limited range forces the designer to build several filters or employ fixed capacitor switching to cover larger tuning ranges. For example, the uhf band requires at least two filters to cover 225 to 400 mhz if varactor tuning is employed.

Another very important factor in the design of a varactor-tuned filter is the variation of Q as the varactor is tuned. The varactor can be simply thought of as a back-biased diode whose capacity is the transition capacity and whose series resistance is the bulk semiconductor resistance. Refer to figure 1-21 for a pictorial representation of the current discussion:

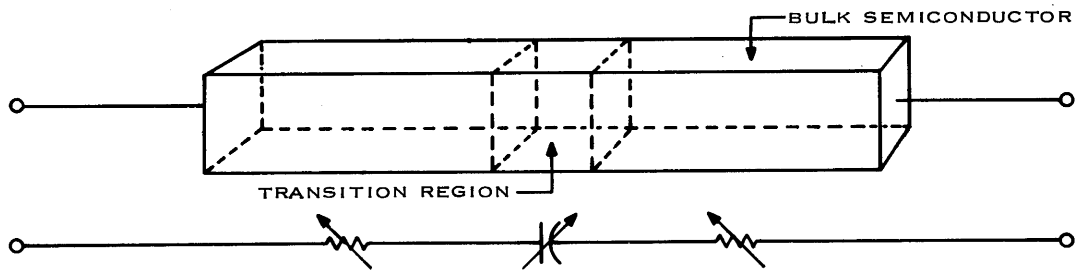

Figure 1-21. Physical varactor model.

When the voltage is varied, the transition width changes with an accompanying change in capacity. However, as the capacity is increased the bulk resistance also increases, which yields a change in Q much larger than predicted by a constant R_S model.

The slope of Q-change also depends on the quality and construction of the diode. For low quality diodes, the bulk resistance is large and the change in resistance percentage-wise is fairly small. For high-quality diodes, the bulk resistance is very small and the change in resistance percentage-wise is very large, although this change is complicated by the fact that epitaxial construction might allow the region to be depleted to the ohmic contact.

An empirical investigation of varactor data has led to the formulation of an equation which reasonably predicts performance. The normalized Q-variation can be expressed as:

$$\frac{Q_V}{Q_{V\,MAX}} = \left(\frac{X_{CV}\Big|_{\omega_O}}{X_{CV}\Big|_{\omega_{MAX}}} \right)^A$$

where

$$1 \leq a \leq 5$$

$$A \cong 1 \text{ for low quality diodes}$$

$$A \cong 5 \text{ for high quality diodes}$$

From previously derived equations the Q-variation of high quality varactor diodes can be expressed in the following equations:

For lumped inductor resonators:

$$\frac{Q_V}{Q_{V\ MAX}} = \left(F_O/F_{MAX}\right)^5$$

For transmission line resonators:

$$\frac{Q_V}{Q_{V\ MAX}} = \left(\frac{\text{TAN}\ \theta_O}{\text{TAN}\ \theta_{MAX}}\right)^5$$

High Quality Varactors

These equations have been employed in a computer program to tabulate the normalized Q-change for both lumped inductor and transmission line resonators.

The equations used are listed below for reference:

Lumped inductor:

$$Q_T/Q_{T\ MAX} = \frac{\dfrac{Q_{V\ MAX}}{Q_{L\ MAX}} + 1 - \left(F_{MAX}/F_P\right)^2}{\left(\dfrac{F_{MAX}}{F_O}\right)^{1/2} \dfrac{Q_{V\ MAX}}{Q_{L\ MAX}} + \left(\dfrac{F_{MAX}}{F_O}\right)^5 \dfrac{\left[1 - \left(F_O/F_P\right)^2\right]^2}{1 - \left(F_{MAX}/F_P\right)^2}}$$

Transmission line:

$$Q_T/Q_{T\ MAX} = \frac{\dfrac{Q_{V\ MAX}}{Q_{L\ MAX}} + \left(1/2 + \theta_{MAX}/\text{SIN}\ 2\ \theta_{MAX}\right)^{-1}}{\left(\dfrac{F_{MAX}}{F_O}\right)^{1/2} \dfrac{Q_{V\ MAX}}{Q_{L\ MAX}} + \left(\dfrac{\text{TAN}\ \theta_{MAX}}{\text{TAN}\ \theta_O}\right)^5 \left(1/2 + \theta_O/\text{SIN}\ 2\ \theta_O\right)^{-1}}$$

Figures 1-22 through 1-24 illustrate the results obtained from this analysis for lumped inductors.

Figures 1-25 through 1-27 illustrate the results obtained from the analysis for transmission line inductors.

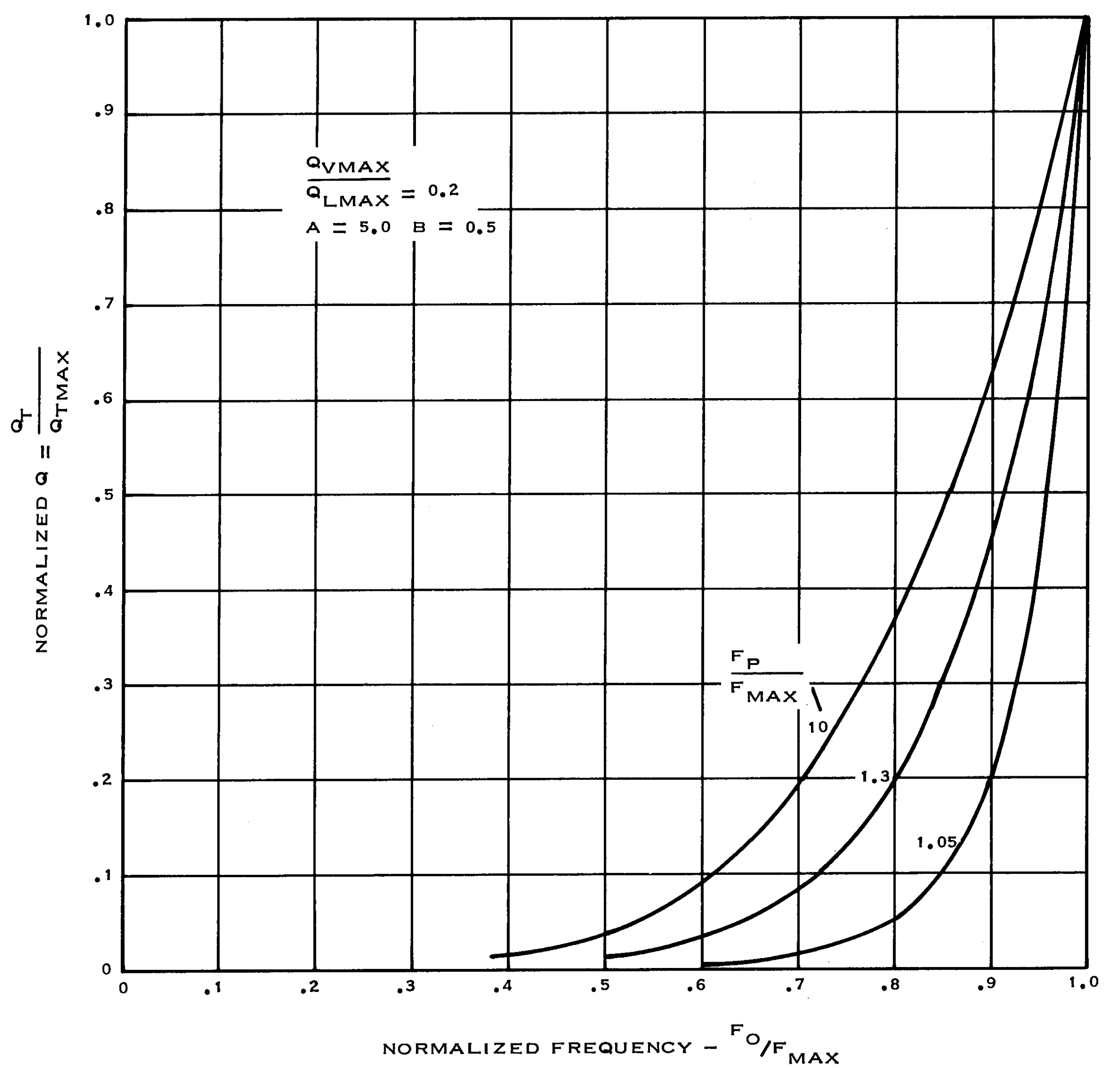

Figure 1-22. Normalized Q versus normalized frequency for lumped inductor.

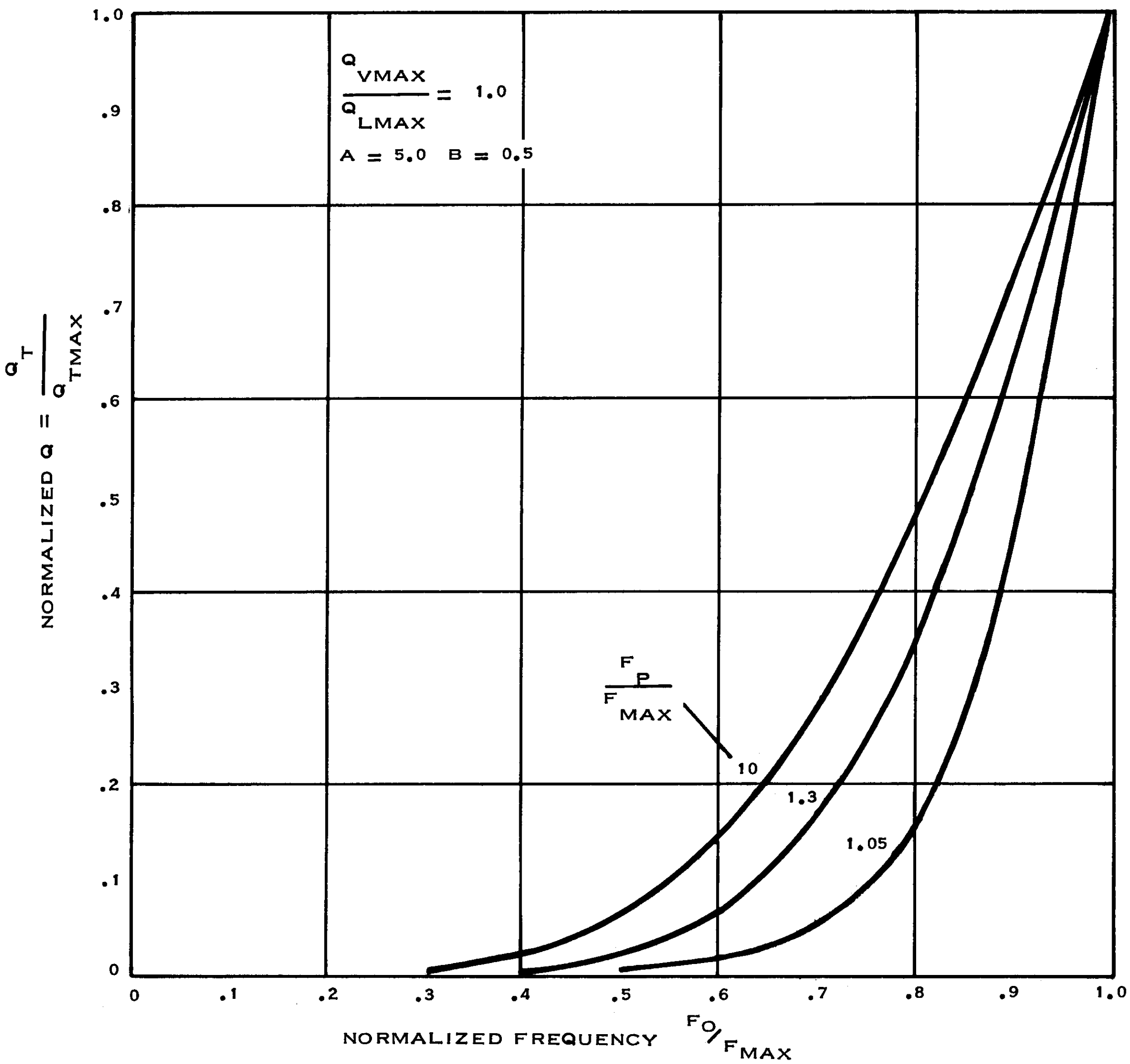

Figure 1-23. Normalized Q versus normalized frequency for lumped inductor.

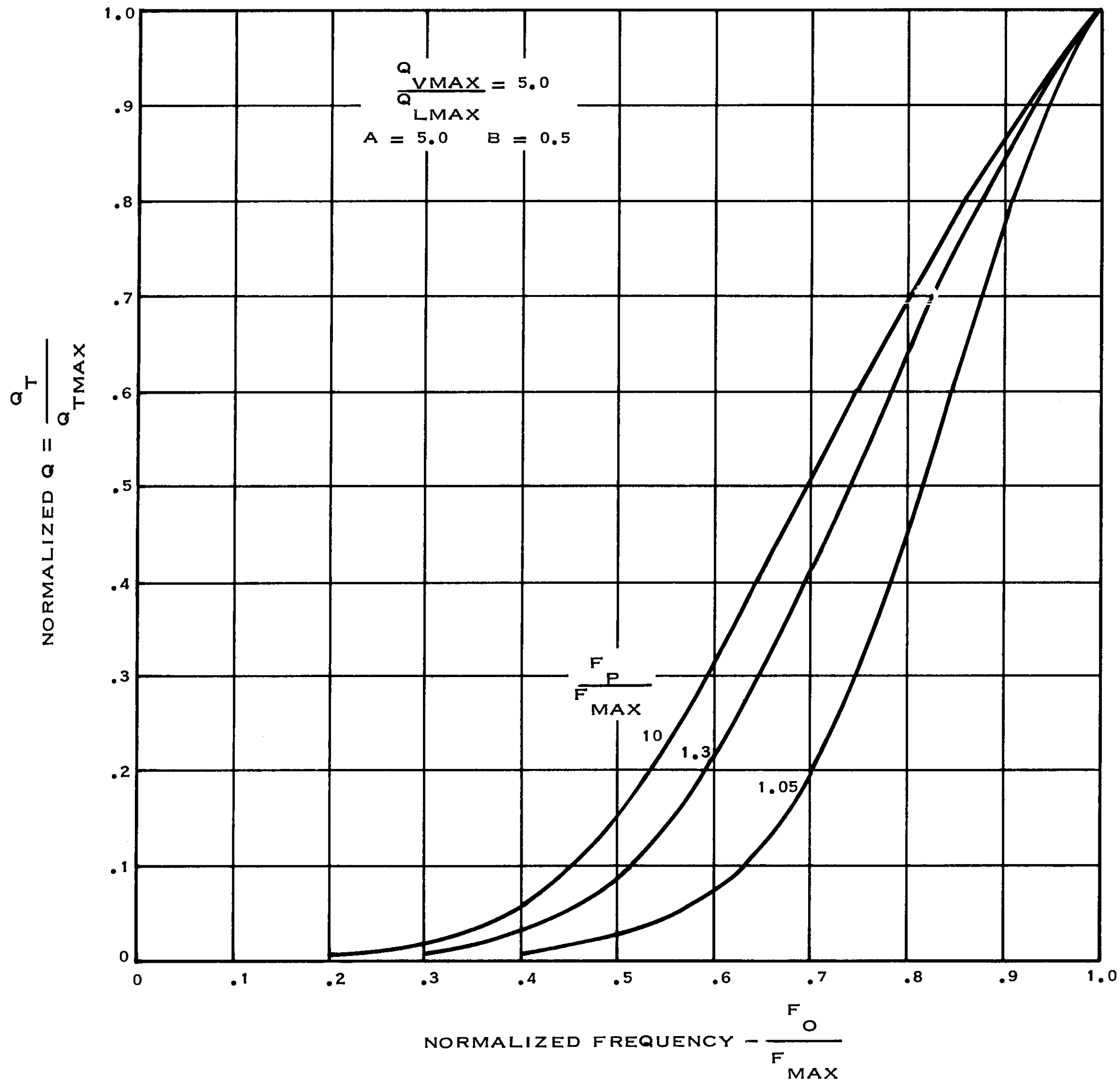

Figure 1-24. Normalized Q versus normalized frequency for lumped inductor.

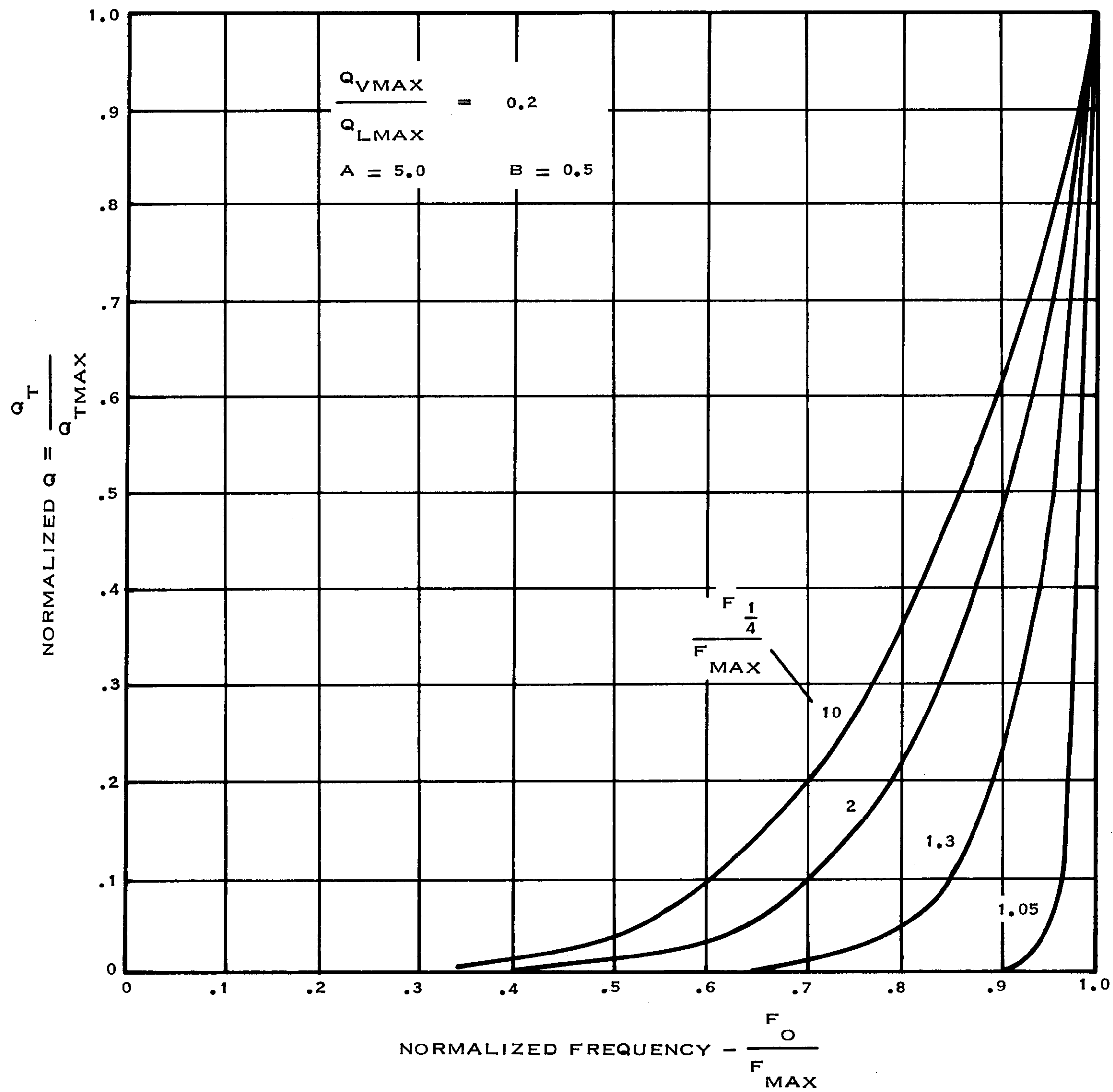

Figure 1-25. Normalized Q versus normalized frequency for transmission line.

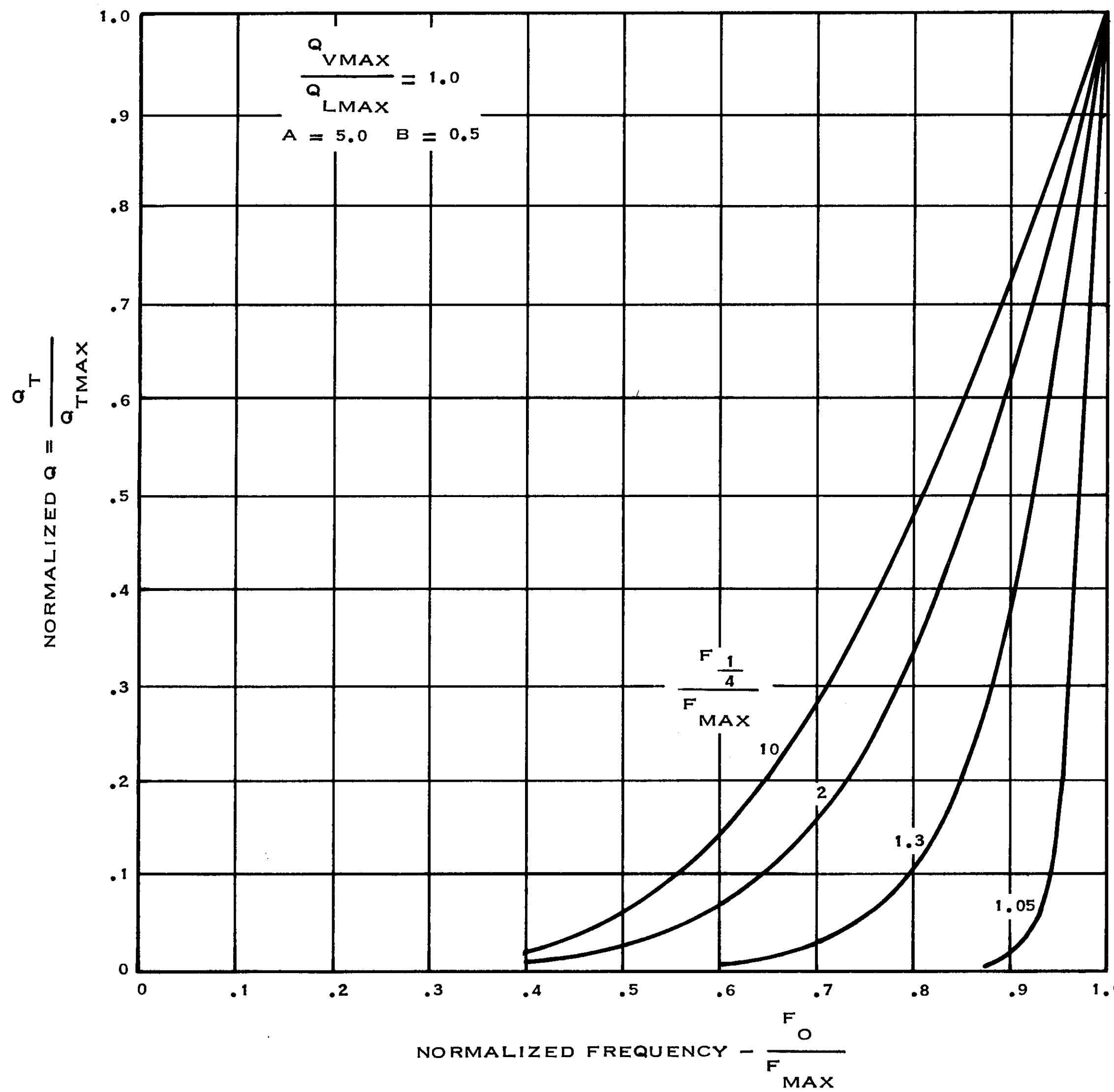

Figure 1-26. Normalized Q versus normalized frequency for transmission line.

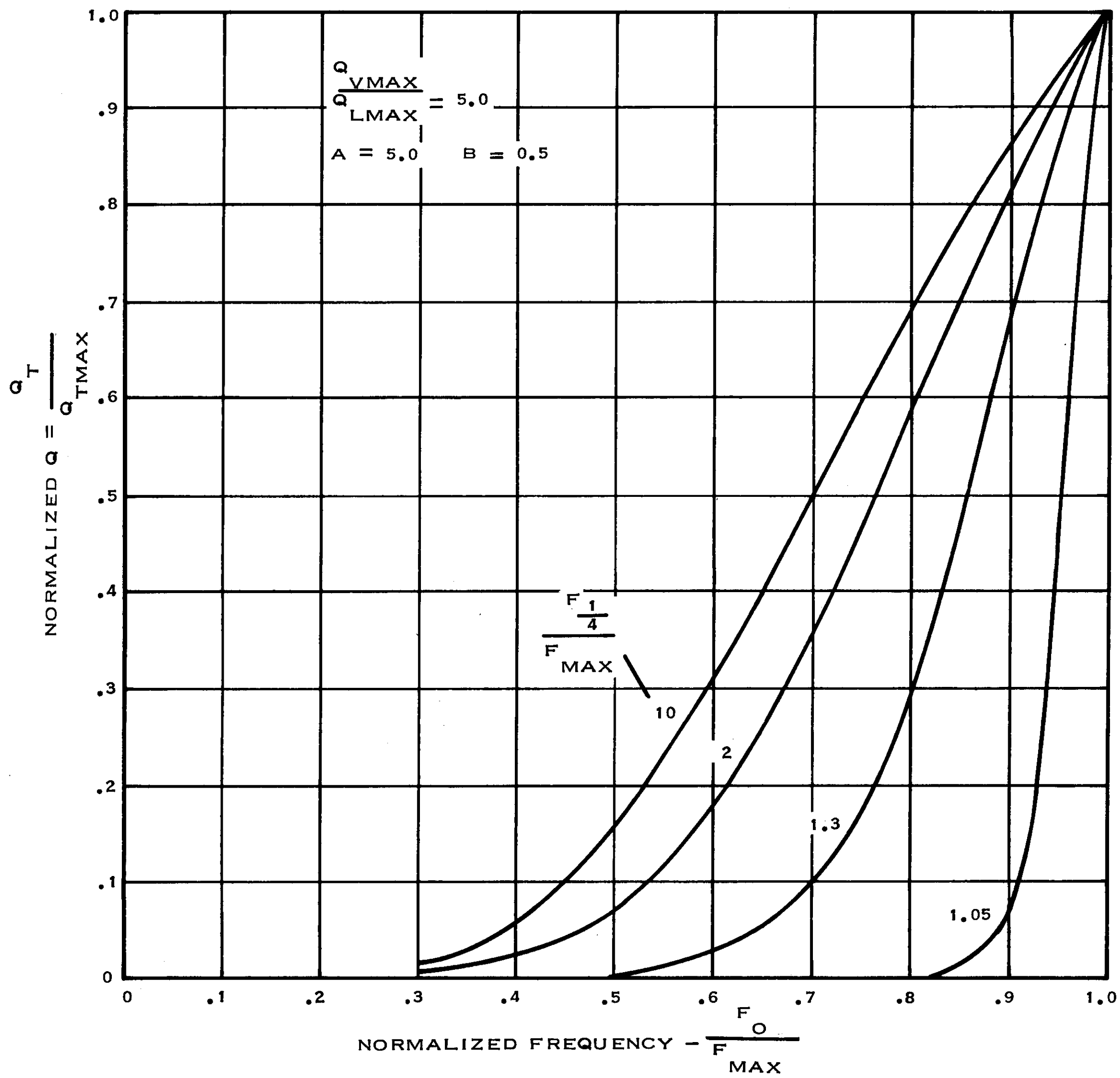

Figure 1-27. Normalized Q versus normalized frequency for transmission line.

These curves dramatically illustrate the large percentage Q-change for resonators employing high Q-varactors while figures 1-15 and 1-19 illustrate the improved Q-variation when low Q-varactors are used. This illustrates the trade off to be made and also the irony of the situation; if a high Q at F_{MAX} is desired then high quality varactors must be used but the Q-change as the resonator is tuned is very large; on the other hand, the low Q varactor has a much more favorable Q-frequency characteristic but its Q at F_{MAX} is much lower.

An illustrative example is included to outline the basic design approach and to demonstrate the close agreement between measured data and the predicted behavior demonstrated by the graphs in figures 1-25 through 1-27.

Let it be required to tune a transmission line resonator having a quarter-wave frequency of 800 mhz from 300 mhz to 400 mhz. It is further specified that a coaxial resonator shall be a employed having Z_O = 100 ohms. The length of the resonator is determined as follows:

$$L = \frac{3.0 \times 10^8}{8 \times 10^8} = 0.375 \text{ cm} = 37.5 \text{ cm}$$

$$\therefore \quad L = \frac{37.5 \text{ cm}}{4} \times \frac{1 \text{ in}}{2.54 \text{ cm}} = 3.69 \text{ in}$$

The required capacitive reactance to achieve resonance at 400 mhz is found from

$$X_{C_{400}} = Z_O \, \text{TAN} \beta \ell = 100 \text{ ohms}$$

$$C_{400} = \frac{1}{2\pi F X_{C_{400}}} = 3.98 \text{ pF.}$$

Since it is further assumed that there are no stray reactances present, a Motorola 1N5461A[1] varactor will resonate at approximately 17.0 Vdc. The varactor Q at 17.0 Vdc bias and 400 mhz is found to be 750.

The ratio $\frac{Q_{V\ MAX}}{Q_{L\ MAX}}$ is specified as unity. Coaxial dimensions follow from

$$Q_{L\ MAX} = 12.78 \, Z_O \sqrt{F_{1/4}} \left(\frac{R_1 R_2}{R_1 + R_2} \right)$$

where

$F_{1/4}$ = 800 mhz, the quarter-wave frequency

R_1 = center conductor radius

R_2 = outer conductor radius

Therefore

$$12.78Z_O\sqrt{800}\left(\frac{R_1R_2}{R_1+R_2}\right) = 750\left(\frac{800}{400}\right)^{1/2}$$

$$\frac{R_2}{R_1} = 5.30$$

$$\frac{R_1R_2}{R_1+R_2} = 0.2938$$

from which

$$R_1 = 0.03498 \text{ inches}$$

$$R_2 = 0.1852 \text{ inches}$$

Total tuning capacitance at 300 mhz is found from

$$Z_O \text{ TAN}\left(\frac{300}{800}\right)90° = 66.8 \text{ ohms}$$

$$C_{300} = 7.96 \text{ Pf}$$

and, from available data,

$$V_{T300} = 2.0 \text{ volts}$$

and the varactor Q is approximately 116.8 at 2.0 volts bias and 300 mhz. Then, from the graph of K^{-1} versus θ_O, figure 1-20,

$$\frac{Q_V}{K^{-1}} = \frac{750}{.778} = 964$$

$$\frac{1}{Q_T} = \frac{1}{964} + \frac{1}{750} = .001038$$

$$Q_{T\ MAX} = 422$$

As the resonator is tuned lower than F_{MAX}, the variation of Q_T from Q_{TMAX} is found from

$$Z_O \text{ TAN } \beta \ell = 100 \text{ TAN } 42.2° \text{ at } F_O = 375 \text{ mhz.}$$

$$C_T = \frac{1}{2\pi F_O X_C} = 4.68 \text{ pF.}$$

From diode curves,

$$V_T = 12.0 \text{ volts}$$

and varactor Q = 507. For $\theta_O = 42.2°$, $K^{-1} = .805$ and varactor Q is

$$Q_V = \frac{507}{.805} = 629$$

$$Q_L = 750\left(\frac{375}{400}\right)^{1/2} = 741$$

$$\frac{1}{Q_T} = \frac{1}{629} + \frac{1}{741}$$

$$QT = 340$$

$$\frac{Q_T}{Q_{T\ MAX}} = .805$$

Ratios of Q_T to $Q_{T\ MAX}$ are similarly computed for various other values of F_O and are presented in table 1-3.

TABLE 1-3. RATIO COMPUTATIONS OF Q_T TO $Q_{T\ MAX}$.

F_O	θ_O	K^{-1}	$Q_T/Q_{T\ MAX}$
400 mhz	45°	.778	1.0
375	42.2°	.805	.805
350	39.4°	.833	.630
325	36.5°	.858	.409
300	33.75°	.880	.261

These data are plotted on the following curve, Figure 1-28, of $Q_T/Q_{T\ MAX}$ versus F_O/F_{MAX} and indicate that, while Q-degradation from $Q_{T\ MAX}$ is very severe, the predicted curve is somewhat more pessimistic than the measured data would indicate.

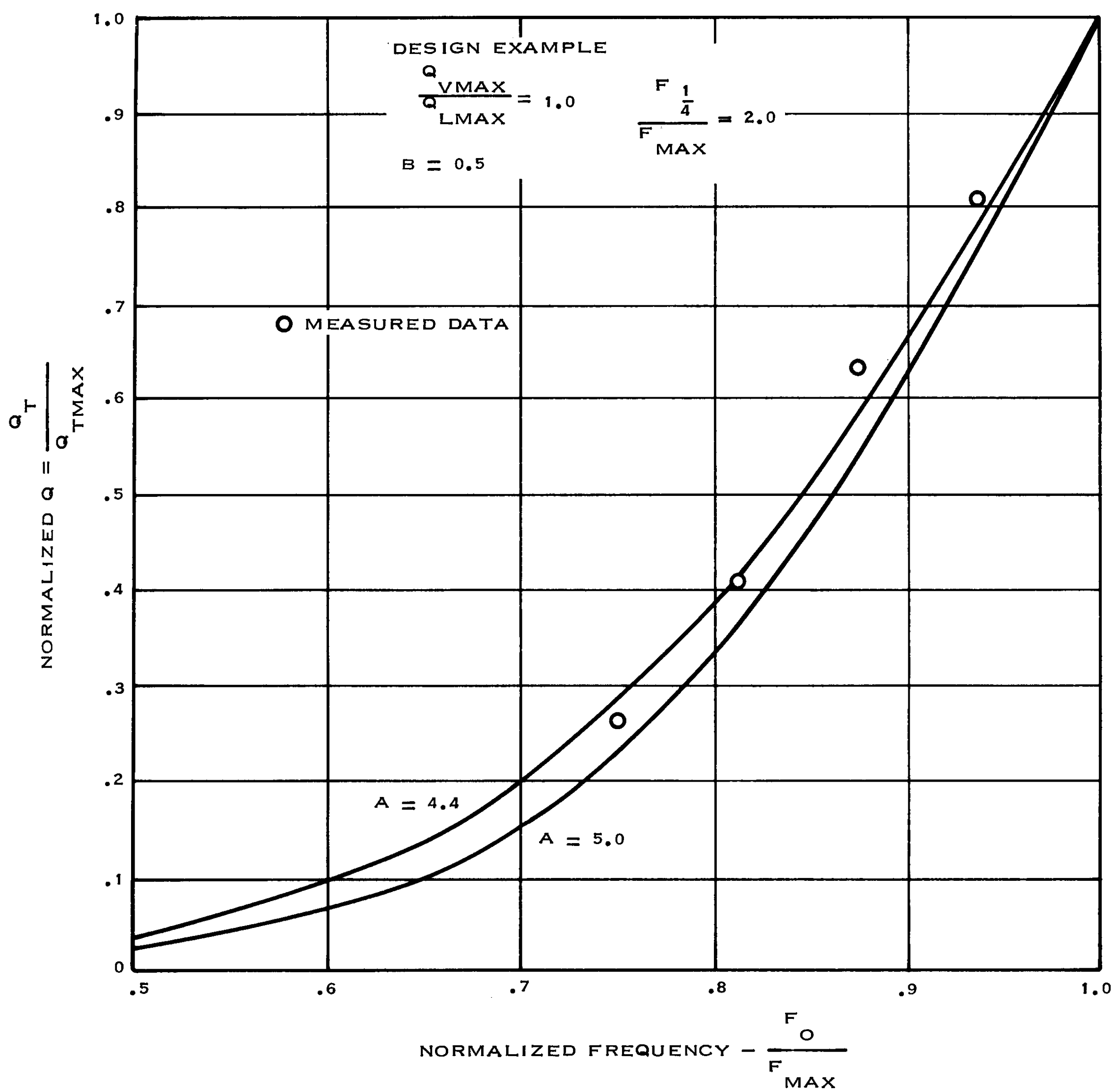

Figure 1-28. Normalized Q versus normalized frequency for transmission line.

3.1.2.1.5 Diode-Switched Capacitor Matrix Tuning

Economical component miniaturization now makes it possible to consider a uhf filter design where the resonators are tuned by switching in and out an array of capacitors. In past designs, it was considered too costly and volume consuming to consider a resonator tuned by switching fixed capacitors, but with the improved thin film and epitaxial technology available today it is quite possible to conceive of a miniature array of MOS capacitors tuning a uhf filter.

Because of the good potential for future development with this concept, considerable project time has been spent conceptualizing a design approach. Several approaches to the problem were conceived but a multitude of design and analysis considerations resulted in the selection of the circuit shown in figure 1-29.

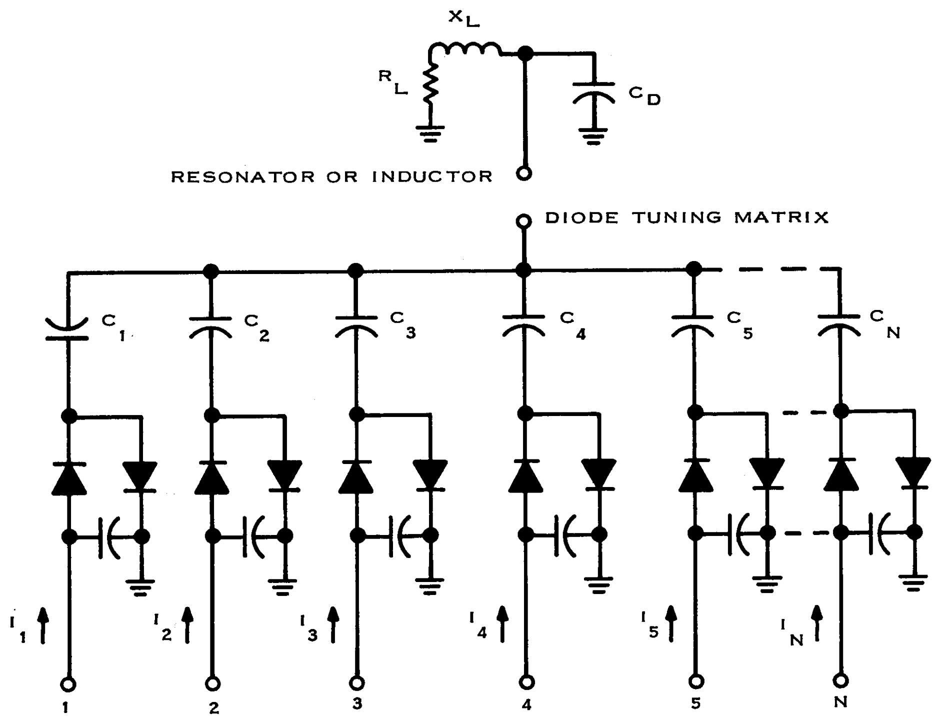

Figure 1-29. Resonator circuit for diode matrix tuning.

The following choices for the equivalent circuits of each capacitor branch were made on the basis of maintaining a minimum of complexity while obtaining adequate accuracy.

In the ON condition (figure 1-30) each capacitor branch can be represented as:

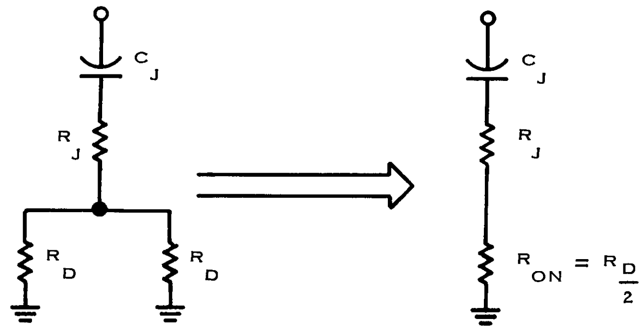

Figure 1-30. Equivalent circuit for capacitor branch in the on state.

In the OFF condition (figure 1-31) each capacitor branch can be represented as:

Figure 1-31. Equivalent circuit for a capacitor branch in the off state.

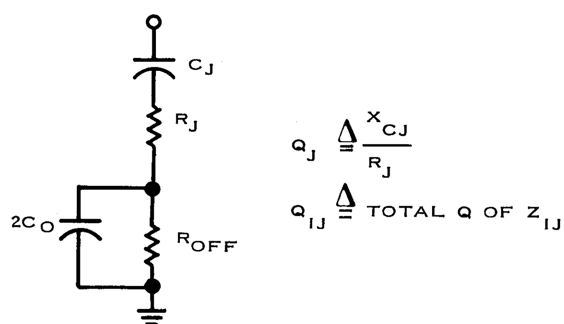

Let Y_{IJ} represent each capacitor circuit (figure 1-32) where I = 1 or 0 for the on-off conditions respectively and J = 1, . . . n represent the Jth capacitor circuit.

Figure 1-32. Switching schematic.

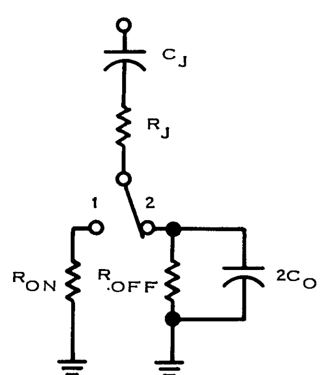

An example is shown in figure 1-33.

The tuning scheme can be analyzed on the basis of previous sections with only slight modifications to account for the fact that the tuning is not continuous. The admittance, Y_T, of the diode tuning can be obtained by summing up all of the branch admittances as

$$Y_T = \sum_{J=1}^{N} Y_J \text{ (STATE I)}$$

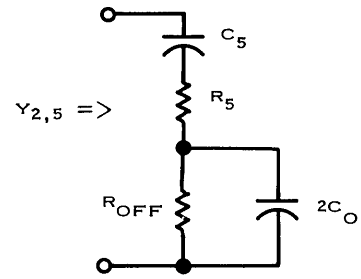

Figure 1-33. Schematic notation.

where I = 0 or 1 for diode J off or on and T is used to represent the channel designation T = 1, ... 2^N

The variables in the equivalent circuit are defined as follows:

R_L = loss resistor associated with X_L.

X_L = inductance reactance for net resonator inductance.

C_D = stray capacity.

C_J = capacity of the Jth branch capacitor.

R_J = loss resistor of the Jth capacitor obtained from Q measurements.

R_D = diode ac resistance in the on condition.

R_{OFF} = parallel combination of the reverse biased ac resistance of each diode.

C_O = reverse bias capacity of each diode.

To determine a tuning code and to keep a record of channel information it is necessary to develop a tuning progression. One example of this would be to consider a binary code progressing from the smallest capacity combination in order of increasing magnitude. That is,

$$Y_{R+1} > Y_R$$

Table 1-7 represents an example of the type of coding possible in a simple case.

The exact nature of the tuning code selected will be explained in the programming approach to this problem.

TABLE 1-4. TUNING PROGRESSION.

CHANNEL NO	ADMITTANCE Y_T	BINARY CODE
1	$Y_{0N} + \ldots\ Y_{03} + Y_{02} + Y_{01}$	n 00000
2	$\ldots + Y_{02} + Y_{11}$	n 00001
3	$\ldots + Y_{12} + Y_{01}$	n 00010
4	$\ldots + Y_{12} + Y_{11}$	n 00011
5	$\ldots + Y_{02} + Y_{01}$	n 00100
6		n 00101
.		
.		
.		
.		
2^n	$Y_{1N} + \ldots\ Y_{13} + Y_{12} + Y_{11}$	n 11111

The compact notation for the array of capacitor branch admittances is given for simplicity of notation and to make the possible combinations more visible for analysis. For example the Y matrix is:

$$\left((Y_{IJ}) = \begin{matrix} Y_{01} & Y_{02} & Y_{03} & \cdots & Y_{0N} \\ Y_{11} & Y_{12} & Y_{13} & \cdots & Y_{1N} \end{matrix} \right)$$

The primary task of designing the diode matrix is to develop a criteria for determining the number of filter channel steps and the center frequencies associated with each channel. Figure 1-34 represents the filter passband stepping across the tuning range for a typical approach to the problem.

The tuning matrix of each resonator must tune the resonator to the center frequency specified by the filter bandwidth. The filter need not be stepped according to the bandwidth of each resonator but rather to the bandwidth of the complete filter. The criteria used to determine the filter channel frequencies was selected to give a minimum specified tuning "notch." This is illustrated in figure 1-35. The amount of filter bandpass overlap determines the amount of notching present in the filter loss variation curve.

For example, the maximum insertion loss over the band is determined by $L_O + \alpha_R$. The loss due to α_R is caused by the fact that the filter passbands have incomplete overlap causing a specific number of α_R notches over the band. The degree of overlap and hence the value of α_R directly determines the minimum number of filter channels required. A trade off exists between the increased insertion loss caused by α_R and the minimum number of filter channels. Practical values of α_R will range between 0.2 and 3 db.

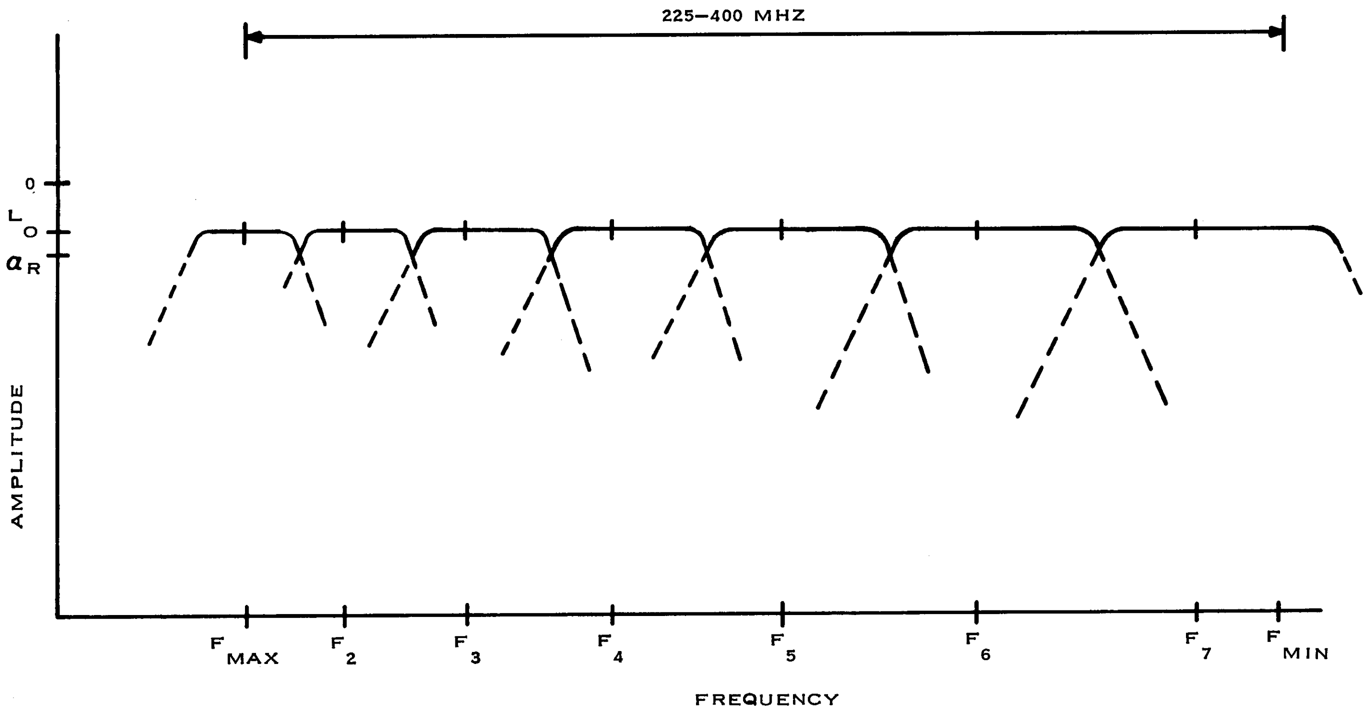

Figure 1-34. Filter channel spacing.

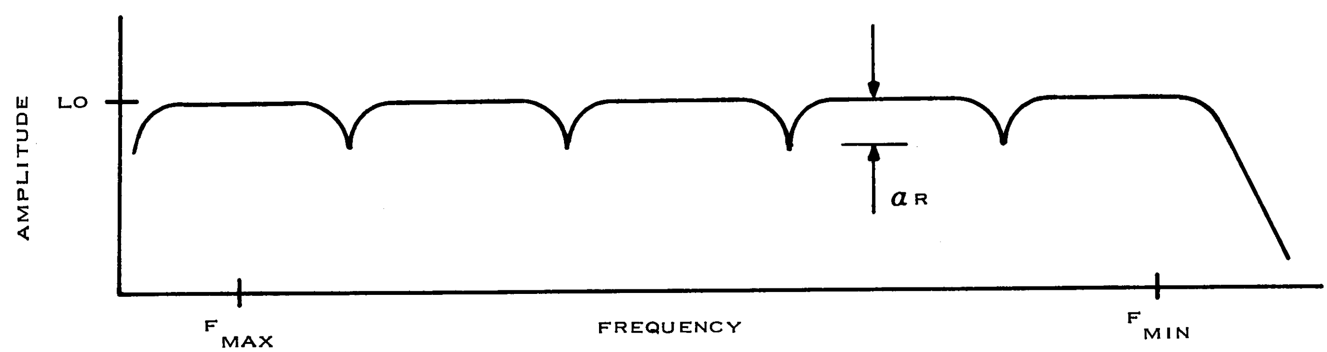

Figure 1-35. Filter loss variation.

Another complication to the problem of specifying filter channels is caused by the changing Q_U of the circuit elements. The design program must compensate for this effect which generally causes the design to have at least one more filter channel than would otherwise be needed for a given minimum stopband requirement.

Several circuit functions and problems were discussed before an attempt was made to synthesize the network. A few of the most obvious problems will now be discussed.

a. The total Q-variation as the diode matrix is tuned is a very unpredictable quantity because the Q at each filter channel depends on:
   1. The Q of X_L.
   2. The Q of each capacitor switched on.
   3. The Q of each diode switched off.
   4. The diode on current and ac resistance.

   To solve this problem it was decided to adjust the diode current of each branch so that it is possible to set the Q of any capacitor branch. The adjustment allows the diode currents to be tailored to produce any desired Q versus frequency response from the diode matrix. To specify any Q-frequency shape, the diode currents must be changed as frequency is changed; but this generally complicates the design to such a degree that the designer is willing to accept more restrictions on the specified Q shape. Generally, it will be possible to obtain a limited control by making each diode current different but not changing the on current as frequency is tuned. One possible combination of diode currents is to set the Q's of all capacitors in the on condition equal at the same frequency. This condition would make the diode matrix Q-linear with frequency A = 1.0, and would also minimize the required tuning current.
b. The filter bandwidth is a function of the filter class (Chebischev, Butterworth, minimum-loss . . .), the number of resonators, and the unloaded Q of each resonator. If the resonator Q changes with frequency the design must compensate for the changing filter bandwidth. This can be done by approximating the filter bandwidth with the tailored Q-function and then iterating until a desired degree of accuracy is obtained.
c. The tuning code for selection of the on-off state for each capacitor must be obtained in such a manner that input coding from a bcd tuning code can be interfaced with the diode matrix by as simple a conversion as is practical.
d. The reverse capacity, C_O, adds significantly to the total tuning capacity of the matrix. The addition of C_O in the equivalent circuit was necessary to account for this effect. C_O should be made as small as possible to reduce this effect. The most promising reduction of C_O is with the use of pin diodes.
e. The tuning accuracy of the matrix affects the value of α_R because of the frequency offset on the nose shape of the filter A small tuning tolerance requires more capacitors for a given filter and a large tolerance increases α_R. A rule of thumb in this case might be to assign the tuning frequency error a value of 5 to 10 percent of the filter bandwidth.
f. Obviously, the maximum number of capacitors in any matrix will be no greater than the number of filter bandwidths. The optimum number of capacitors required generally is not calculable but experience with the design program will give much insight for a method to determine this optimum.

A computer program has been written to synthesize a diode matrix tuned filter. The program approach as well as a design example will be presented on the following filter design.

Frequency range:	Uhf band, 225-400 MHz
Filter characteristic:	Minimum-loss, number of resonator = 3
Filter stopband:	80 db down @ 310 MHz when tuned to 400 MHz (45 MHz if)
Filter bandwidth:	BW (80 db) = 206 MHz at 400 MHz
Filter noise figure:	3.3 db (L_O = 3.3 dB)
Notch loss:	α_R = 1 dB BW (1 dB) = 18 MHz at 225 MHz

The number of filter channels required can be calculated given the minimum total Q, the minimum Q of the lumped inductor, and the 1 db bandwidth at f_{min} (225 mhz). It is desired, however, to normalize the total C to 1 pf at f_{max} (400 mhz). Therefore, the 1 db bandwidth at f_{max} must be calculated and the channels calculated down in frequency from f_{max}. Next, it is necessary to know what capacitance, C, is required to resonate the lumped inductor at each of the channel frequencies. This is calculated remembering that 1 pf must be resonated at f_{max}. Once the desired C values are known, it must be decided how many diode-switched capacitors are needed and how the values are to be assigned.

Once the number of capacitors and the selection at each frequency is determined, the mean square error of the resonant frequencies with respect to the channel frequencies is minimized by adjusting the C values. N capacitors can cover at most 2^N filter channels if it were possible to use each state of the diode-switched matrix. (State is defined as a particular combination of capacitors switched in.) In general, for a nonlinear function it is not possible to use all states and more than N capacitors are required. The exact number of capacitors depend on the closeness of fit desired. However, N such that $2^N \geq$ the number of filter channels is a good starting trial value.

A frequency tolerance can also be specified as the maximum error allowable between a channel frequency and the frequency at which the lumped L and C matrix resonate. Once the number of capacitors is determined, initial values must be established. The method chosen is to divide the frequency band at the geometric mean frequency and assign the minimum value of C in each band minus C_d, to two different capacitors. Thus, these two capacitors are band switched and are never both in. The capacitance change needed to get from f_{max} to the next lowest channel is the minimum change needed and a capacitor is set to this value. The capacitance change from f_{max} to two channels lower is used for the fourth C value. The largest total capacitance change occurs from f_{min} to the geometric mean frequency. If 1/2, 1/4, 1/8, 1/16 ..... $1/2^{N-4}$ of the difference for the remaining values of C is taken, it will approach C at f_{min} in a binary fashion as N gets larger.

Now that values have been calculated for the capacitors to be switched, it must be decided which ones to switch in at each frequency. One capacitor can be selected on the basis of frequency since that is how its value is originally chosen. The difference between the desired capacitance and the frequency selected capacitor is now compared to the remaining values which are in sorted order, largest to smallest. Any value less than the difference is selected and the difference is decreased by this amount. This process continues to the smallest capacitor value which is selected or not selected on the basis of which provides the smallest error from the desired C. This selection is done at all channel frequencies. This is not necessarily an optimum way of assigning initial C values or switching states at each frequency channel: however, it does provide a good intuitive approach. Once initial values and states have been assigned, optimum C values for the specified states are calculated using the Fletcher-Powell algorithm for minimization. The particular routine used has been developed by R. W. Carroll at Collins. Once the C values are optimized, a check is made to see if the frequency error criterion is met at each frequency; if it is, the problem is solved. If not, another capacitor is added and the process repeated.

When the frequency channels were selected, they were based on a specified Q-distribution. The capacitors that are switched off have a very high Q and can be ignored in determining the overall Q. However, the capacitors that are switched on have an ac on resistance, R_D, that affects the Q. Since the C values are different, R_D affects the Q of each capacitor differently. However, R_D is a function of the selection current. Thus, a selection current can be calculated such that it will degrade each Q by the same amount. In this way the total Q is the same as the Q of each capacitor and is predictable. A Q-degradation factor is input

data to the program; 0.9 for example, states that the original capacitor Q is degraded to 0.9 Q by R_D. The program calculates R_D and the selection current, I_{on}, necessary to degrade the Q.

The example filter problem was run and figures 1-36 and 1-37 illustrate the results.

DIODE SWITCHED CAPACITOR TUNED LUMPED INDUCTOR

FMIN	FMAX	BW	QTMIN	QLMIN	Q-DEGRADE	FTOL	NCS
225.00	400.00	18.00	100.00	200.00	.90	2.00	6

NUMBER OF CAPACITORS REQUIRED = 6

C 1 = .750000 C 2 = 1.800413 C 3 = .700351 C 4 = .350176 C 5 = .245076 C 6 = .113422

FREQUENCY	C DESIRED	C ERROR	C 1	2	3	4	5	6
223.567	3.2011	-.0132	0	1	1	1	0	1
241.807	2.7364	-.0227	0	1	0	1	1	1
260.401	2.3596	-.0494	0	1	0	0	1	1
279.343	2.0504	.0000	0	1	0	0	0	0
298.627	1.7942	-.0196	1	0	1	0	0	1
318.247	1.5798	.0027	1	0	0	1	0	1
338.199	1.3989	.0487	1	0	0	1	0	0
358.477	1.2451	.0000	1	0	0	0	1	0
379.079	1.1134	.0000	1	0	0	0	0	1
400.000	1.0000	.0000	1	0	0	0	0	0

Figure 1-36. Program input data and starting values.

CH FREQ	ACT FREQ	TOTAL C-PF	EQUIV L-UH	QC	QL	QT	1	2	3	4	5	6	7
223.567	223.345	3.207	.158	200.	199.	99.9	0	1	1	1	0	0	1
241.807	240.795	2.759	.158	216.	207.	106.3	0	1	0	1	1	0	1
260.401	259.866	2.369	.158	234.	215.	112.2	0	1	0	0	1	0	1
279.343	280.734	2.030	.158	252.	223.	117.7	0	1	0	0	0	0	0
298.627	298.884	1.791	.158	269.	230.	123.9	1	0	1	0	0	0	1
318.247	318.291	1.579	.158	287.	238.	130.0	1	0	0	1	0	1	0
338.199	338.784	1.394	.158	306.	245.	135.9	1	0	0	1	0	0	0
358.477	359.455	1.238	.158	325.	252.	141.7	1	0	0	0	1	0	0
379.079	379.903	1.109	.158	345.	260.	147.8	1	0	0	0	0	0	1
400.000	399.226	1.004	.158	367.	267.	154.8	1	0	0	0	0	0	0

N	C-PF	RD-OHMS	ION-MA
1	.64167	.625	41.58
2	1.66831	.430	60.48
3	.70192	1.022	25.45
4	.40922	1.753	14.84
5	.25297	2.431	10.69
6	.20349	1.737	14.97
7	.12190	5.883	4.42

MINIMUM Q OF CAPACITORS = 222.22

Figure 1-37. Computer solution to example filter problem.

3.1.2.2 Switched Bandpass Filters

The switching of bandpass filters as a means of preselection is a natural progression from the incremental tuning by means of switched capacitors. Several benefits may be derived from such a technique. Each pole of the filter will exhibit higher Q_U and will not be Q limited due to series diode resistance losses. In a filter having many resonant elements, the total number of diodes, and consequently the dissipation, is less. One prime disadvantage is that if one assumes the inductive element comprises the majority of the volume, and if many bandpass filters are required to cover the 225 to 400 mhz range, then the switched bandpass filter technique is likely to consume more volume. The analysis of the switched bandpass filter technique is greatly influenced by the constraints placed on the filter design. The filter design desired for this analysis is the one which offers the least volume for a given selectivity requirement, in particular, the image rejection requirement. Such a filter design has been analyzed and presented in section 3.3.1 and the results will be used here. The physical volume of a spiral coil is related to its Q_U by the expression,

$$V = CQ_U^2$$

where C is a proportionality constant, and the exponent, 2, is referred to as the law of variation, p. From section 3.3.1, it is stated that the optimum number of resonators, N_V, required to meet a specified attenuation specification, α_R, and insertion loss, L_O, is

$$N_V = \frac{p}{p+1} \cdot \frac{\alpha_R + 6 + L_O}{8.686}$$

To implement these results, it is necessary to assume some practical requirements. Consider a preselector having 4 db insertion loss and requiring 60 db of image rejection. Also, assume an if frequency of 45 mhz. Using the preceding equation, it is found that six resonators are sufficient to do the job. By means of minimum-loss filter design curves, it is found that only three bandpass filters designed at center frequencies of 255, 315, and 375 mhz are necessary to tune the entire uhf military band with less than 2 db degradation at the band edge overlap. In addition to providing the necessary information to determine the number of resonators, section 3.3.1 also provides the expression,

$$L_O Q_U \frac{BW}{F_O} \cong \frac{pE^{\frac{p+1}{}}}{2(p+1)} (\alpha_R + 6)$$

which enables the determination of the required resonator Q_U. For the filters having center frequencies of 255, 315, and 375 mhz, the required Q_U's are 27.5, 34.5, and 44, respectively. These Q's are fairly consistent with what can be obtained in microminiature lumped inductors as will be seen in section 3.2.2.

In examining this approach, it is evident that the low number of filters required is due to the fact that a 6-resonator filter has a fairly good shape factor. In this example, the BW_{60}/BW_2 ratio is slightly greater than 3.4. The use of this preselection technique requires that the succeeding active networks be capable of withstanding the equipment's specified undesired signal levels within its nose bandwidth. Also, certain close-in spurious responses may not be aided appreciably by preselection. For example, the 1/2-if spurious lies only 22.5 mhz away from the desired frequency and is not attenuated by the filter. Fortunately, as can be seen from the spurious table, table 1-3 in the Interim Development Report, this response as measured in a JFET mixer is 60 db down, comparable to the image requirement.

3.1.2.3 Parametric Up-Converter Technique

A review of the inductive elements considered thus far indicates that higher Q can be obtained with increased volume at a given frequency or conversely for a given volume, higher Q can be obtained at higher frequencies. To take advantage of this volume, Q-relationship, one should consider performing the primary filtering at an increased frequency.

To translate to a higher frequency requires some form of mixer. The conventional FET mixer will not suffice because of its decreased gain capability and increased noise figure in this application. A loss mixer such as the diode ring in the input circuits cannot be used in that its loss added to the loss of the output frequency filter plus the second stage noise figure would not yield an adequate noise figure. It becomes increasingly evident that a low noise mixer having gain such as the parametric up-converter is the only way that the translation to the high if can be accomplished and still meet the system requirements.

Parametric up-converters have been extensively used in designs whose input frequencies range from hf through X-band. The basis of the parametric device is the nonlinear or time-varying reactance. The device holds the promise for low noise performance because reactance implies no thermal noise such as exhibited by resistance. The two primary parametric amplifiers that may be considered for a uhf translator are the usb up-converter and the negative-resistance amplifier (lsb). Either would enable the preselection to be carried out at a higher frequency, and the advantages and disadvantages of each will be discussed. The theory of parametric devices shall be held to a minimum and only those areas of concern pertinent to the uhf preselector design and consequent trade off analyses will be presented. If further knowledge of the subject is desired, the reader is referred to the reference by Blackwell and Kotzebue.[2]

Almost every discussion of parametric devices can be initiated by introducing the Manley-Rowe power relationships.[3] These establish the definitions of the parametric usb up-converter and negative resistance amplifier as well as provide insight into the maximum gains available. Consider the model in figure 1-38. Each branch is connected across a

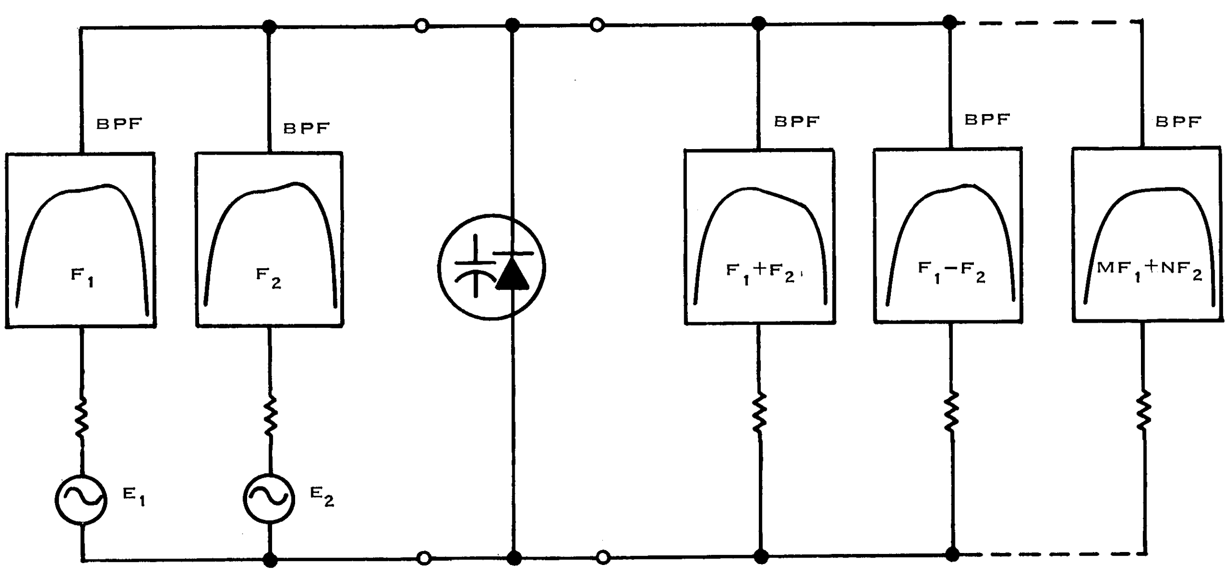

Figure 1-38. Manley-Rowe model.

nonlinear capacitance. Each left-hand branch consists of a bandpass filter and voltage generator. Each right-hand branch consists of a bandpass filter and load resistance such that power is dissipated only at its prescribed frequency, which is generated by the nonlinear capacitance. The Manley-Rowe relationship may be stated as

$$\sum_{M=0}^{\infty} \sum_{N=-\infty}^{\infty} \frac{M P_{M,N}}{MF_1 + NF_2} = 0$$

and

$$\sum_{N=0}^{\infty} \sum_{N=-\infty}^{\infty} \frac{N P_{M,N}}{MF_1 + NF_2} = 0$$

where $P_{M,N}$ is the power flow into the reactance at MF_1 and NF_2. Consider now the parametric up-converter where $F_{SIG} = F_1$, $F_3 = F_1 + F_2$. The preceding equations state that:

$$\frac{P_1}{F_1} + \frac{P_3}{F_3} = 0 \text{ and } \frac{P_2}{F_2} + \frac{P_3}{F_3} = 0$$

Power is being supplied at F_1 and F_2 to the reactance and absorbed by the load at F_3. The gain of this configuration is P_{OUT}/P_{SIG}, which is

$$\frac{P_{OUT}}{P_{SIG}} = \frac{P_3}{P_1} = \frac{F_3}{F_1}$$

This states that the maximum gain available from the up-converter is the ratio of output to input frequency.

The negative-resistance amplifier can also be considered using the same simple model. Let $F_1 = F_{SIG}$ and $F_3 = F_1 + F_2 = F_{PUMP}$. Now,

$$F_{OUT} = F_2$$

Power is being supplied at $F_1 + F_2$, therefore P_3 is positive; consequently, both P_1 and P_2 are negative. This means that the power is being delivered to the source resistance at both F_1 and F_2. If gain is defined as the ratio of power delivered to either source resistance to the power delivered by the source, then the gain can be infinite. This stems from the fact that power can be delivered to the source resistance even if that source is delivering an infinitesimal amount of signal power. Therefore, the negative-resistance amplifier is inherently unstable and requires a circulator for best performance. Conversely, the usb up-converter is a unilateral stable device. Because of this, most of the following discussions will be directed toward the use of the usb up-converter.

It should be remembered that the intention of up-converting to the high if is to simplify the preselection tuning requirement and obtain a favorable volume trade-off. Perhaps the greatest difficulty is obtaining sufficient gain to overcome the second stage noise figure. The upper limit on the output frequency is set by practical considerations such as injection and if filtering requirements. For example, if the if and pump frequencies become too high, it becomes difficult to provide the short circuit termination at the if port to the pump frequency. Also, noise sidebands on the pump signal occurring at the if signal may degrade the overall system noise figure if sufficient if selectivity cannot be provided. In discussing the if selectivity requirement, one must not only consider the pump - if interface, but also consider cross-modulation performance. The parametric up-converter preselection needs to consist only of a 225 to 400 mhz bandpass filter with large rejection at 200 mhz to satisfy spurious requirements. It would be expected that the up-converter would be overloaded by any large undesired signal within this bandpass filter. However, if the up-converter is represented by a linear 4-terminal network, then R_{IN} can be recognized as:

$$Z_{IN} = Z_{11} - \frac{Z_{12}\, Z_{21}}{Z_{22} + Z_T}$$

where Z_{NM} are the effective self-impedance of the nonlinear element and Z_T is the external circuit impedance at the output frequency. This illustrates that the input impedance of the converter is inversely proportional to the load impedance presented to its output. If the up-converter is matched to its antenna when the output is terminated at the center of the if passband, then outside of the if filter passband where the driving point impedance of the filter is drastically different from the midband value, the up-converter will present a very large mismatch to the antenna circuit. Thus, a considerable portion of the undesired signal power will be rejected from the up-converter due to the mismatch. In view of this situation, it can be seen that it is desirable to have an if bandwidth that is no wider than that which can be obtained at uhf using conventional preselection techniques. This places a stringent requirement on the Q_U of the resonator(s) to be used at the if frequency if low losses are maintained. Considerable insight into the problem may be gained by examining the up-converter shown in figure 1-39. The worst-case theoretical maximum gain available is the ratio of output to input frequencies, 3200/400, or 9 db. Because of losses due to imperfect matching, a practical number for this gain is 7 db. The noise figure of the up-converter is chosen to be 2 db and is due primarily to diode and matching losses. It is the purpose of this model to illustrate the Q_U requirements for the if resonator(s). To fully define the problem, it is necessary to establish the selectivity requirements of the if filter. Current state-of-the-art mechanically tuned preselectors utilizing helical resonators are capable of providing 30 db of relative attenuation at a frequency ±2.5 percent away from resonance. To get comparable

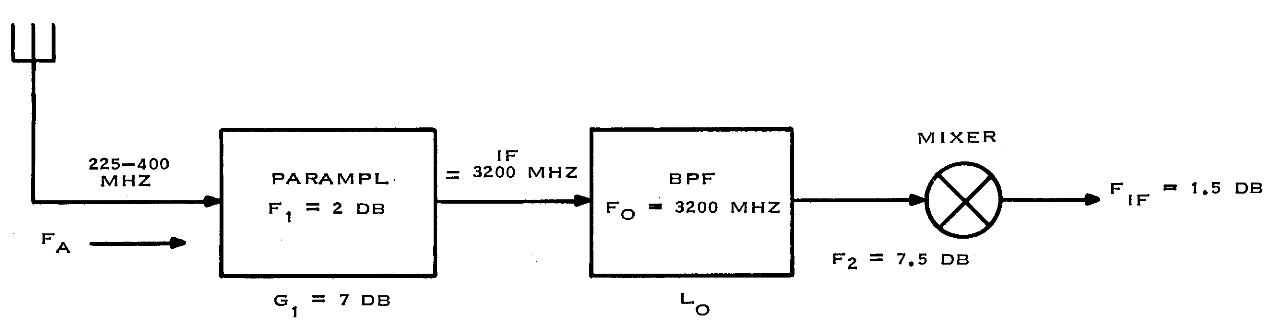

Figure 1-39. Parametric up-converter, block diagram.

performance at an output frequency of 3200 mhz, the filter requirement is 30 db of relative attenuation at a frequency ±.03125 percent from resonance. Using this as the selectivity criteria and employing the well-known Friis relationship as well as Taub's minimum loss filter curves, the curve of figure 1-40 is obtained. The curve shows how the input noise figure of the system in figure 1-39 is affected by the if resonator Q with the selectivity constraint mentioned above. It is immediately apparent that a single resonator is far inferior to a multipole filter even with extremely high Q_U's. Also, it appears that the performance of a 3-pole filter compared to that of the 2-pole filter does not justify the additional volume. For all cases, it should be noted that extremely good Q_U's are required and they cannot be obtained from resonant line structures using microminiature techniques. To obtain Q_U's of the magnitude of those indicated requires the use of resonant cavities. For example, a right circular cylindrical cavity at 3200 mhz operating in the TE-111 mode has a Q_U of approximately 20,000[4] but, unfortunately, its volume is approximately 9 cubic inches. In addition, the absolute frequency stability of such a high Q cavity is poor when temperature and humidity effects are considered. In the literature are applications where significant reductions in the volume of high Q resonant structures have been obtained using TiO_2 dielectric resonators. Harrison[6] shows that at 3200 mhz, a disc of TiO_2, 0.43 inch in diameter by 0.22 inch long, exhibits a Q_U of 8000 when centered axially in a 0.75-inch silver-plated tube. Even though the size reduction is possible, the dielectric resonator suffers from very bad temperature characteristics. Harrison's dielectric resonator exhibited a shift of 0.5 mhz/°F which would be intolerable unless some type of oven were employed. This would tend to reduce or eliminate any advantage with regard to volume over the conventional cavity. In fact, if an oven were employed, one could just as well use a YIG resonator whose Q_U would be in excess of 6400.

The results of the discussion thus far are due to the somewhat low gain capability of the parametric up-converter, because if sufficient gain occurred ahead of the if filter, its loss could be considerably higher and consequently lower Q_U's could be specified. The negative resistance amplifier is capable of producing the desired higher gain and is a relatively well-behaved unilateral amplifier if a circulator is used. Commercial units at S-band are

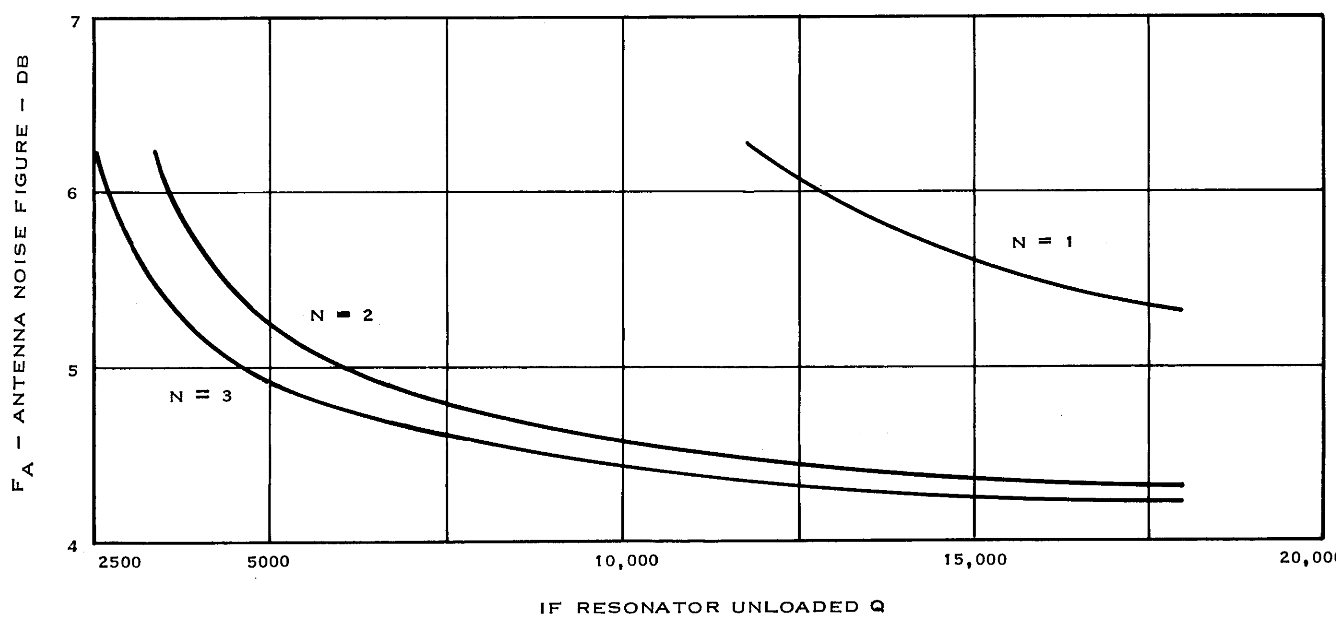

Figure 1-40. System noise figure degradation as a function of if resonator Q for fixed selectivity specification of 30 db at 0.03125 percent ΔF.

available in integrated form that exhibit a 2.5 db noise figure and 17 db gain[7]. This does not provide the ultimate solution at uhf, however, as the radius of the circulator is inversely proportional to frequency and at uhf the circulator becomes large and bulky. Currently available uhf circulators are up to 60 cubic inches in size and weigh 6 to 6.5 pounds.

It is now readily apparent that although up-converting does simplify the tuning problem, the anticipated volume reduction cannot be realized primarily due to the increased resonator Q_U requirement.

3.2 Components for Microminiature UHF Tuner Design

Presented in this section are discussions of both active and passive components for use in tuner designs including amplifiers and lumped inductors. Also presented is an analysis of distortion in varactor tuned circuits.

3.2.1 Active Device

3.2.1.1 Amplifier Circuits

The low Q's exhibited in resonator components for ultraminiature or integrated circuit applications suggests that perhaps rf amplification is required ahead of the mixer to simultaneously satisfy reasonable selectivity and noise figure requirements. The choice of rf amplifier circuits and components can be quite large depending on the requirements of the inductive components. It is evident that inductors having usable Q's at uhf cannot be fabricated in strict monolithic form using silicon substrates. Consequently, if extreme miniaturization is desired as well as usable performance, it is likely that the components will be fabricated on a foreign substrate such as alumina or sapphire. This presents isolation capability such that almost any device or component may be fabricated.

With this in mind, it is beneficial to examine state-of-the-art circuits and devices, and discuss their relative advantages and disadvantages.

Both bipolar and field-effect transistors are available for use as uhf amplifiers. Many articles have been written[8] describing the relative performance advantages of FET's over bipolar transistors such as increased signal handling capability, improved agc characteristic, and higher operating impedance levels; therefore, this area will be treated quite briefly. Shown in table 1-5 is a comparison of dynamic range and noise figure at 400 mhz of several FET and bipolar amplifiers.

TABLE 1-5. DYNAMIC RANGE AND NOISE FIGURE COMPARISON.

CIRCUIT $R_s = R_{sopt}$	DYNAMIC RANGE (db)	NF (db)
2N2857 Common Emitter (I_C = 3MA)	83.8	4.3
2N4417 FET Cascode (I_{DS} = 4MA)	104	3.7
2N5470 Common Base (I_C = 15MA)	105	4.1

Again, the definition of dynamic range is the ratio in db of the undesired signal level required for -10 db cross-modulation distortion to that desired signal level required to produce a 10-db signal-plus-noise to noise ratio for a 50-ohm am receiver with a 3-kilohertz audio bandwidth.

The 2N2857 amplifier is a conventional common emitter amplifier representative of current bipolar designs. The 2N4417 FET cascode circuit is shown in figure 1-41 and represents the latest in uhf FET amplifier design. The application of FET's to uhf design presents several problems that are best solved using the cascode configuration. The FET has a relatively low transconductance compared to bipolar transistor and consequently requires fairly high impedance levels to achieve adequate gain. At uhf, it is essential to keep capacitance levels at a minimum and utilize high Q components to ensure acceptable QX levels. In a common source configuration, it becomes necessary to neutralize the amplifier to maintain stability and realize the lowest noise figure. It is extremely difficult to employ tapped inductors or inductance links for neutralization over even a relatively small frequency range at uhf. Neutralization by means of capacitive bridge techniques eases the frequency problem, but requires the addition of capacitance components which lower the overall QX levels and degrades performance.

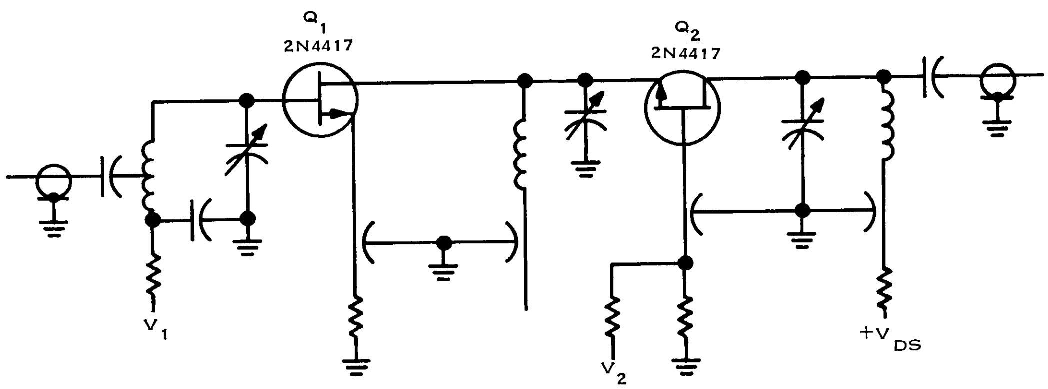

Figure 1-41. Uhf FET cascode circuit.

The best overall solution lies in the utilization of the cascode. The first stage, Q_1, is loaded by the 1/gm resistance presented by the inherently stable common gate stage, Q_2. This configuration suffers a very slight degradation in noise figure due to the fact that the second stage sees a source resistance that is far removed from optimum with regard to its noise performance; however, this degradation is essentially negligible. The optimum source resistance with regard to noise performance for the cascode is approximately 1000 ohms, nearly a power match.

An alternate solution to the neutralization problem would be the use of a common gate circuit. This configuration is inherently stable, however it suffers from a selectivity, noise figure compromise. The optimum noise source resistance is nearly that of the common source configuration. The input resistance is relatively low; consequently, it is impossible to drive the stage from its optimum source without severely loading the input tank and destroying its selectivity. One could drive the stage through a series tank, but the reactance levels become impractical at uhf. Also, if driven from the high source resistance, it becomes

illustrating the excellent noise figure obtainable over a wide current range. The source resistance for this data is 50 ohms. The power gain at 400 mhz is 18 db when terminated in a 50 ohm load. Such low impedance levels eliminate the QX limitation on available gain that can be experienced with FET amplifiers. It should be pointed out that although the 2N5470 bipolar amplifier exhibits approximately the same dynamic range as the FET circuit, it does so at the cost of additional power consumption. The FET cascode dissipates 80 mW whereas the 2N5470 circuit has a dissipation of 300 mW. In addition, the bipolar amplifier exhibits a decreasing signal handling capability as it is reverse-bias-gain controlled. This is also true of a common source neutralized circuit. Shown in figure 1-44 are the signal handling capabilities of the 2N5470 and 2N4417 circuits as they are gain-controlled. Along the ordinate is the undesired signal voltage (open-circuit) at a 50-ohm impedance level that results in -10 db cross-modulation distortion at a specified attenuation. As can be seen, the signal handling ability of the 2N5470 amplifier and subsequently its dynamic range decreases as the amplifier is turned off. Improved distortion characteristics can be obtained by forward agc (increased emitter current), but this is undesirable due to the loading and detuning effects of the resonant circuits. The 2N4417 cascode circuit also exhibits a decreased dynamic range when the gate of Q_1 is biased toward cutoff. However, by leaving the bias on the gate of Q_1 fixed, and reverse gain controlling the gate of Q_2, an increase in signal handling capability is achieved. Since the noise figure of the cascode is not degraded as fast as the signal handling characteristics are improved, a net increase in dynamic range is realized.

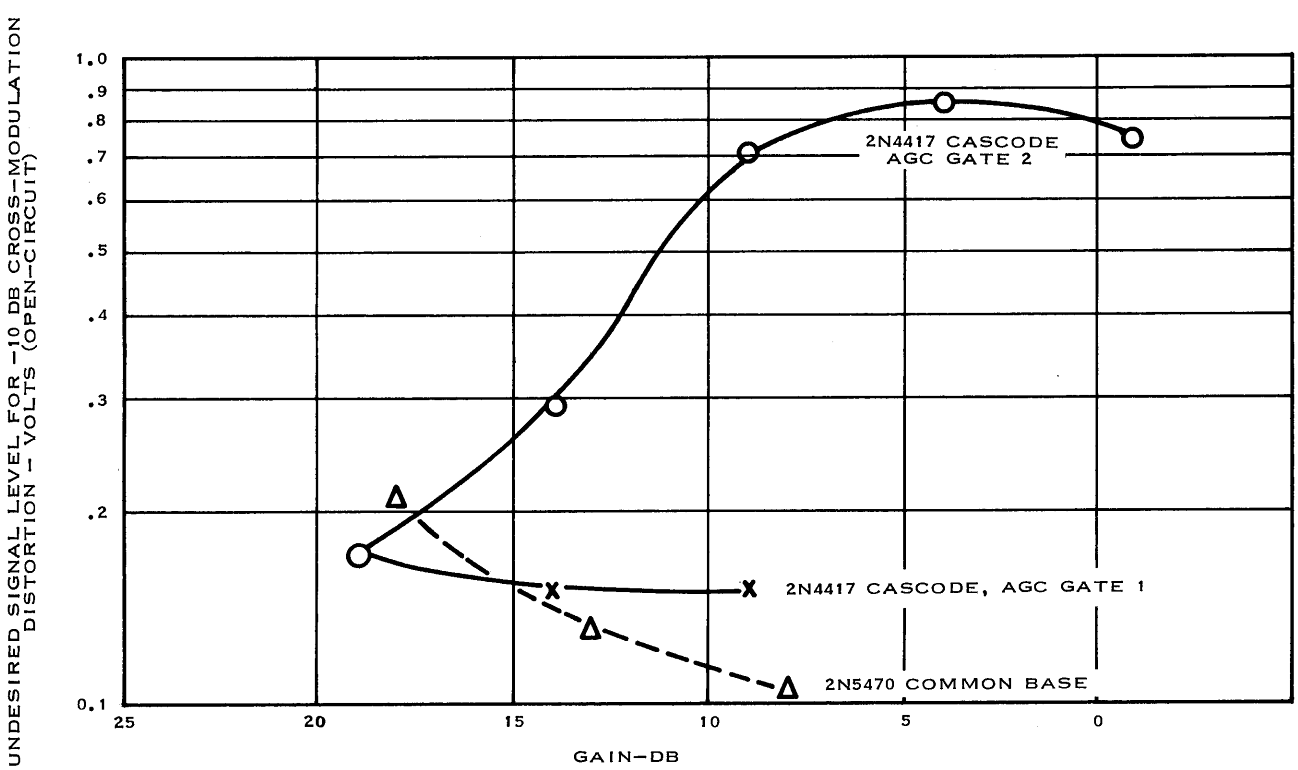

Figure 1-44. Signal handling capability for typical uhf amplifier circuits, F = 400 mhz, R_S = 50 ohms.

If an amplifier cannot meet a specific distortion requirement over its entire agc range, a passive attenuator ahead of the amplifier may be necessary. At uhf, the pin diode provides excellent control and distortion characteristics.[9] Even when used as a simple shunt element at an impedance level of 50 ohms, it can yield 20 db of control. The passive attenuator or "losser" can only offer 1 db of improvement in signal handling capability for a 1-db degradation in noise figure, therefore no real gain in dynamic range is obtained. Feedback techniques such as used at hf to achieve increased dynamic range versus agc have not proved practical at uhf.

Thus far, only state-of-the-art discrete devices and techniques have been discussed. The current trend in new active device research is aimed at extending high gain and low noise performance to higher frequencies. One technique that has demonstrated promising results is that of ion-implantation. In the current literature[10] there have been reports of a transistor with a gain-bandwidth product of 9 ghz that exhibits a noise figure of 4 db at 4 ghz. The results are due to the ability of the ion-implantation to give extremely fine control of base thickness leading to low base resistances which in turn determine the device gain and noise figure.

Another area of concern which is equally as significant to this project is the fabrication of silicon devices on foreign substrates. In assuming the premise that the preselector inductive components are likely to be fabricated on alumina or sapphire substrates, it would be highly desirable to have device fabrication on this substrate as well. The alternate would be to employ the hybrid chip approach with additional interconnects resulting in higher cost and decreased reliability. The ability to deposit silicon on sapphire using heteroepitaxial techniques is well documented[11]. After the deposition, active element locations are isolated by etching away the excess silicon between these "islands," and the devices are then fabricated using conventional mashing and diffusion processes. Zuleeg[12] reports development of diodes, bipolar transistors, MOS transistors, and space-charge-limited triodes using silicon-on-sapphire techniques. The devices are lateral; that is, they are made up of side-by-side diffusions of p and n impurities. The vertical junction areas formed are quite small because they are essentially the product of the silicon film thickness and "island" width. These small junction areas yield depletion-layer capacitances of .02 to .05 pf, giving rise to excellent frequency characteristics. A bipolar transistor constructed in this manner had a gain-bandwidth product of 4 ghz and exhibited a power gain of 12 db at 1 ghz. This points out that the silicon-on-sapphire approach does not necessarily mean compromised performance in order to be compatible; rather, the technique can actually offer improved performance.

3.2.1.2 Distortion in Varactor Tuned Circuits

In addition to the discussion of amplifiers and their limitations and capabilities, it is convenient at this time to discuss the signal handling capability of the varactor.

Since the varactor is a nonlinear capacitance, a large signal present in a varactor tuned circuit will be distorted by the nonlinearity. Furthermore, a small signal will be distorted by the presence of a large signal at a different but closely spaced frequency. This latter effect is responsible for cross modulation which means the transfer of the modulation of a large signal to a small signal.

For a single tuned circuit, it is possible to derive an expression showing the effects of circuit Q, varactor tuning voltage, exponent, and capacitance upon cross modulation. The details of the calculation are presented in part III, section 8, and the resulting expression is

$$\overline{V}^2 = 3\sqrt{2}\ \frac{1}{N(N+1)Q} \cdot \frac{C}{C_B} \cdot \frac{M_A}{M_U}$$

where

$\overline{V} = \dfrac{E_U}{V_B + \phi}$

E_U = peak carrier voltage of undesired signal

V_B = varactor bias

ϕ = varactor contact potential, usually 0.6 volt

N = varactor exponent

Q = operating Q of tuned circuit

C = total circuit capacitance

C_B = varactor capacitance at V_B

M_A = modulation index acquired by desired signal due to undesired modulation

M_U = modulation index of undesired signal

This equation includes in the derivation a very important worst-case situation; the desired signal frequency is placed at a particular point on the selectivity curve where the slope is the greatest. The bandwidth between the two points of maximum slope is related to the half-power (3 db) bandwidth by

$$BW = \frac{BW_3}{\sqrt{2}}$$

which is equivalent to the bandwidth at 1.76 db points. This aspect is often overlooked in casual measurements of cross modulation in varactor tuned circuits and is important because of tracking errors in practical front-end circuits. Indeed, consideration of the analysis in part III, section 8, shows that when the desired signal is placed at resonance, cross modulation is minimal and consists only of transferral of the second and higher even harmonics of the undesired modulation to the desired signal.

Experimental tests of the cross-modulation equation have been conducted. A single tuned circuit was constructed with a Q of 100 at 15 mhz using a Philco V4092 varactor having an exponent N of 0.48. No fixed capacitance was used such that $C/C_B = 1$. The bias voltage V_B was 6.85 volts and a 30 percent modulated undesired signal was applied at 13.5 mhz ($M_U = .3$). A small unmodulated signal at approximately 15 mhz was also applied and adjusted in frequency for the largest amount of cross modulation. For -20 db cross modulation (acquired modulation 20 db below 30 percent, or $M_A = .03$), a 0.46-volt rms undesired signal level was measured.

The calculated level is obtained as follows:

$$N = .48$$

$$Q = 100$$

$$\frac{C}{C_B} = 1$$

$$\frac{M_A}{M_U} = \frac{.03}{.3} = .1$$

$$\overline{V}^2 = 3\sqrt{2}\ \frac{1}{(.48)(1.48)(100)} \cdot (1) \cdot (.1)$$

$$\overline{V}^2 = .00597$$

$$\overline{V} = .0772 = \frac{E_{U\ PEAK}}{V_B + \phi}$$

$$V_B = \phi = 6.85 + .6 = 7.46 \text{ volts}$$

$$E_U = (7.46)(.0772) = .575 \text{ volt peak}$$

$$E_U = (.707)(.575) = .406 \text{ volt rms}$$

Thus, the calculated undesired voltage level is pessimistic and in error by 13 percent. This may be considered good correspondence in view of measurement error and the inherent non-linearity of the process.

3.2.1.3 Inductors

In earlier discussions of inductive elements, considerable attention was given to distributed inductors, specifically microstrip and the coaxial and helical resonators. The Q versus volume relationships were established and a discussion of their relative advantages was presented. It is the purpose of this section to discuss the lumped inductive components available for use in microminiature uhf preselector design.

The requirement for lumped inductive elements stems from the fact that transmission line components, such as those utilizing microstrip techniques, are necessarily a given physical length dependent on the frequency, dielectric constant, and degree of foreshortening. Consequently, in the uhf frequency range, the line may be physically larger than desired. All efforts to reduce size result in reduced performance. For example, the dielectric constant can be made very large reducing the line length by $\sqrt{\epsilon_r}$, but even if the loss tangent of the material is very low, it has been shown that the conductor losses increase just due to decreased size. Also, only a certain degree of foreshortening can be tolerated if the line is to be used with a variable capacitance in which tuning range is limited. Lumped elements intended for use in the uhf band are subject to a different set of constraints. The ultimate size limitation is imposed by the ability to accurately reproduce the component. Photolithographic techniques that have evolved due to technological advances in the semiconductor industry have enabled the production of components having line geometrics defined within a fraction of a mil on smooth substrates. It is this capability that permits the lumped element approach to be practical at frequencies extending beyond the 225 to 400 mhz spectrum.

The inductive geometry most compatible with integrated circuits is that of the spiral. Both the circular and square spiral configuration can be utilized but generally the circular configuration is preferred because it offers slightly higher Q. This is due to the fact that it has a higher volume to surface ratio[13]. The microminiature spiral can be calculated to a fair degree of accuracy by means of the expression[14].

$$L_{-UH} = \frac{A^2 N^2}{8A + 11C}$$

where

N is the number of turns,

$$A = \frac{D_O + D_I}{4},$$

$$C = \frac{D_O - D_I}{2}$$

where D_O is the outer diameter of the coil in mils and D_I is the inner diameter of the coil in mils. These parameters are also defined in figure 1-45. Examination of

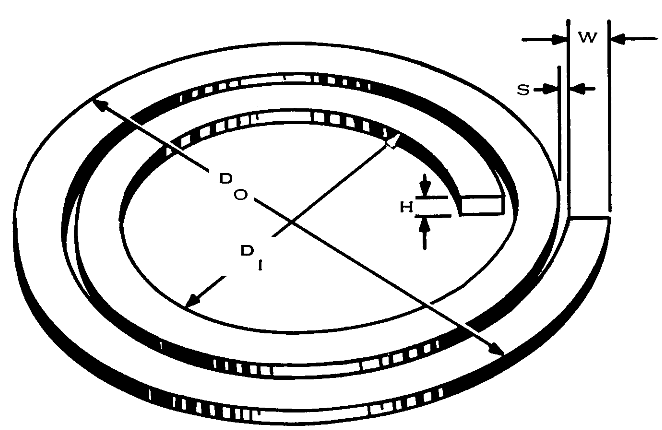

Figure 1-45. Spiral coil configuration.

this expression reveals that coil values in excess of 100 nanohenries can be fabricated in an area of not more than 100 mils square.

Daly, et al[15], derives an expression for Q,

$$Q = \frac{2LW}{NA}\sqrt{\frac{F\sigma}{\pi\mu}}$$

where L, A and N are defined as before, and

W is the conductor width

F is the frequency

σ is the conductivity and

μ is the permeability.

This relationship assumes that the current flows within a skin depth of the top and bottom surfaces and vertical surfaces. Also, it is assumed that the Q is dependent only on conductor losses and is not influenced by the substrate loss tangent. The expression predicts that Q will vary as the square root of frequency. A 50-nanohenry spiral inductor was fabricated on a .025 inch, 99.5 percent pure alumina substrate. It is shown in figure 1-46. The behavior of Q for this inductor was nearly that which was expected as may be seen in the plot of Q^2 versus frequency shown in figure 1-47. The data was obtained by lightly coupling the spiral inductor to a signal generator and an rf millivoltmeter by means of a small inductive link and a capacitive probe. The coupling was adjusted to give an insertion loss in excess of 50 db. The spiral coil was tuned over the frequency range by means of a high Q multisection MOS capacitor. Initially, all the sections of the capacitor were wire-bonded together to give a net capacitance of 24 pf. The frequency was increased by breaking the desired capacitor bonds. The largest available increments were 3.5 pf each and the smallest were 0.5 pf. The minimum obtainable capacitance is 3.5 pf giving rise to a maximum frequency of approximately 350 mhz. Examination of the expression for Q indicates that the spiral coil is limited in this respect for although the Q is directly proportional to conductor width, W, it is inversely proportional to the average radius. Therefore, for a given reactance level, the turn-to-turn capacitance increases as the conductor width is increased. This results in a decreased self-resonant frequency which eventually renders the coil unusable. Some Q improvements can be

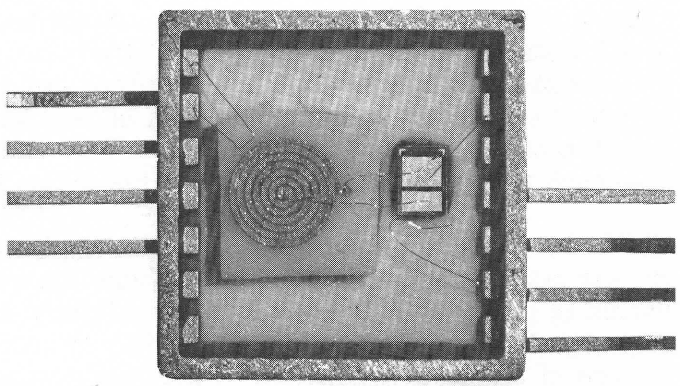

Figure 1-46. 50-nanohenry spiral coil.

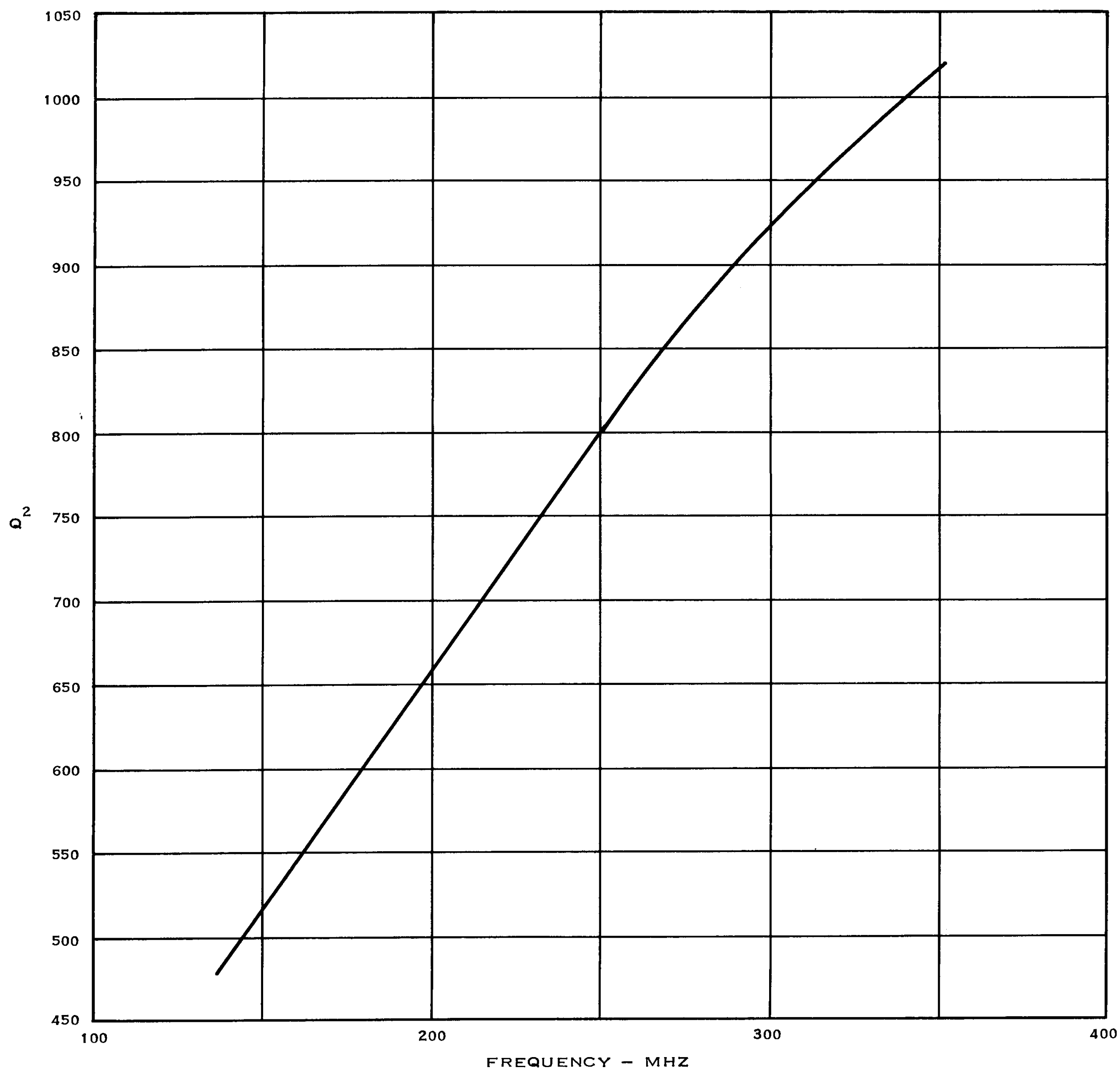

Figure 1-47. Q^2 versus frequency for 50-nanohenry spiral coil.

obtained by refined fabrication techniques. The material used for the conductor should have very high conductivity and it should be several skin depths deep. The substrate also is of extreme importance. In addition to the requirement that it possess a low loss tangent, Keister[16] has conducted tests that indicate that high purity and surface smoothness contribute to higher Q's. One conclusion drawn by Keister is that purity contributes more to high Q than surface smoothness. One practical problem that is virtually ignored in nearly all discussions of microminiature components is the performance of the component in close proximity to shields and/or ground planes as might be encountered in final assembly. Shown in figure 1-48 is the degradation of Q as the distance between the spiral coil, and a parallel ground plane is decreased. The distance shown on the abscissa includes the .025 inch alumina substrate. As can be seen, the ground plane exerts a significant influence on inductor performance and should be considered in Q versus volume analyses. Although the Q's obtained for the spiral coil are quite low compared to those obtained using conventional discrete components, it is believed that they offer the highest Q's obtainable in a given volume using planar microminiature techniques.

Although not necessarily compatible with monolithic integrated circuit techniques, additional lumped inductive components which can be employed using hybrid fabrication techniques should be discussed. The toroid coil using ferrous core materials is of interest because it offers a potential solution to the problem of the enclosed or shielded inductance. The use of a ferrous material for an inductor core complicates any analysis of Q behavior. Rand[17] has shown that the maximum Q of such an inductor occurs when the core losses equal the conductor losses and is equal to one-half of that obtainable from the core material. A brief search for materials usable in the uhf range indicates that very little material is available. In general, as the frequency increases, the relative permeability of the material decreases. Ferrites intended for use at uhf, such as Ceramag 2285A, have relative permeabilities of approximately 7.5 but, unfortunately, the ferrites exhibit temperature characteristics which

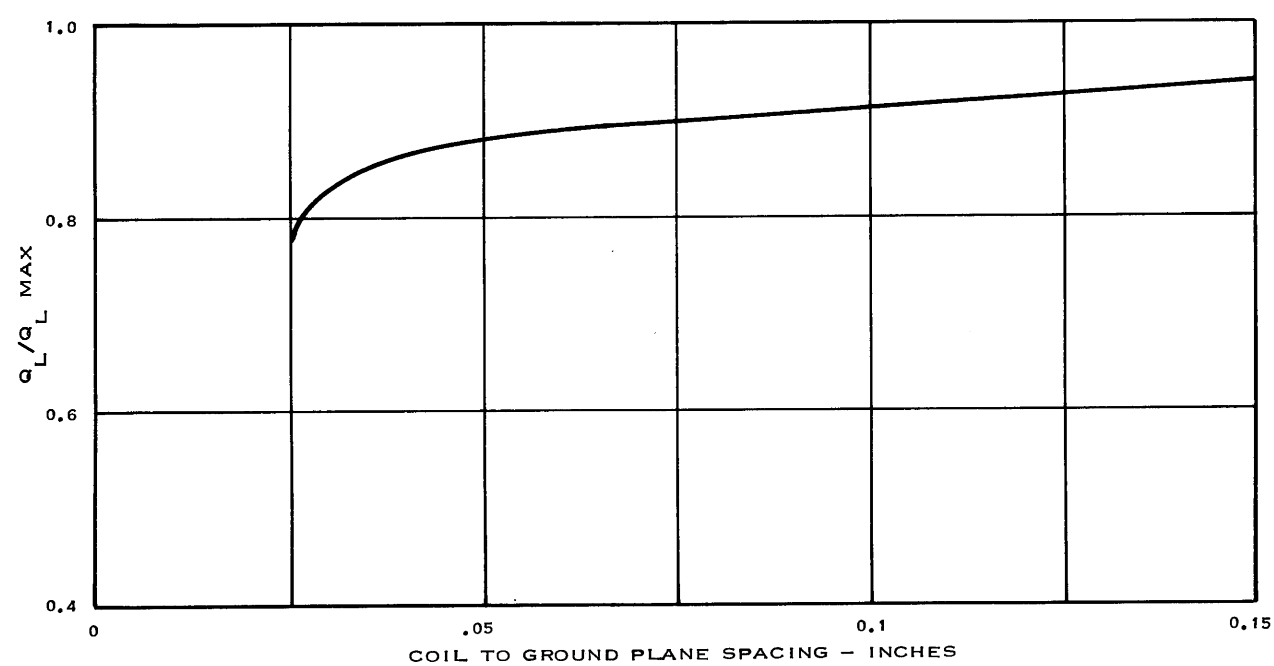

Figure 1-48. Effects of shielding on 50-nanohenry spiral coil at 250 mhz.

eliminate their use as precision tuning elements. For example, the typical temperature coefficient of permeability for Ceramag 2285A is 0.36 percent per degree Celsius. Powdered iron cores offer adequate temperature stability but are not very useful in the uhf range as the permeability is quite low. The only commercially available powdered iron core material indicated for use at frequencies as high as uhf is IRN-9. The specified permeability at low vhf frequencies is 3.3 to 3.6. A small 0.1 inch od toroidal coil was fabricated using two turns of no 34 wire on an IRN-9 core. The measured inductance at 250 mhz is 41 nanohenry. The Q versus frequency relationship over the uhf range is shown in figure 1-49. The decreasing Q with increasing frequency illustrates the strong influences of the core loss. The actual value of inductance appeared lower than expected and subsequent measurements at 250 mhz indicated that the permeability was less than 1.3. This low value would suggest that the toroidal coil's Q would also be affected when centered between two parallel ground planes. Shown in figure 1-50 is the characteristic illustrating this effect.

The low value of permeability obtained for the toroid would indicate that nearly equal reactance levels and improved Q's could be obtained using the ordinary solenoid configuration. The expression for the inductance of a single-layer solenoid is[18]

$$L_{-UH} = FN^2D$$

where

N is the number of turns

D is the mean diameter

and

F is a constant dependent on the shape factor of the coil.

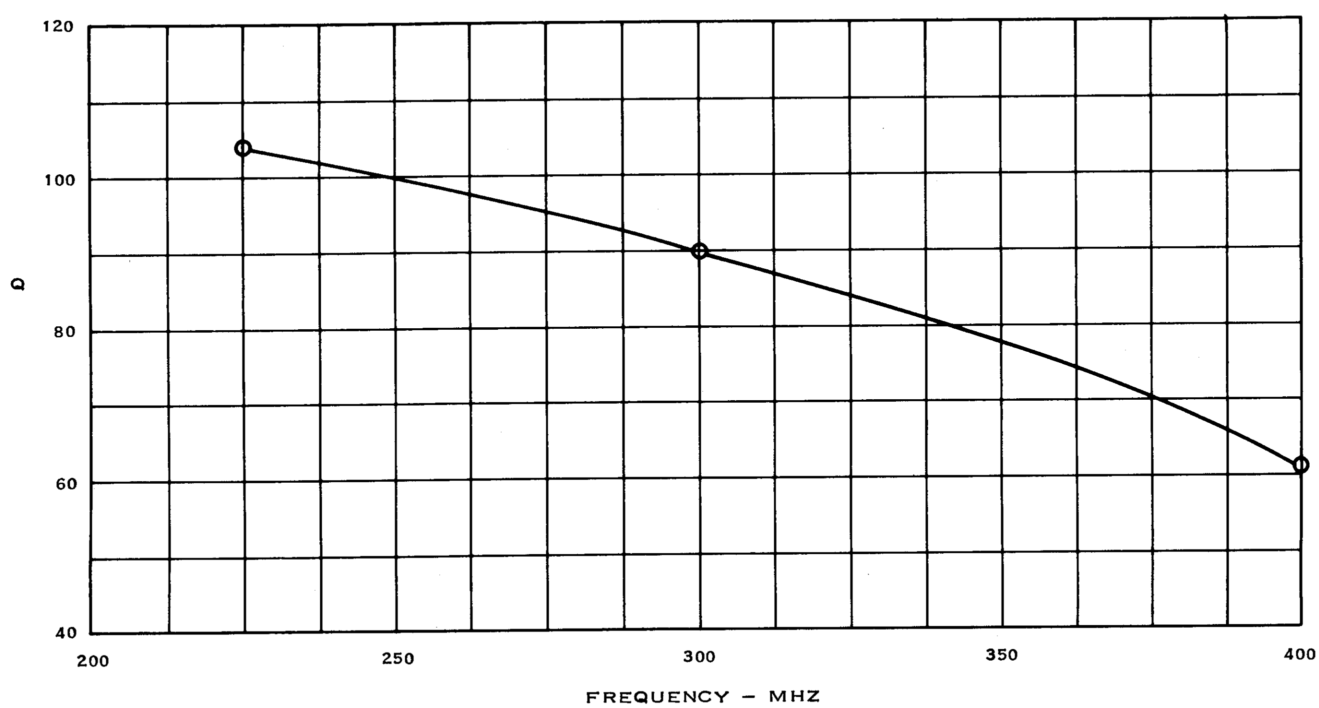

Figure 1-49. Q versus frequency for 0.1-inch od IRN-9 toroidal coil, L = 41 nanohenrys.

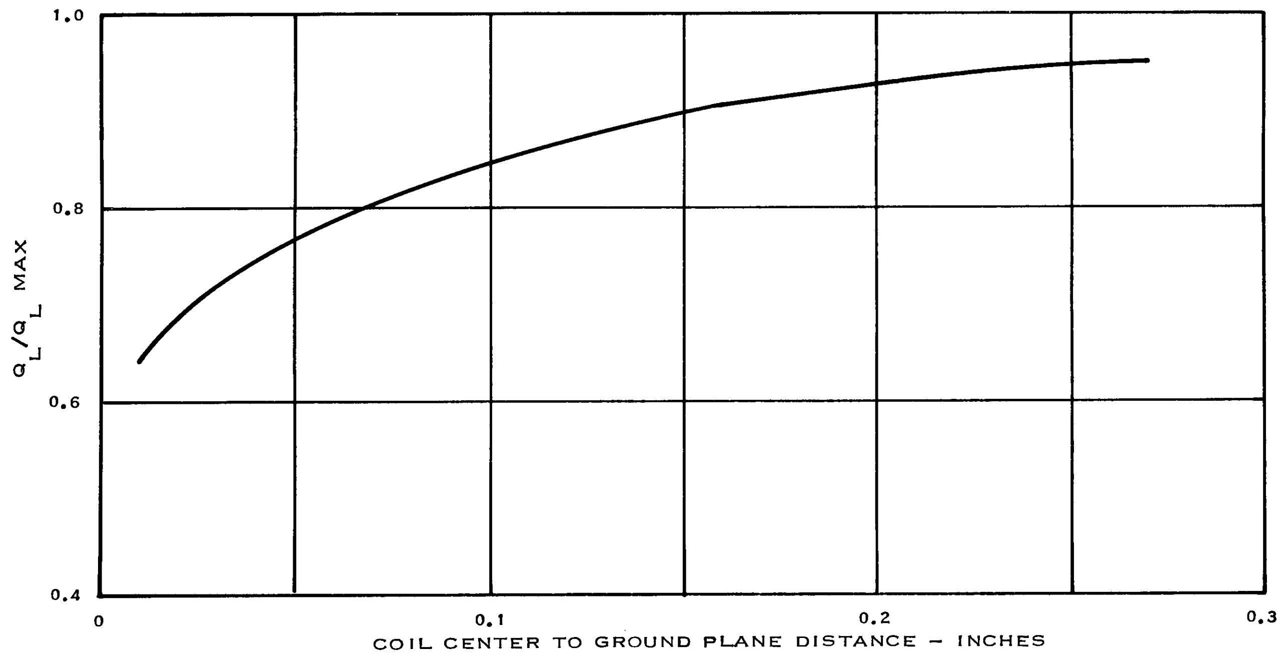

Figure 1-50. Effects of shielding on IRN-9 toroidal coil at 250 mhz.

A coil consisting of four turns of no 32 wire and an id of 0.070 inch was constructed and tested. The measured value of inductance is approximately 20 nanohenries. As expected, the Q varied as the square root of frequency - 138 at 255 mhz and increasing to 173 at 400 mhz. To observe the effects of shielding at 250 mhz, two ground planes were placed on each side of the coil parallel to its axis. Figure 1-51 illustrates the degradation in Q as the spacing is varied.

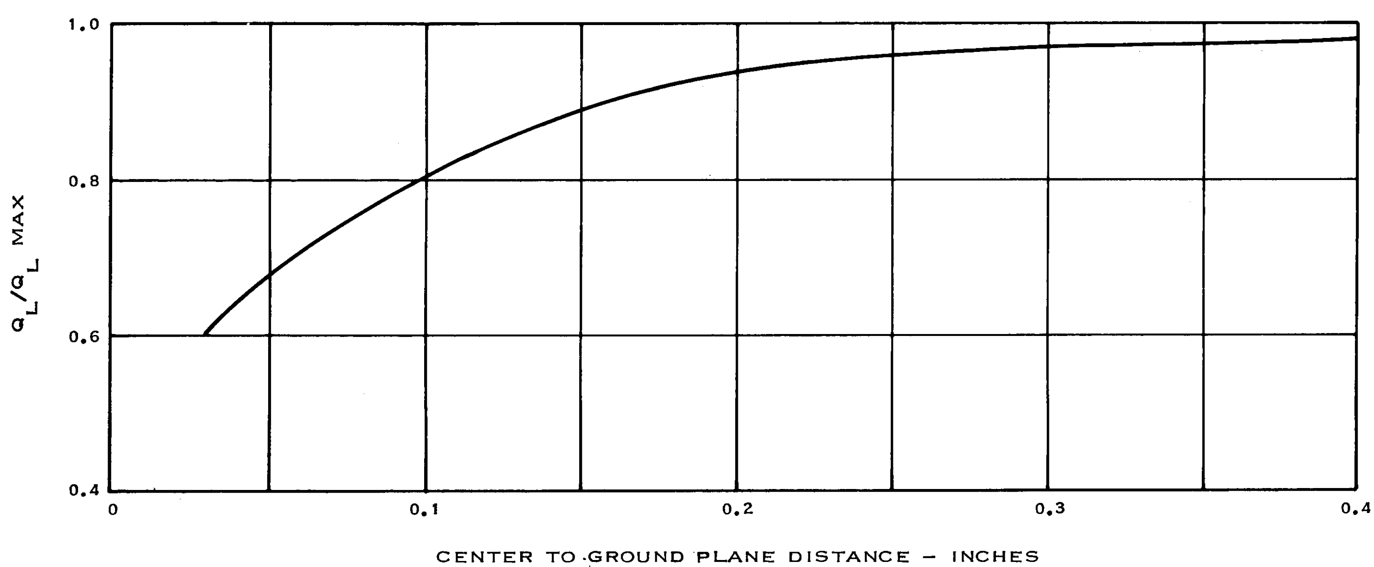

Figure 1-51. Effects of shielding on miniature solenoid at 250 mhz, ID = .070 inch.

Knowing that a shielding problem exists, it is logical to ask whether or not the shielding could be provided in such a manner to optimize Q. The helical resonator does exactly this. In the preceding discussion, it was determined that ground planes spaced 0.125 inch degraded the Q to 90 percent of its initial value. At 400 mhz, this corresponds to a Q of approximately 155. If a helical resonator were constructed in this volume, it would exhibit a Q of 300, nearly a 2 to 1 improvement. The major disadvantage of the use of the helical resonator is that its fabrication is difficult and expensive particularly when its size is decreased. The size reduction of a helical resonator is limited by the ability to make the helix. Resonators have been constructed with a helix pitch of 80 turns per inch and 100 turns per inch appears to be a practical limit using conventional techniques. Shown in figure 1-52 is a plot of the pitch - $F_{1/4}$ versus resonator volume characteristic for the helical resonator. Knowing the quarter-wave frequency, $F_{1/4}$, and assuming a practical limit on helix pitch, one can ascertain the minimum volume obtainable, as well as the unloaded Q. For example, consider the fabrication of a helical resonator having an $F_{1/4}$ of 600 mhz. Assuming a helix pitch of 100 turns per inch, figure 1-52 shows the minimum volume to be 0.007 cubic inch. Using the relationship,

$$Q_U = 51 \sqrt{F_O} \quad \sqrt[3]{V}$$

yields a Q_U of 191 at 400 mhz.

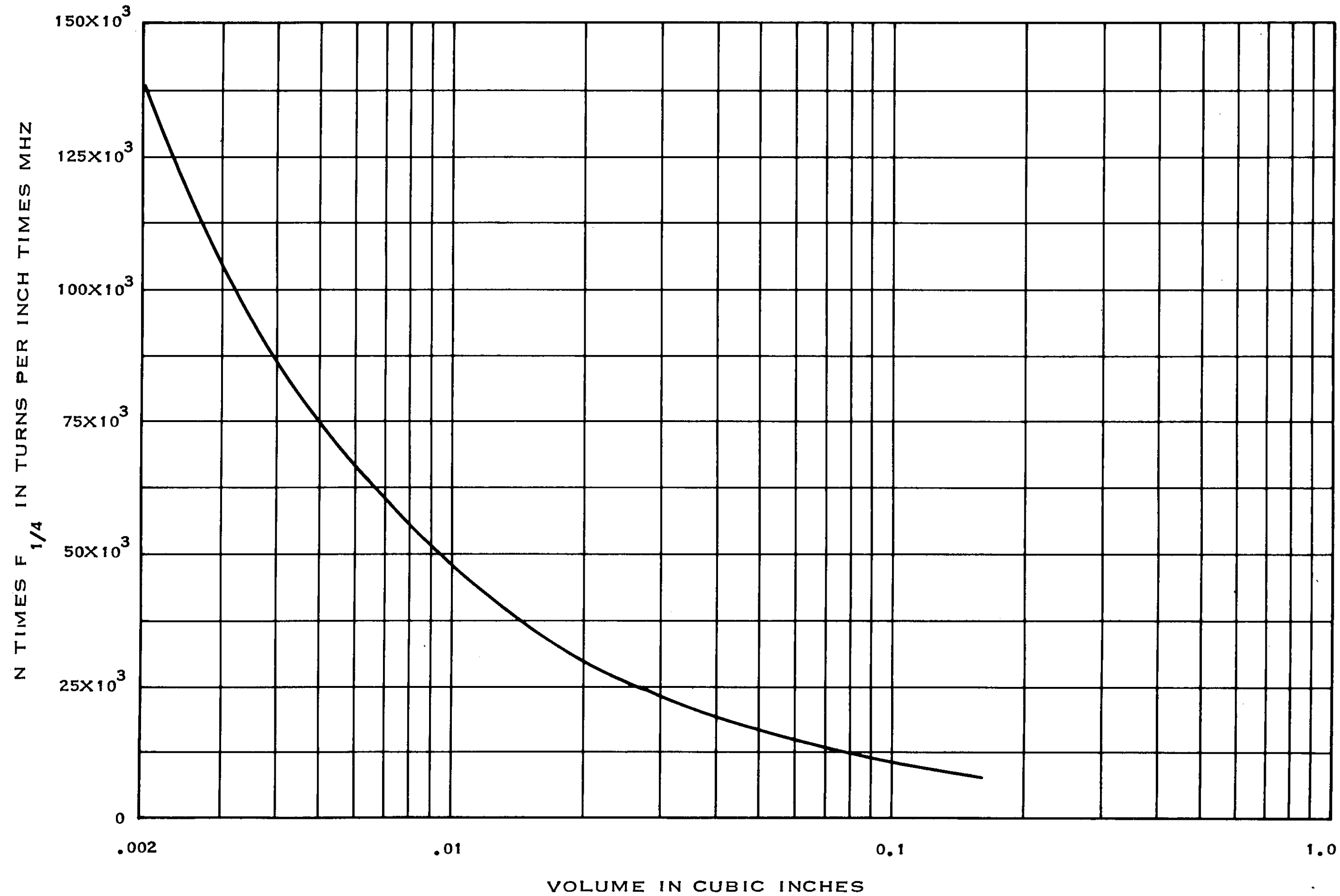

Figure 1-52. N times $F_{1/4}$ versus volume for helical resonator.

3.3 Trade-Off Analysis

This section will present the results of trade-off studies conducted during the course of the investigation. The trade-offs associated with the basic block diagram of a uhf tuner can be described in largely an analytical manner; for example, the relationships between filter Q requirements, loss, and selectivity. In the areas of fabrication, circuit and component techniques, however, the parameters are so interrelated that a compact analysis of one as a function of others is not clearly definable. However, comparisons between techniques are readily drawn on the basis of experiment and as a result of the literature search. Trade-offs of this type are presented in chart form.

3.3.1 Image and Spurious Responses Trade-off Analysis

Table 1-1 of the Interim Development Report (IDR) has shown in a comparative way the trade-offs existing between the four basic frequency schemes. Of those schemes, the one having an if output frequency approximately one-tenth of the signal frequency has been shown to be the optimum from the standpoint of minimum volume of the if filter. There are two choices of injection frequency for this scheme, low or high side injection. Part III of the IDR has shown the spurious responses which cross the desired frequency in the 225 to 400 mhz band when low side injection is employed; this is compared in table 1-6 which illustrates that high side injection results in a smaller number of crossovers whose minimum order is larger. Therefore, high side injection is better from a high order spurious response standpoint only.

TABLE 1-6. CROSSOVER SPURIOUS RESPONSES IN THE 225 TO 400 MHZ BAND FOR A DOWN-MIXER WITH 30 MHZ OUTPUT FREQUENCY (MAXIMUM ORDER = 20).

H	L	F_O/F_{SIG}	H	L	F_O/F_{SIG}
-6	7	.1250	-7	8	.1250
-7	8	.1111	-8	9	.1111
-8	9	.1000	-9	10	.1000
8	-9	.1250	9	-10	.1250
-9	10	.0909			
9	-10	.1111			
Low side injection.			High side injection.		

The worst spurious response, however, is the image since the relative response of the mixer is unity to the signal and image frequencies. The image can only be reduced with selectivity which is obtained with physical volume. (See the IDR for discussion of the image phasing mixer and selectivity.) The signal and image responses have arithmetic symmetry about the injection frequency, while filters possess geometric symmetry of attenuation about the resonant frequency. If the normalized image bandwidth, BW_2/F_O, for both low and high side injection is calculated as a function of normalized intermediate frequency, IF/F_O, the

plot shown in figure 1-53 is obtained. (See derivation in part III, section 9.) This shows that low side injection is to be preferred from an image standpoint. Indeed, for all spurious responses lying between the signal and injection frequencies but not crossing the signal frequency, (for example, half-if spurious) low side injection results in better filter rejection of the undesired signal.

A trade-off between the if and the number of spurious responses for low side injection is shown in figure 1-54. The curve shows the total number of spurious responses up through the 20th order which cross the desired frequency. Since no selectivity is provided by the preselector for these responses, the ordinate is indicative of the number of channels which will be subject to interference from close-in undesired signals. The curve indicates a trend only; specific frequency schemes must always be examined in detail for responses which do not cross the desired frequency but which may approach it closely.

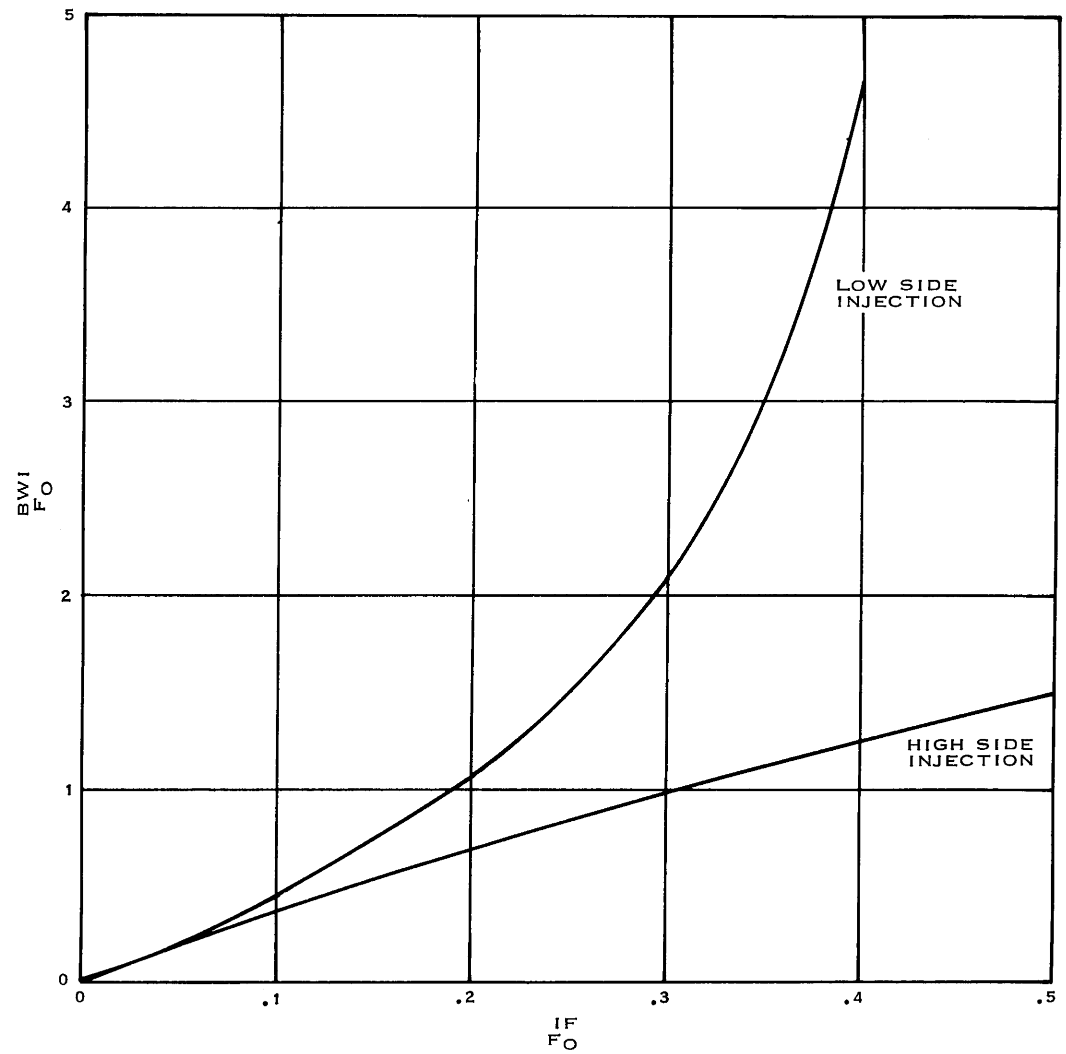

Figure 1-53. Image bandwidth versus intermediate frequency.

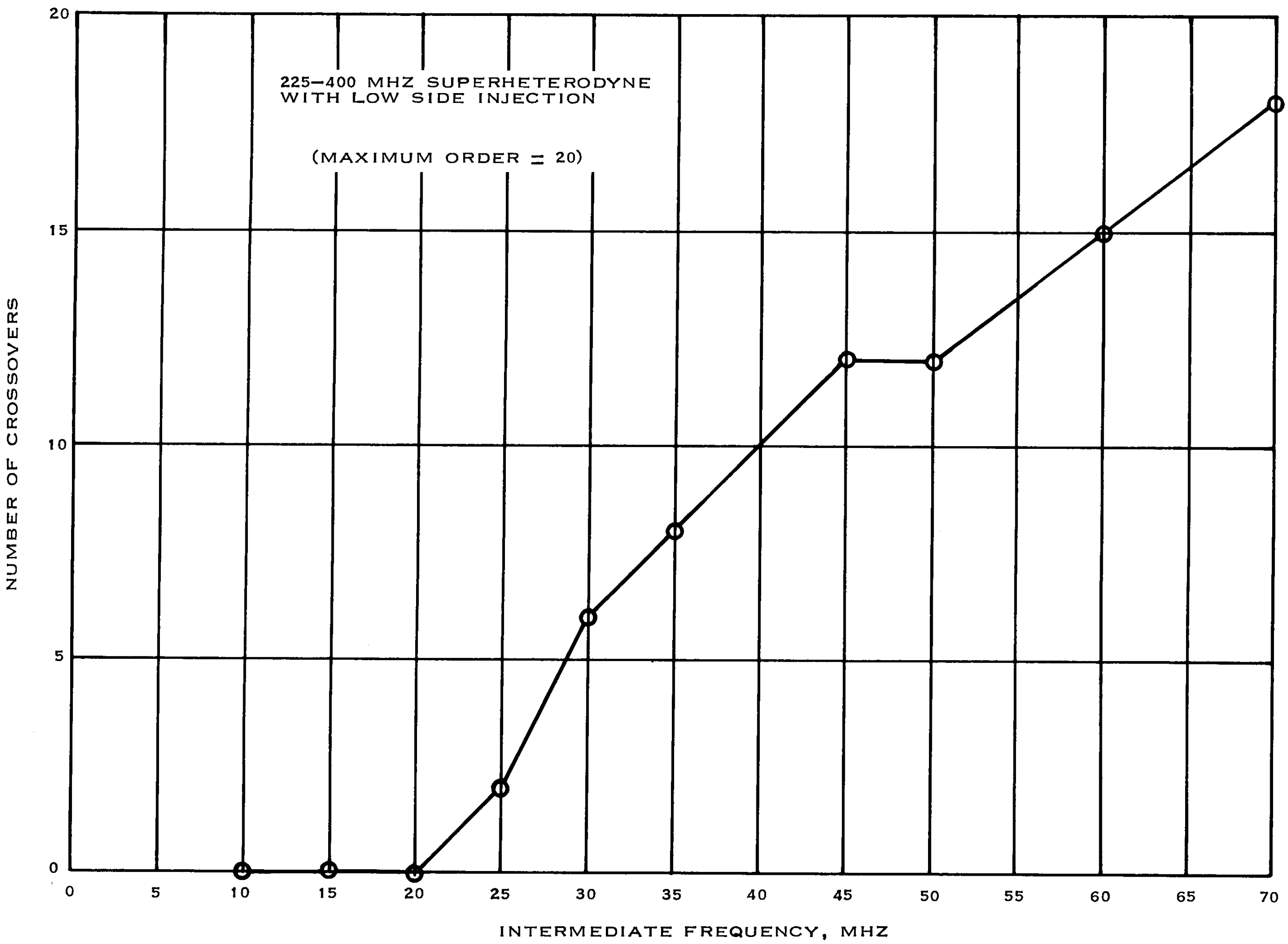

Figure 1-54. Number of crossover spurious responses versus intermediate frequency.

Since image and noncrossing spurious responses are all reducible with rf selectivity, it is instructive to examine the trade-offs between selectivity and other parameters. The equal element or minimum loss filter postulated by Cohn[19] will be used in the selectivity trade-off calculations because such a design has the greatest stopband attenuation for a given passband loss. The minimum loss synthesis is to be preferred for receiver rf filtering since the exact shape of the passband is usually unimportant, while the center frequency loss and stopband attenuation are of major importance.

If, for a minimum loss filter, the number of resonators is allowed to vary while holding the stopband attenuation at some point constant, it is found that a minimum in passband loss is obtained for a certain optimum number of resonators. This was mentioned in the IDR and is due to Taub[20]. The equation for N_o is

$$N_o = \frac{\alpha_r + 6 = L_o}{8.686}$$

where α_r is the relative attenuation in db at some stopband bandwidth. As demonstrated in part III, section 10, α_r is given by

$$\alpha_r = -6 - L_o + 20\ N\ \mathrm{LOG}\left(\frac{L_o}{4.343N} Q_U \frac{BW}{f_o}\right)\ ,\ \mathrm{DB}$$

where L_o is the passband insertion loss in db, N is the number of resonators, Q_U is the unloaded quality factor of the resonators, BW is the bandwidth between points of equal attenuation α_r and f_o is the filter's center frequency. When $N = N_o$, the relationship

$$L_o\ Q_U \frac{BW}{f_o} \cong 1.359\ (6 + \alpha_r)$$

is obtained which is true whenever the number of resonators is optimum for a given selectivity specification. The left-hand term of this expression shows that loss (or noise figure) may be directly traded with selectivity for a given amount of stopband attenuation. This result may be combined with the intermediate frequency versus bandwidth plot of figure 1-53 to arrive at the family of curves in figure 1-55. The latter shows the image attenuation, α_r versus the normalized if when the number of resonators is optimum for a given α_r. For example, when a 30-mhz if is used with the front end tuned to 300 mhz, an $L_o\ Q_U$ product of about 280 is required to obtain an 80-db image response when a single filter is employed in the front end. If a preselection and interstage filter are used, an $L_o\ Q_U$ product of 140 is required when each filter attenuates the image by 40 db. These curves are truncated at 30 db where approximations in the derivation begin to be significant.

Another way of looking at image selectivity trade-offs is to optimize the physical volume of the filter for a given selectivity. This has also been done by Taub[21]. The derivation, framed in the symbology of this report, is given in part III, section 2. Briefly, the general stopband selectivity equation for the minimum loss filter is solved for Q_U, giving

$$Q_U = \frac{4.343N}{L_o} \cdot \frac{f_o}{BW} \cdot 10^{\frac{\alpha_r + 6 + L_o}{20N}}$$

As pointed out by Taub, the physical volume of a distributed resonator is related to Q_U (at least over a restricted range) by the equation

$$V = CQ_U^p$$

where C is a proportionality constant and p is an exponent describing the variation. The total volume of the filter is then

$$V_T = NCQ_U^p$$

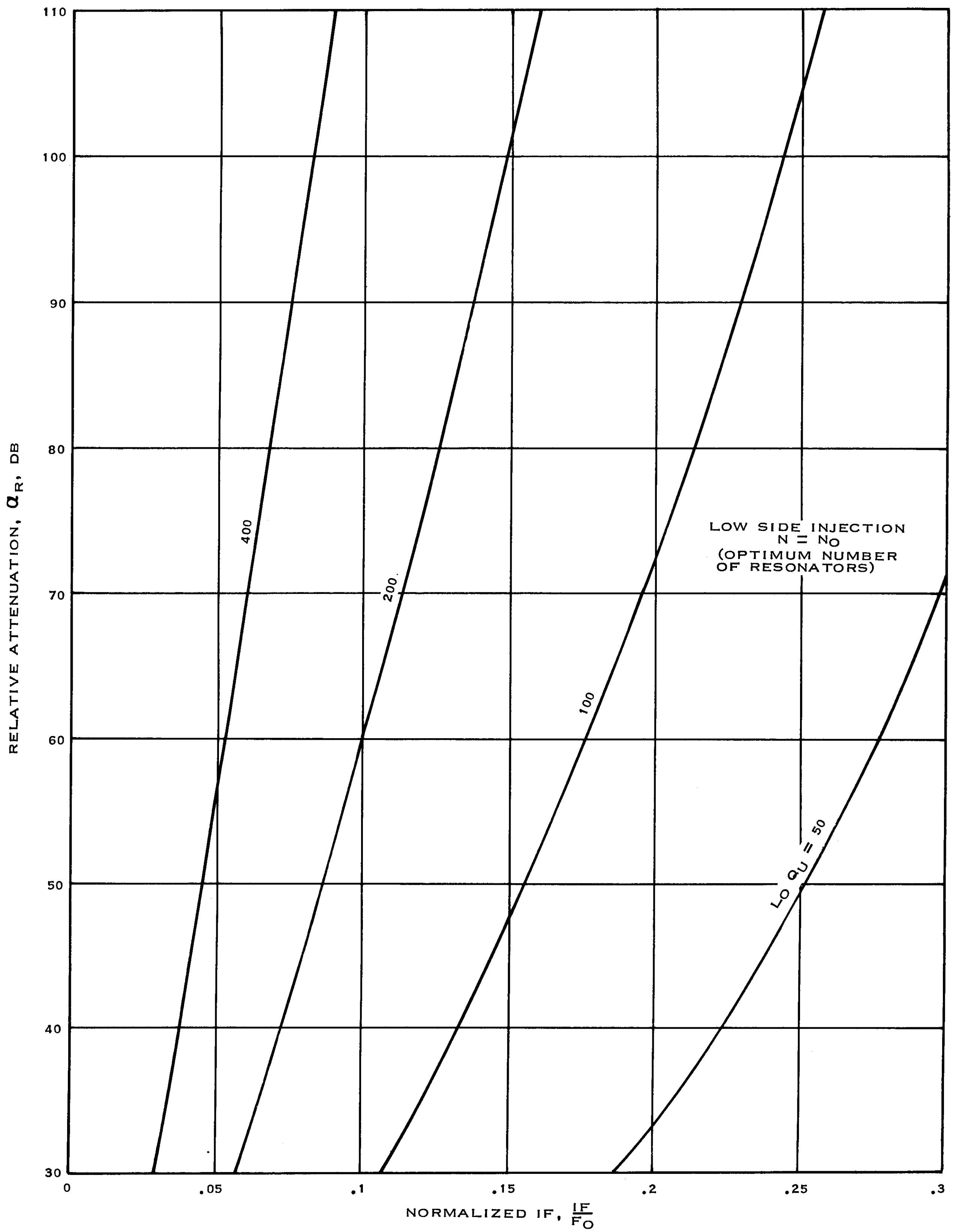

Figure 1-55. Image attenuation versus intermediate frequency.

This is combined with the above selectivity equation and the derivative with respect to N is set equal to zero. Solution of that equation for the optimum number of resonators, N_V, from a volumetric standpoint yields

$$N_v = \frac{p}{p+1} \cdot \frac{\alpha_r + 6 + L_o}{8.686}$$

When this N_V is substituted into the relative selectivity equation, a new and optimal relationship between loss, bandwidth, quality and selectivity is obtained:

$$L_o Q_U \frac{BW}{f_o} \cong \frac{pe^{\frac{p+1}{p}}}{2(p+1)} (\alpha_r + 6)$$

This relation is plotted in figure 1-56 for the case p = 3 (helical resonator) and for low side injection so that the selectivity versus loss relationship can be seen as a function of the ratio of intermediate to signal frequencies.

The trade-offs implied in figure 1-56 express a very fundamental limit on the performance versus size of a receiver front end. First, the selectivity has been optimized by the use of Cohn's minimum loss synthesis. Second, the volume of the Cohn filter providing a specified selectivity has been minimized by finding an optimum number of resonators from a total volume standpoint. Since N must be an integer whereas N_V is usually noninteger, it follows that the performance of any real design must generally be less than this theoretical limit. Fortunately, the optimum is a fairly shallow one so that an integer value of N does not cause a drastic performance change.

3.3.2 Process Trade-Offs

Table 1-7 lists the electrical, physical, reliability, and cost performance of several fabrication processes. The discrete component method of construction is included to allow comparison with present established technology in the uhf tuner field. The thin-film hybrid approach generally uses a high purity alumina substrate onto which spiral inductors, tantalum capacitors and resistors, and interconnections are attached, using metal deposition and selective etching processes. Active components such as transistors and diodes along with some passive components are also attached to the substrate and interconnected with gold wire bonds. The monolithic process pertains to diffusion of the entire circuit into a silicon wafer using photographic masking and etching procedures. The multiphase monolithic process is an extension of the silicon monolithic one in which isolation between diffused regions is obtained through layers of silicon dioxide and high purity polycrystalline silicon. The silicon-on-sapphire process uses a highly polished sapphire substrate on which islands of single crystal silicon are formed to allow diffusion of active devices and some passive elements. Thin-film inductors, resistors, capacitors, and interconnection paths are also deposited on the sapphire using vapor deposition and photographic selective etching.

The resistor quality column in table 1-7 pertains to the degree of freedom from parasitic shunt distributed capacitance. The quality factor column indicates the relative Q obtainable in capacitors and inductors. Impedance level relates to the QX product attainable in process

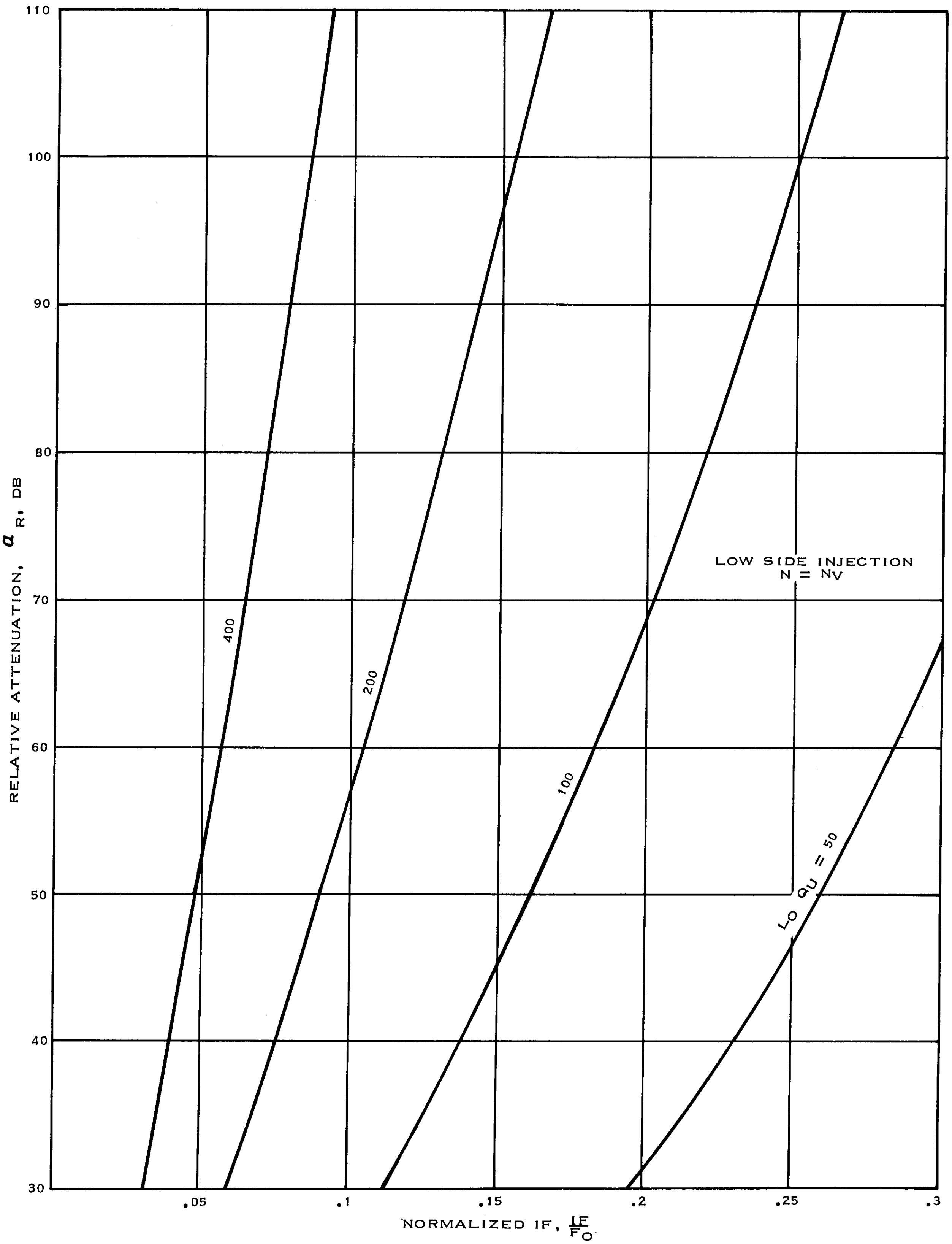

Figure 1-56. Image attenuation versus intermediate frequency, minimum total volume.

TABLE 1-7. TRADE-OFF CHART FOR FABRICATION PROCESSES APPLICABLE TO UHF MICROMINIATURE TUNERS.

PROCESS	VOLUME	RESISTOR QUALITY	INDUCTOR QUALITY	CAPACITOR QUALITY	QUALITY FACTOR "Q"	IMPEDANCE LEVEL	ISOLATION	RELIABILITY	DEVELOPMENT COST	PRODUCTION COST
Thin-film hybrid	Medium	Good	Low values	Wide range	Medium	Medium	High	Medium	Medium	Medium
Discrete	Very high	Excellent	Wide range	Wide range	High	High	Highest	Lowest	Low	Medium
Silicon on sapphire	Low	Good	Low values	Low values	Fair	Medium	Medium	Medium	High	High
Monolithic	Very low	Poor	Nil	Non-linear	Unusable	Low	Lowest	Highest	High	Low
Multiphase monolithic	Low	Medium	Nil	Non-linear	Unusable	Low	Low	High	High	High

resonators and directly affects the stage gain available from high impedance FET active circuits. Isolation means the degree of electrostatic coupling present which limits the stability of active stages and the control of filter response shapes due to undesired coupling coefficients.

3.3.3 Active Circuit Trade-Offs

Table 1-8 compares the performance trade-offs available in the active circuits used for uhf amplification and heterodyne mixing. The noise figure column lists the typical performance of the best devices currently available for uhf use. The dynamic range column is based on the same circuits and devices used in the noise figure column. It can be noticed that the lowest noise figure is available from very small geometry bipolar transistors; however, the dynamic range of such an amplifier is relatively poor. It is possible, by using rf power bipolar transistors, to obtain more dynamic range than that of the FET amplifiers; however, the noise figure of such a bipolar amplifier is higher than for an FET stage. The injection noise column pertains to the ability of a mixer to reject the spectral noise on the injection signal lying at frequencies removed from the injection by plus and minus the intermediate frequency. This is of considerable importance in high dynamic range mixers operating from digital frequency synthesizer injection sources. The spurious column compares the relative spurious response level of mixers to high order mixing products such as the "half-if" spurious, caused by twice the injection frequency beating with twice an undesired signal frequency to produce the if.

3.3.4 Passive Circuit Trade-Offs

Table 1-9 indicates the relative characteristics of passive circuits useful for the preselection filtering function. Passive is used in the small signal sense; the large signal nonlinearity of varactor and YIG tuned resonators is well appreciated. Of considerable importance is the tuning control power requirement; varactor tuning is the only electrical tuning method that minimizes this parameter.

TABLE 1-8. TRADE-OFF CHART FOR ACTIVE CIRCUITS USED IN UHF MICROMINIATURE TUNERS.

ACTIVE CIRCUIT	BEST NOISE FIGURE (db)	DYNAMIC RANGE (db)	GAIN (db)	TYPICAL DC POWER (mW)	INJECTION POWER (mW)	INJECTION NOISE REJECTION	GAIN CONTROL	SPURIOUS
Neutralized rf amplifier (FET)	3.5	104	10	50	--	--	Fair	--
Cascode rf amplifier (FET)	3.7	104	15	100	--	--	Good	--
Single FET mixer	6	104	9	50	80	Poor	--	Fair
Balanced FET mixer	7	114	12	100	50	Good	--	Good
Single diode mixer	10	--	-10	0	5	Poor	--	Poor
Balanced quad diode mixer	8	115	-8	0	100	Excellent	--	Excellent
Bipolar rf amplifier	1.5	80	15	10	--	--	Poor	--

TABLE 1-9. TRADE-OFFS BETWEEN PASSIVE CIRCUITS USED IN UHF PRESELECTORS.

PASSIVE CIRCUIT	QUALITY FACTOR "Q"	LARGE SIGNAL LINEARITY	TUNING RANGE	VOLUME	CONTROL POWER (mW)
Varactor tuning	Medium	Poor	Narrow	Smaller	Negligible
Switched C tuning	Medium	Good	Medium	Small	1,000
Switched BPF	High	Excellent	--	Large	300
YIG	High	Poor	High	Largest	3,000

3.3.5 Performance Trade-Offs

Table 1-10 compares, in a relative way, the trade-offs between electrical and physical specifications of a tuner. The chart is read by letting a single specification in a vertical column improve. For example, better sensitivity or high rejection of spurious responses would be improvements. The entries in the horizontal rows interesecting the single vertical column then indicate the dependency of other specifications. Since tuner design is very interdependent, with a change in the block diagram occurring as a function of specifications, some of the entries may indicate trends only.

TABLE 1-10. UHF TUNER PERFORMANCE TRADE-OFFS.

	PARAMETERS IMPROVED ONE AT A TIME							
PARAMETER AFFECTED	SENSITIVITY OR NOISE FIGURE	IMAGE REJECTION	SPURIOUS RESPONSE	CROSS-MODULATION	INTERMOD-ULATION	POWER INPUT	VOLUME	COST
Sensitivity or noise figure	--	D	NDR	D	D	NDR	I	IL
Image rejection	D	--	I	NDR	NDR	NC	I	I
Spurious response	NDR	I	--	SI	I	I	I	IL
Cross modulation	D	NDR	I	--	I	I	IL	IL
Intermodulation	D	NDR	I	I	---	I	IL	IL
Power input	NDR	NDR	SI	I	I	--	NDR	NDR
Volume	NDR	I	I	I	I	NDR	--	R
Cost	I	I	I	IL	IL	NDR	D	--

LEGEND:
D = Degradation
NDR = Not directly related
I = Improvement or increase
NC = No change
SI = Small improvement or increase possible
IL = Improvement limited by technology
R = Reduction

3.3.6 Q-Volume Trade-Offs for Transmission Line Resonators

The following equations obtained from Zverev and Blinchikoff[22] and Cline[23], et al, serve as a basis for deriving a set of equations which describe the Q-volume trade-offs.

For helical resonators:

$$Q = 60S\,(F_O)^{1/2}$$

$$Z_O = \frac{81500}{F_{1/4}\,S} = \frac{95355}{F_{1/4}\,V^{1/3}}$$

For coaxial resonators:

$$Q = 12.78\, Z_O\, (F_O)^{1/2} \left(\frac{R_1 R_2}{R_1 + R_2} \right)$$

where S = shield length in inches

Z_O = characteristic impedance in ohms

F_O = frequency of resonance in mhz

$F_{1/4}$ = 1/4-wave frequency in mhz

R_1 = inner conductor radius in inches

R_2 = outer conductor radius in inches

$Z_o = \frac{138}{\sqrt{\epsilon}} \log_{10} (r_2/r_1)$

ϵ = Dielectric constant

Opt Q, Air

$r_2/r_1 = 3.59$

and it is assumed the resonators have air dielectrics and copper conductors.

Figures 1-57 and 1-58 are repeated from the interim report for convenience and to clarify the definition of the terms.

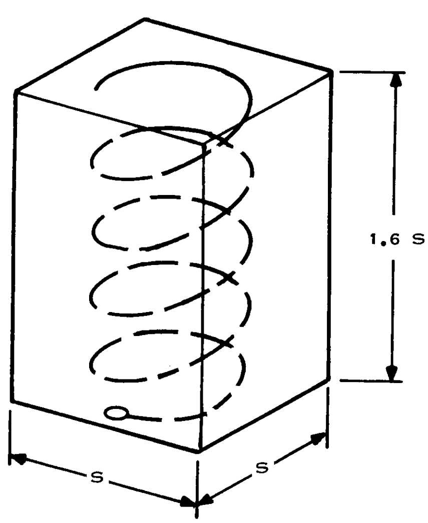

Figure 1-57. Helical resonator.

$R_2 > R_1$

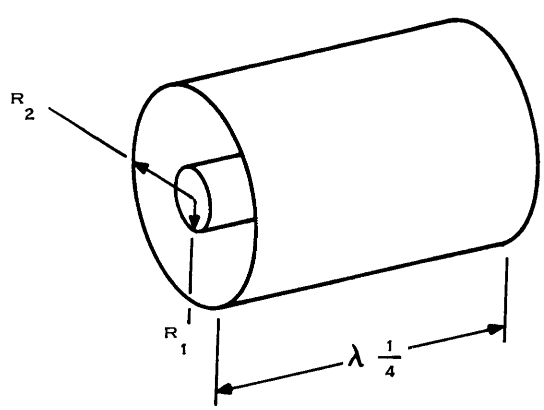

Figure 1-58. Coaxial resonator.

It was shown in the interim report that the unloaded Q for a helical resonator can be expressed in terms of its volume and resonant frequency as

$$Q_U = 51\, (F_O)^{1/2}\, (V)^{1/3}$$

In a similar manner it is possible to derive the equation for maximum Q in a coaxial resonator as follows:

$$Q_U = 12.78\, Z_O\, (F_O)^{1/2} \left(\frac{R_1 R_2}{R_1 + R_2} \right)$$

For maximum Q at $F_{1/4}$ we require that $R_2/R_1 = 3.59$ and $Z_O = 76.7$ ohms, then the Q at quarter-wave frequency can be written as

$Q_{1/4} = 215\, (F_{1/4})^{1/2} R_2$

$$Q_{1/4} = 12.78(76.7)(F_{1/4})^{1/2}\, R_2 \left(\frac{1}{1 + R_2/R_1} \right)$$

Obtaining R_2 in terms of volume, $V = \pi R_2^2\, \lambda_{1/4}$ where $\lambda_{1/4}$ is the quarter wavelength of the resonator in inches. $\lambda_{1/4} = 2950/F_{1/4}$ for air dielectric.

$\lambda_{1/4} = \frac{2050}{F_{1/4}}$ for most coaxial lines with teflon dielectric

Solving for R_2 and substituting;

$$R_2^2 = \frac{F_{1/4}\, V}{2950\pi} \qquad R_2 = \frac{(F_{1/4}\, V)^{1/2}}{(9267.69)^{1/2}}$$

$$Q_{1/4} = 12.78\ (76.7)\ (F_{1/4})^{1/2}\ \frac{(F_{1/4}\, V)^{1/2}}{(9267.69)^{1/2}} \left(\frac{1}{1 + 3.59} \right)$$

and finally

$$Q_{1/4} = 2.218\, F_{1/4}\, (V)^{1/2}$$

or

$$Q_U = 2.218\, F_{1/4}\, (V)^{1/2} \left(\frac{F_O}{F_{1/4}} \right)^{1/2} = 2.218 \sqrt{F_{1/4} F_O V}$$

The fact that large values of C_{TMIN} require a coaxial resonator for maximum Q led to the conclusion that there must be a unique solution to the problem of determining which resonator type will give maximum Q in a particular design. This unique solution was obtained by combining the tuning equations for each resonator with the Q-volume equations. This analysis has shown that there is a direct relationship between the minimum tuning reactance level X_{CTMIN} and volume. The following equations were used to derive these relationships:

$X_{CTMIN} = Z_O$ TAN βL for both resonators but for a specific value of X_{CTMIN} the characteristic impedances and the electrical wavelength will be different. This requires that the Z_O and βL values used in the derivation apply specifically to either the coaxial or helical resonator.

Let

F4COAX = 1/4-wave frequency for coaxial resonator

F4 HEL = 1/4-wave frequency for helical resonator

then,

$$X_{CT\,MIN} = 76.7 \text{ TAN}\left(\frac{\pi}{2}\,\frac{F_{MAX}}{\text{F4 COAX}}\right) \text{ (coaxial resonator)}$$

Also

$$X_{CT\,MIN} = \frac{95355}{\text{F4 HEL } V^{1/3}} \text{ TAN}\left(\frac{\pi}{2}\,\frac{F_{MAX}}{\text{F4 HEL}}\right) \text{(helical resonator)}$$

If we set the $Q_{HEL} = Q_{COAX}$ then

$$51\,(F_{MAX})^{1/2}\,V^{1/3} = 2.218\,(\text{F4 COAX})\,(V)^{1/2}\left(\frac{F_{MAX}}{\text{F4 COAX}}\right)^{1/2}$$

solving for volume.

$$V^{1/6} = \frac{51\,(F_{MAX})^{1/2}}{2.218\,(\text{F4 COAX})\left(\frac{F_{MAX}}{\text{F4 COAX}}\right)^{1/2}} = \frac{51}{2.218\,(\text{F4 COAX})^{1/2}}$$

now

$$\text{F4 COAX} = \frac{\pi}{2}\,\frac{F_{MAX}}{\text{TAN}^{-1}\left(\frac{X_{CT\,MIN}}{76.7}\right)}$$

so that

$$V = \left(\frac{51}{2.218\,(\text{F4 COAX})^{1/2}}\right)^6 = \frac{3.82 \text{ X } 10^7}{F_{MAX}^{\;3}}\left[\text{TAN}^{-1}\left(\frac{X_{CT\,MIN}}{76.7}\right)\right]^3$$

Thus for any value of $X_{CT\,MIN}$ and F_{MAX} there is a unique F4 COAX which specifies a unique volume at which the helical resonator and coaxial resonator have equal Q.

$$X_{CT\,MIN} = 76.7 \text{ TAN}\left[\frac{F_{max}}{337}\,V^{1/3}\right]$$

For uhf resonator designs where $F_{MAX} = 400$ MHZ. Figure 1-59 is a plot of the equal Q-curve for varying values of $X_{CT\ MIN}$ and volume.

Values other than unity for the coaxial resonator Q, to helical resonator Q are shown to illustrate the relative Q difference between the two resonator types.

a. Examples

1. A varactor tuning scheme has a minimum tuning capacity of 4 picofarads at $F_{MAX} = 400$ mhz/$X_{CT\ MIN} = 100$ ohms. Figure 1-59 shows that for volumes less than .459 in^3 the highest Q resonator is of helical construction.

   This can be verified from the basic equations,

   coaxial resonator,

$$100 = 76.7 \text{ TAN } (90° \frac{400}{\text{F4 COAX}})$$

$$\text{F4 COAX} = 685 \text{ mhz}$$

$$Q_{COAX} = 2.218\ (685)(.459)^{1/2} \left(\frac{400}{685}\right)^{1/2} \approx 786$$

   helical resonator,

$$Q_{HELICAL} = 51\ (400)^{1/2}\ (.459)^{1/3} \approx 786$$

2. A helical resonator and a coaxial resonator are constructed for the uhf band with equal volumes of .2 cubic inches and they both must resonate a capacitive reactance of 150 ohms at 400 mhz. Their Q's are compared;

   coaxial resonator,

$$150 = 76.7 \text{ TAN} \left(90° \frac{400}{\text{F4 COAX}}\right)$$

$$\text{F4 COAX} = 572 \text{ mhz}$$

$$Q_{COAX} = 2.218\ (572)(.2)^{1/2} \left(\frac{400}{572}\right)^{1/2} \approx 474$$

   helical resonator,

$$Q_{HELICAL} = 51\ (400)^{1/2}\ (.2)^{1/3} \approx 596$$

$$\frac{Q_{COAX}}{Q_{HELICAL}} = .795 \approx .8 \text{ as verified by the curve.}$$

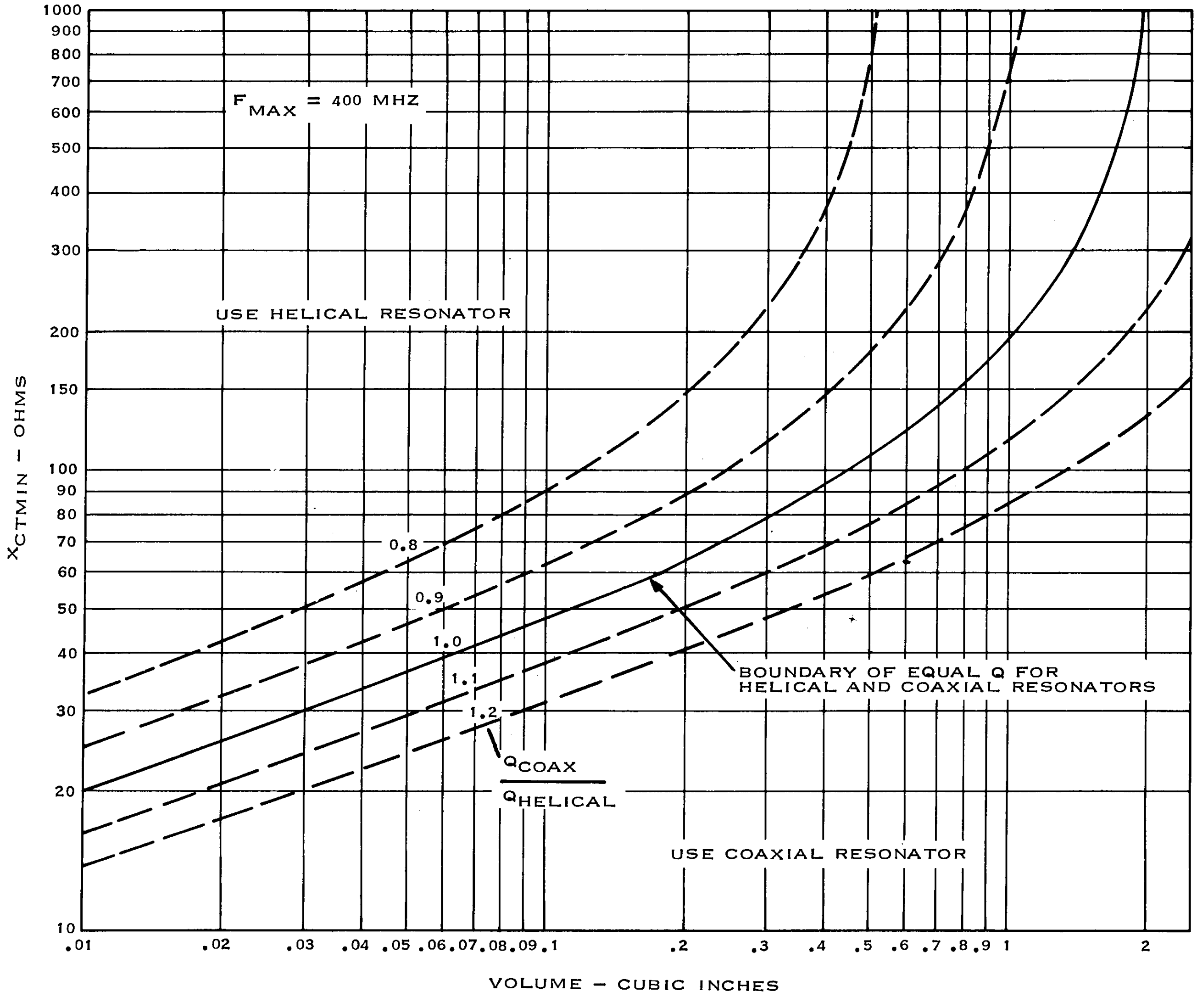

Figure 1-59. Q-volume trade-off for transmission line resonators.

3.4 Project Performance and Schedule Chart

(UNCLASSIFIED)

COLLINS RADIO COMPANY
TUNER FUNCTIONAL GROUP

PROJECT PERFORMANCE AND SCHEDULE (SHEET 1)

(PROJECT SERIAL NO. 62105N XF 52545 001)

CONTRACT NO. N00039-69-C-2602 REPORT DATE: 3 JANUARY 1970

PERIOD COVERED: 9/15/69 TO 1/3/70

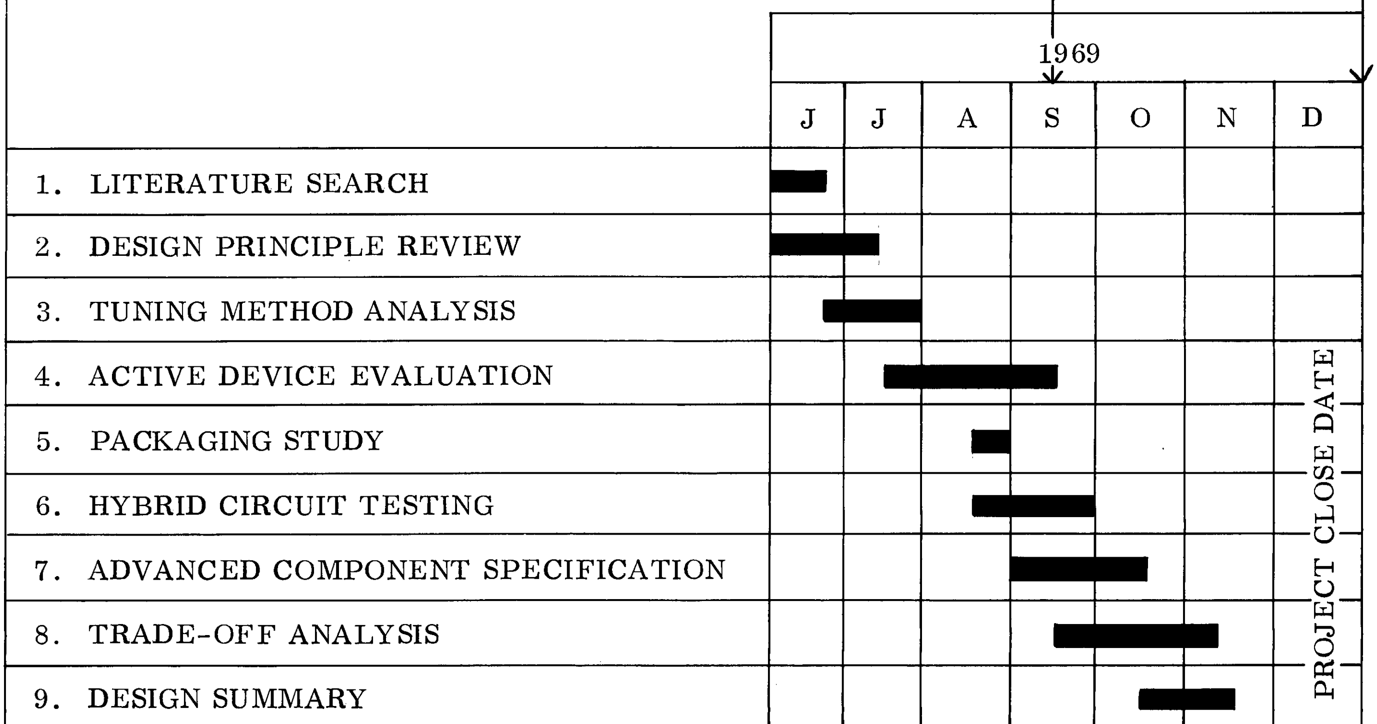

(UNCLASSIFIED)

COLLINS RADIO COMPANY

TUNER FUNCTIONAL GROUP

PROJECT PERFORMANCE AND SCHEDULE (SHEET 2)

CONTRACT NO. N00039-69-C-2602 REPORT DATE: 3 JANUARY 1970

PERIOD COVERED: 9/15/69 TO 1/3/70

LEGEND ■ - - WORK PERFORMED

□ - - SCHEDULE OF PROJECTED OPERATION

ITEM: ESTIMATED COMPLETION IN PERCENT OF TOTAL EFFORT TO BE EXPENDED.

1.	LITERATURE SEARCH	100%
2.	DESIGN PRINCIPLE REVIEW	100%
3.	TUNING METHOD ANALYSIS	100%
4.	ACTIVE DEVICE EVALUATION	100%
5.	PACKAGING STUDY	100%
6.	HYBRID CIRCUIT TESTING	100%
7.	ADVANCED COMPONENT SPECIFICATION	100%
8.	TRADE-OFF ANALYSIS	100%
9.	DESIGN SUMMARY	100%

NOTES AND REMARKS:

N/A

4. CONCLUSIONS

a. High Q varactor tuned resonators have large Q changes versus frequency.
b. Small values of stray capacitance improve Q variation with frequency and minimize needed tuning capacity ratio.
c. Diode switched capacitance matrix tuning can be synthesized by computer techniques; however, optimization of channel selection was not obtained due to lack of time.
d. Large reverse bias capacity values for switch diodes make circuit optimization difficult if not impossible.
e. Bandpass filters consisting of many sections can offer adequate image attenuation with a sacrifice in nose bandwidth.
f. A parametric up-converter does not offer a volume advantage over conventional pre-selection techniques.
g. Varactor tuning cross modulation has major dependence on operating Q and varactor total capacitance ratio.
h. Thin-film spiral inductors offer moderate Q in a very small volume. All air core coils are susceptible to shielding Q degradation.
i. Helical resonator volumes less than .005 cubic inch are not practical.
j. Low side injection gives better image rejection.
k. Minimum volume filters can be constructed using a large number of moderate Q resonators while giving adequate image rejection.
l. Thin-film hybrid construction techniques offer the best promise for microminiaturization in tuner fabrication.
m. Monolithic techniques are not practical as a total construction technique in the near future.
n. The choice of a high Q resonator depends on the volume and reactance level of the resonator.

PART II RECOMMENDATIONS

1. GENERAL DISCUSSION

This study has examined the technical details of uhf tuner design from the standpoints of theoretical analysis of the block diagram, study of the components available today and projected for the future, and the processes for construction which apply to microminiature design. The trade-offs in these areas have been presented in analytical, graphical, and chart form. None the less, a totally formalized method of tuner design is still difficult, if not impossible, because of the many complex branches in the conceptual process. Often, the weighting factors associated with a performance specification are so subjective that analytical trade-offs are not possible.

At this point, it is recommended that further study in the microminiature uhf tuner area be conducted in two major areas, running concurrently in time. These are as follows:

a. Finalize the design of and construct a prototype tuner for the 225 to 400 mhz band.
b. Initiate development of selected new components.

Description of these studies and developments is further defined in the following sections.

1.1 Prototype Tuner

It is recommended that a prototype uhf tuner be developed to further define the theoretical, experimental and process limitations of a very small tuner design. This prototype should be constructed using thin-film hybrid processes and should have usable but not high performance characteristics.

A summary of performance goals required is as follows:

Noise figure:	17 db.
Image rejection:	60 db.
Spurious responses:	60 db below 10 db s+n/n sensitivity.
Cross-modulation:	0 dbm available, 30 percent am, at ±5 mhz for -10 db cm with a 100-microvolt desired signal.
Intermodulation:	Two -21 dbm available signals, spaced 500 khz, one modulated 30 percent at 1000 hz will produce a 3rd order IM product on the desired channel having not more than 10 db s+n/n.
Antenna radiation:	50 microvolts across 50-ohm load.
Antenna, injection, if output impedance:	50 ohms.
Tuner insertion gain:	10 db.

Power requirements:	250 milliwatts dc. 0 dbm injection.
Size:	0.15 cubic inch.

Some discussion of these specifications is in order. The 17-db noise figure requirement is certainly not as low as can be obtained in the 225 to 400 mhz range. In an am system with 3000 hz audio bandwidth, a 17-db noise figure results in 5 microvolt am sensitivity for 10 db s+n/n ratio. This is a useful sensitivity in tactical equipment where the desired signal strength is usually 20 microvolts or more. This sensitivity allows the use of a hot carrier diode balanced mixer in the front end which offers a good trade-off in sensitivity for dynamic range. The necessity for rf amplification is eliminated. The cross-modulation and inter-modulation specifications are commensurate with such a design. The 60-db image and spurious response specification is believed to be ample for interference immunity under most situations. This one specification is directly traded with physical size.

A block diagram of a front end meeting these specifications is shown in figure 2-1. The preselection filters are varactor tuned over their respective ranges. Development of incremental tuning components in silicon integrated chip form would eventually replace the varactors and allow one filter to cover the full range. The injection frequency range is broken into two bands so as to minimize the complexity of an associated, digitally stabilized, injection signal source. High side injection is thus used on the lower half of the band and high side on the other. The if preamplifier is required to provide a low noise figure for the balanced mixer. It is assumed that the if output goes directly to a crystal bandpass filter in the receiver.

Figure 2-2 shows a top view of one of the preselection filters. These filters are designed according to minimum volume theory using Cohn minimum loss synthesis of coupling and end loading. Accordingly, they have a rather large number of small spiral coil resonators, typically six. Silicon varactor chips and MOS capacitors are used for tuning and decoupling together with thin-film tantalum isolation resistors.

1.2 Advanced Component Requirements

It is to be expected that during the next five years steady progress will be made in the components available for uhf tuner fabrication.

Obvious trends include the following:

a. Higher Q varactors.
b. Better exponent control of hyperabrupt junction varactors.

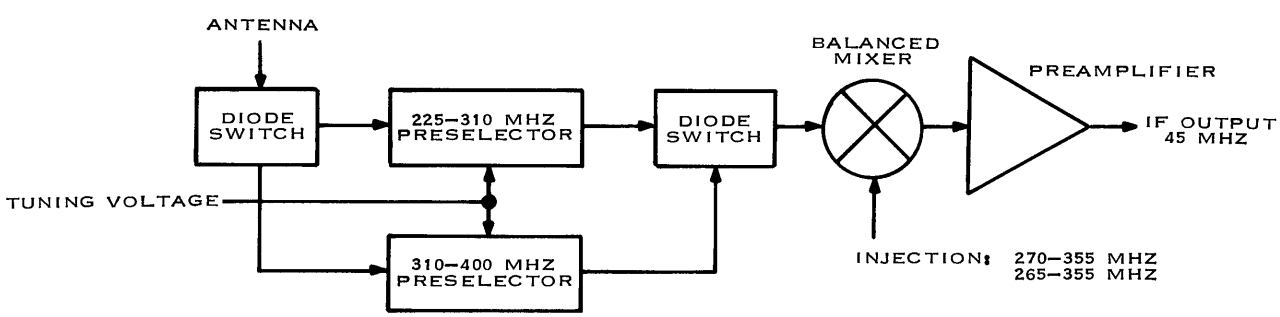

Figure 2-1. Block diagram of 225 to 400 mhz tuner.

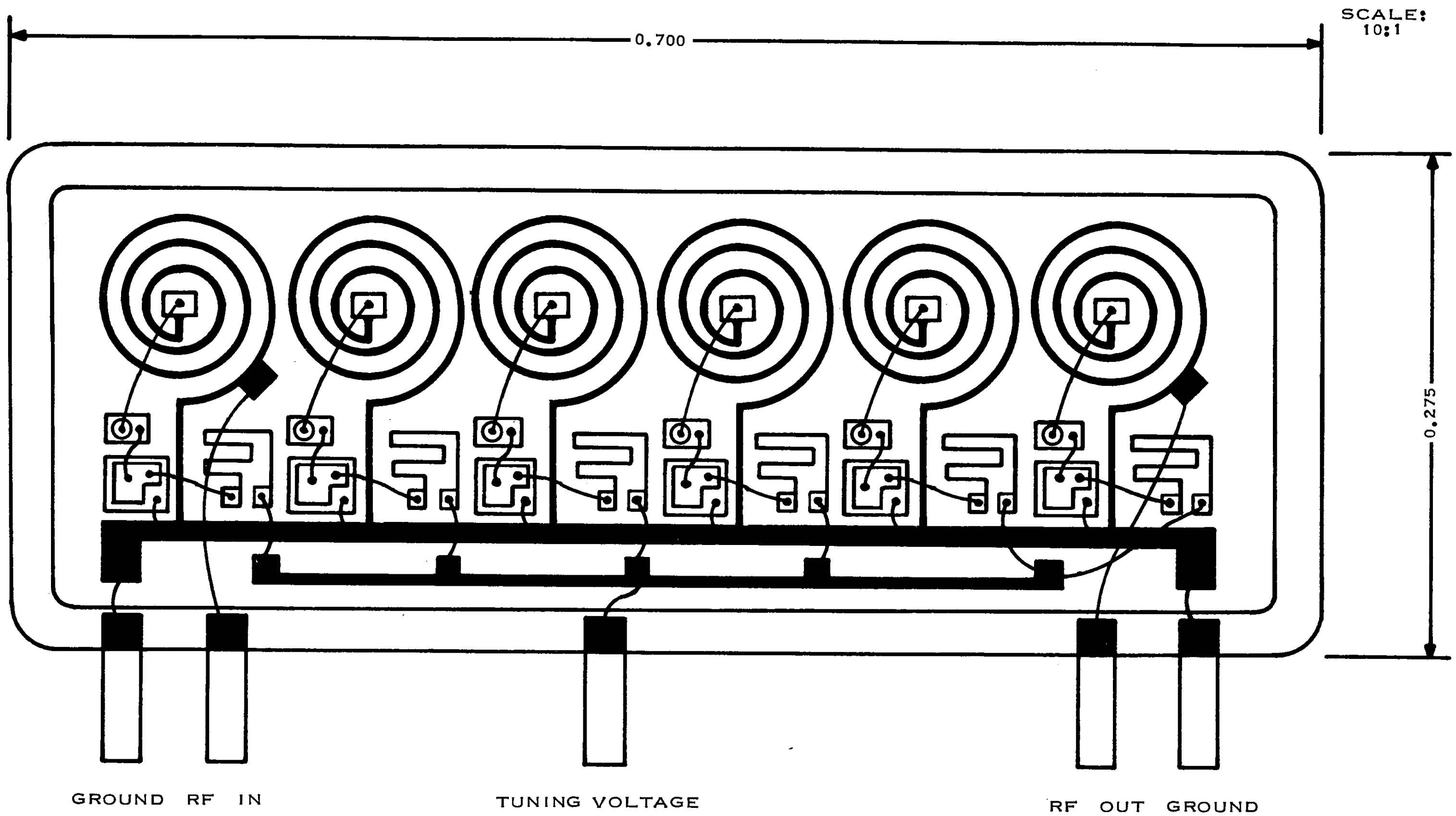

Figure 2-2. Plan view of thin-film hybrid 6-pole uhf preselector filter.

c. Lower active device noise figure.
d. Higher gain bandwidth products of field-effect transistors.
e. Improvements in monolithic diffusion accuracy, notably ion-implantation.
f. Higher reliability through silicon refinement purity and improved manufacturing processes.
g. Cost reduction.

These trends are expected to continue as a direct result of small discrete breakthroughs, competition, and increased manufacturing volume. A major breakthrough in uhf tuner design would occur if materials exhibiting room temperature superconductivity were found. This would reverse the present situation wherein microminiature inductor Q is considerably less than that of fixed and voltage variable capacitors.

The following device development and areas of investigation are needed and recommended for improvement in microminiature uhf tuner design in the next decade:

a. Basic research in high Q ferrite materials for the uhf spectrum. These would find application in toroidal form for winding high value toroidal inductors and in sheet form for deposition of smaller, high inductance spiral inductors. Reasonable permeability to expect would be in the range 5 to 10 and the loss tangent should be such that inductor Q of 100, minimum, at 400 mhz is obtainable. The permeability temperature coefficient should be small and within the compensation range of negative coefficient capacitors. The Curie temperature must exceed 100 °C.
b. Development of a silicon integrated circuit tuning voltage generator for varactors. Specifications should include the following:

Output voltage:	5 to 100 volts.
Output current:	10 microamperes.
Output noise:	0.5 percent low frequency ripple; rms noise at 30 mhz not more than 1.0 microvolt per root megahertz.
Dynamic output impedance:	500 ohms
Control:	Output voltage programmable either by means of a single external variable resistance or by an input control voltage of 0 to 100 millivolts.
Input voltage:	12 to 24 volts.
Total dissipation:	50 milliwatts, maximum.

It is intended that this integrated circuit be used for tuning voltage generation which is programmed either with an external resistance ladder or by a phase discriminator servo loop operating on a tuned circuit at the tuner injection frequency.

c. Integrated MOS binary capacitor. This component would be required for a step-tuned preselector filter having greater dynamic range than a varactor-tuned filter. It would consist of four binary weighted value MOS capacitors that are switched between a node and ground by means of charge storage diodes. The diode currents would be controlled

by integral combinational logic to provide decoding from 100's and 10's digits in bcd input to straight-line-incremented frequency with an inductor connected to the capacitive node. Specifications should include the following:

Capacitance values:	A, B, C, and D. (To be determined.)
Q:	100 minimum at 400 mhz.
Logic level:	TTL 0 to 5 volts.
Operating voltage:	+5 vdc.

d. Uhf JFET cascode amplifier. A low noise integrated cascode amplifier chip is required to implement the rf gain and agc function in a hybrid uhf tuner. The junction field-effect transistor is to be preferred over an MOS field-effect cascode because of uhf noise figure superiority. The node between the common source and the common gate stages must be wide-band to eliminate a tuning requirement. It should include the following specifications.

Input capacitance:	1 pf.
Transconductance:	10,000 micromhos.
Output capacitance:	1 pf.
Reverse transfer capacitance:	0.01 pf.
Gain at 400 mhz:	15 db.
Gain control range:	20 db.
Dynamic range:	110 db.

e. 225 to 400 mhz integrated balanced mixer. An integrated circuit doubly balanced mixer chip with unbalanced input, output, and injection ports is required for the frequency translation function in a hybrid uhf tuner. This may be developed along with the JFET cascode rf amplifier to produce a complete front end on one silicon chip, exclusive of tuning elements. Balanced mixer integrated circuit techniques may be similar to, or based upon, those currently used to produce low-frequency 4-quadrant multipliers. It may be necessary to include a wide-band injection power amplifier stage to provide sufficient local oscillator signal for high dynamic range. Specifications should include the following:

Port impedances:	50 ohms.
Insertion loss:	8 db.
Excess noise:	0.2 db.
Injection to signal port balance:	30 db.
Saturation:	+2 dbm for 1 db gain compression.
Spurious performance:	Equal to or better than present hot carrier diode balanced mixers.

f. A basic semiconductor research study might be profitable in the area of the inversion capacitance variation of an MOS junction as a function of light flux as mentioned by Grove, et al (see reference 24). Grove shows in his figures 13 and 14, that, with proper dc bias, the inversion capacitance is independent of bias over a wide range and dependent on white light illumination. This effect offers the promise of a distortion-free tuning element for uhf preselection filters.

PART III SUPPLEMENTARY DATA

1. RECEIVER NOISE TEMPERATURE

It is often more convenient to work with noise temperature rather than with noise figure or noise factor. The noise factor, F, is the noise figure, NF, expressed as a ratio rather than in decibels so that

$$F = 10^{NF/10}$$

The noise temperature in degrees Kelvin is related to the noise factor by

$$T = 290\ (F-1)$$

and the noise factor to the noise temperature by

$$F = 1 + T/290$$

The overall noise factor, F_E, of a set of cascaded devices is given by Friis[25] equation

$$F_E = F_1 + \frac{F_2-1}{G_1} + \frac{F_3-1}{G_1G_2} + \ldots \frac{F_N-1}{G_1G_2 \ldots G_{N-1}}$$

where F_N is the noise factor of the Nth stage and G_N is the available power gain of that stage expressed as a power ratio. Substitution into this equation gives the overall noise temperature T_E as

$$T_E = T_1 + \frac{T_2}{G_1} + \frac{T_3}{G_1G_2} + \ldots \frac{T_N}{G_1G_2 \ldots G_{N-1}}$$

where T_N is the noise temperature of the Nth stage or device. It is further convenient to define the noise temperature contribution from the Nth stage as

$$T_{CN} = \frac{T_N}{1 \cdot G_1G_2G_3 \ldots G_{N-1}}$$

so that the overall noise temperature now becomes the sum of the temperature contributions of the individual stages or

$$T_E = T_{C1} + T_{C2} + T_{C3} + T_{C4} \ldots T_{CN}$$

For a passive device such as a filter, where only thermal noise is present, the noise temperature of the device is given by

$$T_N = T_A\left(\frac{1}{G_N} - 1\right)$$

where T_A is the ambient temperature of the device in degrees Kelvin and G_N is the available gain (conjugate matched gain) of the device. Note that for a passive device, G_N is always less than or equal to unity.

2. OPTIMAL FILTER VOLUME

The optimum number of resonators, N_v, resulting in minimum total filter volume is found by relating the volume to the selectivity equation and taking the first derivative with respect to N, the number of resonators. It has been proven (section 10) that

$$\alpha_R = -6 - L_O + 20\ N\ \mathrm{LOG}\left(\frac{L_O}{4.343N}\ Q_U\ \frac{BW}{f_o}\right)$$

Solving this for Q_U gives

$$Q_U = \frac{4.343N}{L_O} \cdot \frac{f_o}{BW} \cdot 10^{\frac{\alpha_R + 6 + L_O}{20N}}$$

We postulate the dependency of total filter volume on resonator Q_U by the function

$$V_T = NCQ_U^p$$

where C is a constant of proportionality and p is the law of variation. Combining with the selectivity equation gives

$$V_T = NC\left[\frac{4.343N}{L_O} \cdot \frac{f_o}{BW} \cdot 10^{\frac{\alpha_R + 6 + L_O}{20N}}\right]^p$$

Let $A = (\alpha_R + 6 + L_O)/20$

and $B = \dfrac{4.343}{L_O} \cdot \dfrac{f_o}{BW}$

$$V_T = CB^p\, N^{p+1} . 10^{\frac{Ap}{N}}$$

$$\frac{dV_T}{dN} = CB^p \left[N^{p+1} \cdot \ln 10 \cdot \left(- \frac{Ap}{N^2} \right) + 10^{\frac{Ap}{N}} \cdot (p+1)\, N^p \right]$$

$$= CB^p\, N^p \cdot 10^{\frac{Ap}{N}} \left(p+1 - \frac{Ap}{N} \ln 10\right)$$

when

$$N = N_V, \frac{dV_T}{dN} = 0$$

$$O = p+1 - \frac{Ap}{N_V} \ln 10$$

$$N_V = \frac{Ap \ln 10}{p+1}$$

Replacing A and noting that ln 10 = 1/LOG e = 1/.4343 gives

$$N_V = \frac{p}{p+1} \cdot \frac{\alpha R^{+6+L_O}}{8.686}$$

It is necessary to prove that the above N_V is unique; that is, there are no other minimums in the range $0 \geq N \geq \infty$. This proof was suggested by R. W. Carroll of Collins technical staff. If we show that the second derivative of V_T with respect to N is positive for all positive N and p, then uniqueness is demonstrated.

$$\frac{dV_T}{dN} = CB^p\, N^p\, 10^{\frac{Ap}{N}} \left(p+1 - \frac{Ap}{N} \ln 10\right)$$

$$\frac{d^2V_T}{dN^2} = CB^p \left\{ \frac{d}{dN}\left[N^p\, 10^{\frac{Ap}{N}} \right] \left(p+1 - \frac{Ap}{N} \ln 10\right) + N^p\, 10^{\frac{Ap}{N}} \frac{d}{dN}\left[p+1 - \frac{Ap}{N} \ln 10 \right] \right\}$$

$$= CB^p \left\{ \left(p+1 - \frac{Ap}{N} \ln 10\right) \left[N^p\, 10^{\frac{Ap}{N}} \ln 10 \left(- \frac{Ap}{N^2} \right) + 10^{\frac{Ap}{N}}\, pN^{p-1} \right] \right.$$

$$\left. + N^p\, 10^{\frac{Ap}{N}} \left[Ap \ln 10 \left(\frac{1}{N^2} \right) \right] \right\}$$

This reduces to

$$\frac{d^2V_T}{dN^2} = pCB^p \cdot 10^{\frac{Ap}{N}} \cdot N^{p-3} \cdot (p+1) \left[N^2 - \frac{2Ap \ln 10}{p+1} N + \frac{p(A \ln 10)^2}{p+1} \right]$$

The factors outside the square brackets are positive by inspection. If there are no real roots of the terms in the square brackets, then it is also positive. This follows from the consideration that the bracketed function of N is parabolic and concave upwards. If it is always positive, it must not cross the F(N) = 0 axis and the roots are therefore imaginary. The roots are:

$$\frac{Ap \ln 10}{p+1} \pm \sqrt{\left(\frac{Ap \ln 10}{p+1}\right)^2 - \frac{(Ap \ln 10)^2}{p(p+1)}}$$

The radical reduces to

$$\pm \frac{Ap \ln 10}{p+1} \sqrt{-\frac{1}{p}}$$

and therefore the two roots are imaginary, providing that p is positive. The latter is true for any conceivable resonator. The second derivative is therefore positive for all N, and N_V is accordingly a unique minimum of V = F(N).

Finally, $N=N_V$ can be substituted into the relative selectivity equation

$$\alpha_R = -6 - L_O + 20 \text{ N LOG} \left(\frac{L_O}{4.343N} Q_U \frac{BW}{f_o} \right)$$

giving

$$L_O Q_U \frac{BW}{f_o} = \frac{pe^{\frac{p+1}{p}}}{2(p+1)} (\alpha_R + 6 + L_O)$$

which, when $L_O << \alpha_R$ is simplified to

$$L_O Q_U \frac{BW}{f_o} \cong \frac{pe^{\frac{p+1}{p}}}{2(p+1)} (\alpha_R + 6)$$

3. MINIMUM VOLUME FILTERS WITH MULTIPLE FREQUENCY ATTENUATION REQUIREMENTS

The equations for the design of a minimum volume filter with a stopband loss, L_O db, and a stopband relative attenuation, α db, at a bandwidth, BW, were derived in section 2. In some cases it is desired to specify minimum relative stopband attenuations α_1 and α_2 at bandwidths of BW_1 and BW_2 respectively. There is no loss of generality in specifying that

$$BW_1 \leq BW_2$$

The relative stopband attenuation α_1 at a bandwidth BW_1 for a Cohn filter is shown in section 2 to be

$$\alpha_1 = -6 - L_O + 20\ N\ LOG \left(\frac{L_O}{4.343\ N}\ Q\ \frac{BW_1}{f_o} \right) DB$$

Likewise, the attenuation α_X at a bandwidth BW_X is given by

$$\alpha_X = -6 - L_O + 20\ N\ LOG \left(\frac{L_O}{4.343\ N}\ Q\ \frac{BW_X}{f_o} \right) DB$$

Subtracting α_1 from α_X then gives

$$\alpha_X = \alpha_1 + 20\ N\ LOG\ (BW_X/BW_1)$$

If the attenuation, α_X, of the filter when $BW_X = BW_2$ is greater than the required attenuation, α_2, then the filter designed for the single frequency attenuation specification is also a minimum volume filter for the 2-frequency attenuation filter problem.

Often, however, the minimum volume filters designed for a bandwidth of BW_1 or BW_2 will not provide the required attenuation at the other frequency as shown for filters A and B in figure 3-1. The optimum number of sections for a minimum volume filter was given in section 2 as

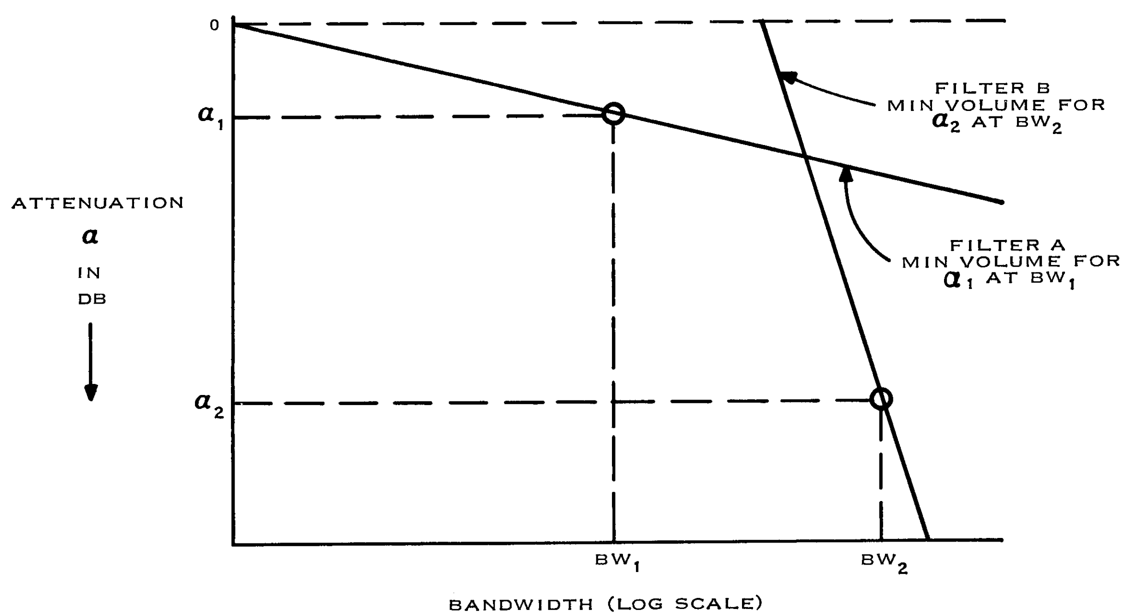

Figure 3-1. Selectivity curves for single frequency attenuation, minimum volume filters.

$$N_V = \frac{p}{p+1} \cdot \frac{\alpha + L_O + 6}{8.686}$$

Since α_2 is greater than α_1, then also the number of sections in minimum volume filter B will be greater than that of filter A. Also, it is evident that the stopband slope of filter B is greater than that of filter A. It was also shown in section 2 that the volume, V, of a Cohn filter has a minimum for a certain number of sections, N, and that d^2V/dN^2 is always positive. The form of the curve of V versus N, therefore, is as shown in figure 3-2. For any given number of filter sections, the Cohn filter design will realize a given stopband attenuation and passband loss with the lowest possible unloaded Q. Since volume is monotonically related to Q, the volume is minimum for that number of sections.

Now consider a sequence of Cohn filters providing a relative attenuation, α_1, and a bandwidth, BW_1, with increasing number of sections as shown in figure 3-3. From figure 3-2 it will be seen that the volume is increasing as N increases. The lowest number of sections, N_O, that just meets the specification at a bandwidth BW_2 is, therefore, the minimum volume filter meeting the attenuation at both BW_1 and BW_2. Increasing the number of sections beyond N_O, while just meeting α_1 at BW_1, results in a larger volume filter. On the other hand, increasing the number of sections beyond N_O while just meeting α_2 at BW_2 results in a lower volume filter, but it will no longer meet the attenuation α_1 at BW_1.

The number of sections that results in a minimum volume filter providing relative attenuations α_1 and α_2 at BW_1 and BW_2, respectively, is obtained by choosing N such that the attenuation curve goes exactly through both attenuation points. This number may be found by setting

$$\alpha_X = \alpha_1 \text{ and } BW_X = BW_1$$

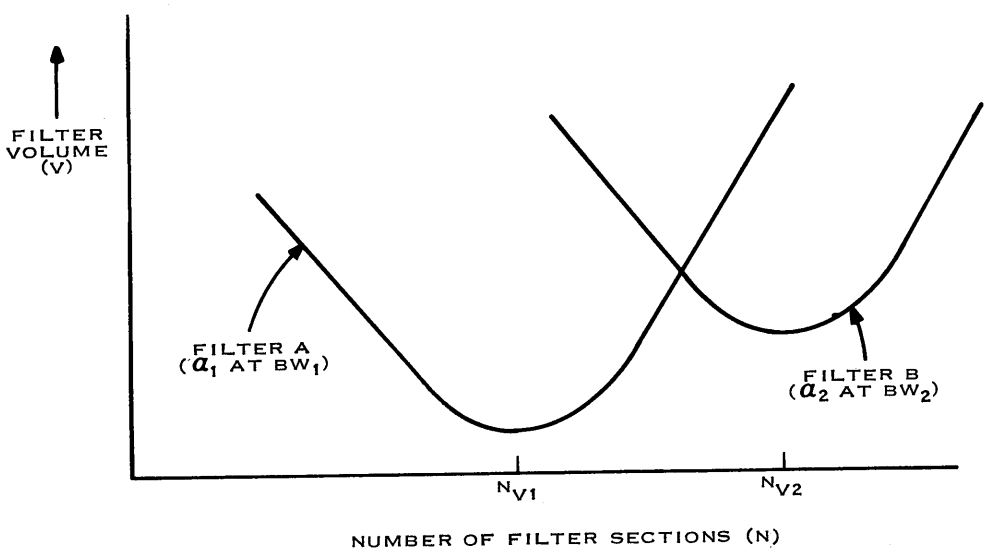

Figure 3-2. Filter volume versus number of filter sections.

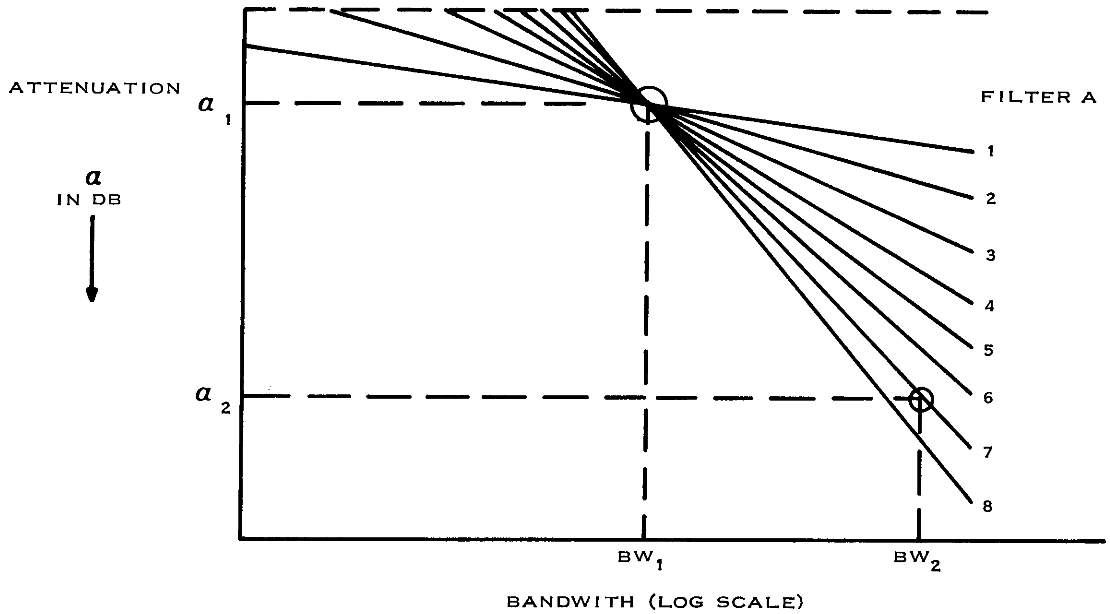

Figure 3-3. Cohn filter attenuation curves for a sequence of filters with increasing numbers of filter selections.

and solving for N_O to obtain

$$N_O = \frac{a_2 - a_1}{20 \text{ LOG } (B\omega_2/B\omega_1)}$$

The resulting filter, is, of course, still a Cohn filter and therefore the general equations given in section 10 still apply.

4. DERIVATION OF TUNING EQUATIONS FOR LUMPED INDUCTOR RESONATOR

Refer to figure 1-7(A) for circuit definition.

The resonance relationships at the high and low ends of the tuning range can be written:

$$X_C = X_L \text{ at resonance}$$

$$\frac{1}{\omega_{MAX}\left(C_{V\,MIN} + C_D\right)} = \omega_{MAX} L_{EQ} \qquad \frac{1}{\omega_{MIN}\left(C_{V\,MAX} + C_D\right)} = \omega_{MIN} L_{EQ}$$

The total capacitor limitation can be obtained by taking the ratio of maximum to minimum capacity.

$$\frac{\left(C_{V\ MAX} + C_D\right)}{\left(C_{V\ MIN} + C_D\right)} = \left(\frac{F_{MAX}}{F_{MIN}}\right)^2 = \frac{\dfrac{C_{V\ MAX}}{C_{V\ MIN}} + \dfrac{C_D}{C_{V\ MIN}}}{1 + \dfrac{C_D}{C_{V\ MIN}}} = \bar{C}_T$$

Reducing this still farther we obtain the equations for the lumped inductor

$$\bar{C}_T \triangleq \frac{(\bar{C}_V + \bar{C}_D)}{(1 + \bar{C}_D)}$$

$$\bar{C}_T = \left(\frac{F_{MAX}}{F_{MIN}}\right)^2 = (\bar{F}_T)^2$$

From the resonance equation

$$\omega^2 = \frac{1}{LC}$$

we get

$$C_T = C_{T\ MIN} \left(\frac{F_{MAX}}{F_O}\right)^2$$

where the subscript T refers to the total capacitance, F_{MAX} is the resonant frequency when $C_T = C_{T\ MIN}$ and F_O is the resonant frequency for a given C_T.

In the analysis of both the transmission line and lumped inductor resonators it became apparent that the lumped inductor resonator could be treated in a way analogous to the transmission line. This was done by including the stray capacity C_D into the equations by defining a pole frequency F_P as:

$$\omega_P^2 \triangleq \frac{1}{C_D\, L_{EQ}}$$

When drawing this analogy the stray capacity for the transmission line circuit is ignored. This, then, makes the tuning curves for both resonator types very similiar as illustrated in figure 1-10 for $C_D = 0$. Although this analogy is introduced, the analysis does not depend upon its existence. Rather, it is a convenient concept to use when presenting the effects of circuit parameters on circuit performance.

At resonance, it is apparent that

$$\omega_O C_V + \omega_O C_D - \frac{1}{\omega_O L_{EQ}} = 0$$

Substituting for L_{EQ} in terms of the pole frequency gives:

$$\omega_O C_V + \omega_O C_D - \frac{\omega_P^2}{\omega_O} C_D = 0$$

$$1 + \frac{C_D}{C_V} - \left(\frac{\omega_P}{\omega_O}\right)^2 \frac{C_D}{C_V} = 0$$

$$\frac{C_D}{C_V} = \frac{1}{\left(\frac{\omega_P}{\omega_O}\right)^2 - 1}$$

When $\omega_O = \omega_{MAX}$, $C_V = C_{V\ MIN}$; hence

$$\frac{C_D}{C_{V\ MIN}} = \frac{1}{\left(\frac{F_P}{F_{MAX}}\right)^2 - 1}$$

Similarly, when $\omega_O = \omega_{MIN}$, $C_V = C_{V\ MAX}$, and

$$\frac{C_D}{C_{V\ MAX}} = \frac{1}{\left(\frac{F_P}{F_{MIN}}\right)^2 - 1}$$

The variable capacitance ratio, $C_{V\ MAX}/C_{V\ MIN}$, is then

$$\frac{C_{V\ MAX}}{C_{V\ MIN}} = \frac{\left(\frac{F_P}{F_{MIN}}\right)^2 - 1}{\left(\frac{F_P}{F_{MAX}}\right)^2 - 1} = \frac{\left(\frac{F_P}{F_{MAX}} \cdot \frac{F_{MAX}}{F_{MIN}}\right)^2 - 1}{\left(\frac{F_P}{F_{MAX}}\right)^2 - 1} = \frac{\left(\frac{F_{MAX}}{F_{MIN}}\right)^2 - \left(\frac{F_{MAX}}{F_P}\right)^2}{1 - \left(\frac{F_{MAX}}{FP}\right)^2}$$

This equation when solved for F_P/F_{MAX} yields

$$\left(\frac{F_P}{F_{MAX}}\right)^2 = \frac{\frac{C_{V\ MAX}}{C_{V\ MIN}} - 1}{\frac{C_{V\ MAX}}{C_{V\ MIN}} - \left(\frac{F_{MAX}}{F_{MIN}}\right)^2}$$

which defines the pole frequency in terms of the variable capacitance ratio and the tuning ratio. The former equation also shows that the variable capacitance ratio approximates the frequency ratio squared as the pole, or the parasitic resonant frequency becomes large compared to the maximum tuned frequency.

The required equivalent inductance is

$$L_{EQ} = \frac{1}{\omega^2_{MAX}\,(C_{V\ MIN} + C_D)} = \frac{1}{\omega^2_{MAX}\, C_{T\ MIN}}$$

or in terms analogous to the transmission line expressions:

$$L_{EQ} = \frac{1}{\omega^2_{MAX}\, C_{V\ MIN}\,(1 + C_D/C_{V\ MIN})}$$

$$L_{EQ} = \frac{1}{\omega^2_{MAX}\, C_{V\ MIN}\left[1 + \frac{1}{\left(\frac{F_P}{F_{MAX}}\right)^2 - 1}\right]}$$

which may be reduced to

$$L_{EQ}\, C_{V\ MIN} = \frac{1}{\omega^2_{MAX}} - \frac{1}{\omega^2_{P}}$$

5. DERIVATION OF TUNING EQUATIONS FOR TRANSMISSION LINE RESONATOR

Refer to figure 1-7(B) for circuit definition.

The resonance relationships at the high and low ends of the tuning range can be written:

$$\frac{1}{\omega_{MAX}\,(C_D + C_{V\ MIN})} = Z_O \,\mathrm{TAN}\frac{\pi}{2}\frac{F_{MAX}}{F_{1/4}}\ ; \quad \frac{1}{\omega_{MIN}\,(C_{V\ MAX} + C_D)} = Z_O \,\mathrm{TAN}\frac{\pi}{2}\frac{F_{MIN}}{F_{1/4}}$$

The total capacitor limitation can be obtained by taking the ratio of maximum to minimum capacity as:

$$\frac{(C_{V\ MAX} + C_D)}{(C_{V\ MIN} + C_D)} = \frac{F_{MAX}}{F_{MIN}}\,\frac{\mathrm{TAN}\frac{\pi}{2}\frac{F_{MAX}}{F_{1/4}}}{\mathrm{TAN}\frac{\pi}{2}\frac{F_{MIN}}{F_{1/4}}} = \bar{C}_T = \frac{\bar{C}_V + \bar{C}_D}{1 + \bar{C}_D}$$

Also, it is possible to write the capacity at any frequency F_O as:

$$C_T = C_{T\ MIN}\left(\frac{F_{MAX}}{F_O}\right)\frac{\mathrm{TAN}\frac{\pi}{2}\frac{F_{MAX}}{F_{1/4}}}{\mathrm{TAN}\frac{\pi}{2}\frac{F_O}{F_{1/4}}}$$

Solving for the maximum allowable C_D we get:

$$\frac{C_D}{C_{V\ MIN}} = \frac{\bar{C}_T - \bar{C}_V}{1 - \bar{C}_T}$$

Finally the needed $\bar{C}_V$ can be obtained from substitution as

$$\bar{C}_V = \bar{C}_T + \bar{C}_D\,(\bar{C}_T - 1)$$

The required Z_O can be calculated from the following equations. At the maximum operating frequency:

$$Z_O = \frac{1}{\omega_{MAX}\,C_{T\ MIN}\,\mathrm{TAN}\frac{\pi}{2}\frac{F_{MAX}}{F_{1/4}}}$$

from which we define a $Z_O C_{V\,MIN}$ product as:

$$Z_O C_{V\,MIN} = \frac{1}{\omega_{MAX}\, C_I \,\mathrm{TAN}\frac{\pi}{2}\, \frac{F_{MAX}}{F_{1/4}}} \qquad C_I = (1 + \overline{C}_D)$$

6. CIRCUIT Q FOR LUMPED INDUCTORS

The nodal Q for the lumped resonator circuit of figure 1-7(A) is computed from the combination of the net Q's of the inductive and capacitive components.

$$\frac{1}{Q_T} \triangleq \frac{1}{Q_C} + \frac{1}{Q_L}$$

The Q for the inductor is

$$Q_L \triangleq \frac{X_L}{R_{L(\omega)}}$$

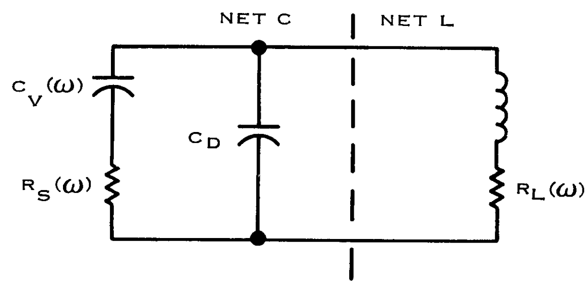

Figure 3-4. Lumped resonator circuit.

and this Q can be written in terms of the inductor Q at the maximum filter frequency F_{MAX} as follows:

$$\frac{Q_L\big|_{\omega_O}}{Q_L\big|_{\omega_{MAX}}} = \frac{\left(\frac{X_L}{R_{L(\omega)}}\right)\Big|_{\omega_O}}{\left(\frac{X_L}{R_{L(\omega)}}\right)\Big|_{\omega_{MAX}}} = \frac{X_L\big|_{\omega_O}}{X_L\big|_{\omega_{MAX}}} \; \frac{R_{L(\omega)}\big|_{\omega_{MAX}}}{R_{L(\omega)}\big|_{\omega_O}}$$

where

$$\frac{X_L\big|_{\omega_O}}{X_L\big|_{\omega_{MAX}}} = \frac{F_O}{F_{MAX}} \qquad \text{and} \qquad \frac{R_{L(\omega)}\big|_{\omega_{MAX}}}{R_{L(\omega)}\big|_{\omega_O}} = \left(\frac{F_O}{F_{MAX}}\right)^X$$

The value of the exponent X ranges between -1/2 and 0 and depends upon the operating frequency and coil construction. The final expression for inductor Q can now be given:

$$Q_L = Q_{L\,MAX} \left(\frac{F_O}{F_{MAX}}\right)^b \qquad 1/2 \le b \le 1$$

SKIN EFFECT (b = 1/2) — CONSTANT R_L (b = 1)

The exponent B of the frequency ratio is adjusted to give results compatible with actual coil operation; but it is a good assumption that the coil losses are due to skin loss in which case the value of B is 1/2. In many practical cases it is necessary to assign a value other than 1/2 for B, but in this report B = 1/2 is the best value presently known.

The Q of the net C portion can be obtained in forms of the pole frequency, F_{MAX}, and $Q_{V\ MAX}$. First, it will be necessary to show how the Q of the variable C is affected by circuit values and operating frequency. The pole frequency has been defined as that frequency at which C_D and L_{EQ} are resonant:

$$\omega_P^2 \triangleq \frac{1}{L_{EQ}\, C_D}$$

The net reactance of the parallel combination of C_D and L_{EQ} can be obtained in terms of L_{EQ} and ω_P as follows:

$$X_L = \omega L_{EQ}$$

$$X_{CD} = \frac{1}{\omega C_D} = \frac{\omega_P^2 L_{EQ}}{\omega}$$

$$X_T = X_L // X_{CD} = \frac{\omega L_{EQ}}{1-\left(\omega / \omega_P\right)^2}$$

The Q of the variable capacitor is defined and derived:

$$Q_V = \frac{1}{\omega C_V R_S} = \frac{1}{R_S} \frac{\omega L_{EQ}}{1-\left(\omega / \omega_P\right)^2}$$

where $X_{CV} = X_T$ at resonance.

The ratio of the variable capacitor Q at any frequency F_O to the Q at maximum frequency F_{MAX} is:

$$\frac{Q_V}{Q_{V\ MAX}} = \frac{R_S\,(\omega_{MAX})}{R_S\,(\omega_O)} \frac{\omega_O}{\omega_{MAX}} \frac{1-\left(\frac{\omega_{MAX}}{\omega_P}\right)^2}{1-\left(\frac{\omega_O}{\omega_P}\right)^2}$$

$$\frac{Q_V}{Q_{V\ MAX}} = \left(\frac{F_O}{F_{MAX}}\right)^A \frac{1 - \left(\frac{F_{MAX}}{F_P}\right)^2}{1 - \left(\frac{F_O}{F_P}\right)^2} \qquad 1/2 \leq A \leq 1$$

where the exponent A accounts for the variations in $R_S(\omega)$ as the resonator is tuned (from section 3.1.2.1.1).

The net Q of the capacitor circuit containing $R_S(\omega)$, $C_V(\omega)$, and C_D can now be computed. The parallel resistance and capacitive reactance are obtained assuming Q > 10.

$$R_P = Q_V^2 R_S \qquad X_P = \frac{1}{\omega(C_V + C_D)} = \omega L$$

The net capacitor Q is;

$$Q_{NET} = \frac{R_P}{X_P} = (Q_V^2 R_S) \cdot \omega(C_V + C_D) = \left(\frac{1}{\omega C_V R_S}\right)^2 R_S \, \omega(C_V + C_D)$$

$$Q_{NET} = Q_V \left(1 + \frac{C_D}{C_V}\right)$$

At resonance the admittance equation for the entire network is:

$$\omega_O C_V + \omega_O C_D - \frac{1}{\omega_O L_{EQ}} = 0$$

which yields an expression for the ratio C_D/C_V as:

$$\frac{C_V}{C_D} = \left(\frac{F_P}{F_O}\right)^2 - 1 \qquad \frac{C_D}{C_V} = \frac{1}{\left[\left(\frac{F_P}{F_O}\right)^2 - 1\right]}$$

Substituting this into the equation for net Q we get:

$$Q_{NET} = Q_V\left(1 + \frac{C_D}{C_V}\right) = Q_V\left(1 + \frac{1}{\left(\frac{F_P}{F_O}\right)^2 - 1}\right) = Q_V \frac{1}{1 - \left(\frac{F_O}{F_P}\right)^2}$$

Also, substituting the equation for Q_V the net Q becomes:

$$Q_{NET} = Q_{V\ MAX} \left(\frac{F_O}{F_{MAX}}\right)^A \frac{1 - \left(\frac{F_{MAX}}{F_P}\right)^2}{\left[1 - \left(\frac{F_O}{F_P}\right)^2\right]^2}$$

The Q's for the inductive and capacitive parts of the total resonator can now be combined to give the total resonator Q.

$$\frac{1}{Q_T} = \frac{1}{Q_L} + \frac{1}{Q_{NET}} \qquad Q_T = \frac{1}{\frac{1}{Q_L} + \frac{1}{Q_{NET}}}$$

$$Q_T = \cfrac{1}{\cfrac{1}{Q_{L\ MAX}\left(\frac{F_O}{F_{MAX}}\right)^B} + \cfrac{1}{Q_{V\ MAX}\left(\frac{F_O}{F_{MAX}}\right)^A \cfrac{1 - \left(\frac{F_{MAX}}{F_P}\right)^2}{\left[1 - \left(\frac{F_O}{F_P}\right)^2\right]^2}}}$$

which is written in final form as:

$$Q_T = Q_{V\ MAX} \cfrac{1}{\left(\frac{F_{MAX}}{F_O}\right)^B \frac{Q_{V\ MAX}}{Q_{L\ MAX}} + \left(\frac{F_{MAX}}{F_O}\right)^A \cfrac{\left[1 - \left(\frac{F_O}{F_P}\right)^2\right]^2}{1 - \left(\frac{F_{MAX}}{F_P}\right)^2}}$$

Also the ratio of total Q at F_O to total Q at F_{MAX} can be taken to illustrate the Q variation across a band of frequencies.

$$\frac{Q_T}{Q_{T\ MAX}} = \frac{\dfrac{Q_{V\ MAX}}{Q_{L\ MAX}} + 1 - \left(\dfrac{F_{MAX}}{F_P}\right)^2}{\left(\dfrac{F_{MAX}}{F_O}\right)^B \dfrac{Q_{V\ MAX}}{Q_{L\ MAX}} + \left(\dfrac{F_{MAX}}{F_O}\right)^A \dfrac{\left[1 - \left(\dfrac{F_O}{F_P}\right)^2\right]^2}{1 - \left(\dfrac{F_{MAX}}{F_P}\right)^2}}$$

Although the Q of the variable capacitor as an individual element is not used in the design analysis, it is curious to note the actual charge in this Q as a function of F_P and F_O. A curve has been presented to illustrate this interesting effect in figure 3-5.

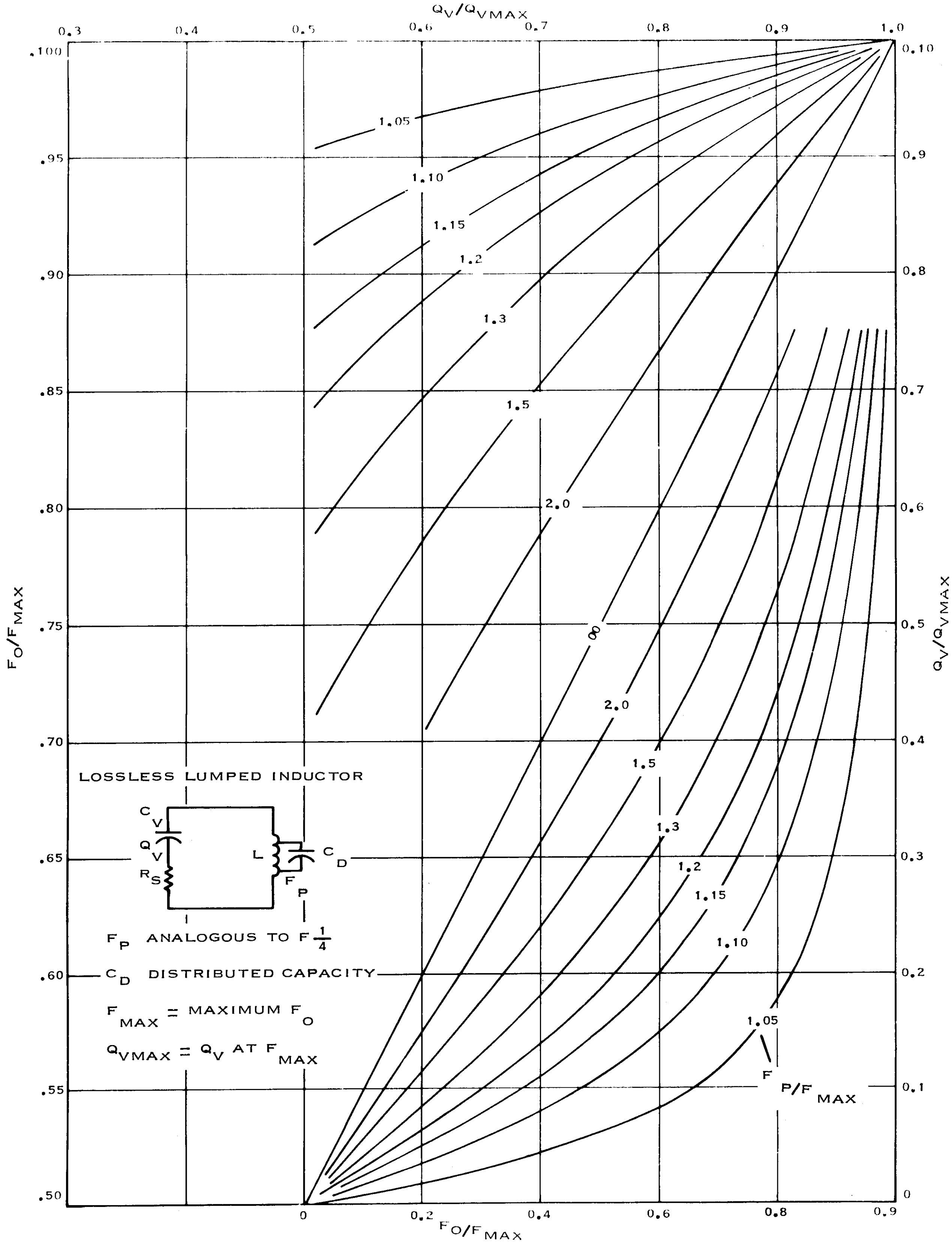

Figure 3-5. Q-behavior of tuning capacitor.

7. CIRCUIT Q FOR TRANSMISSION LINE RESONATORS

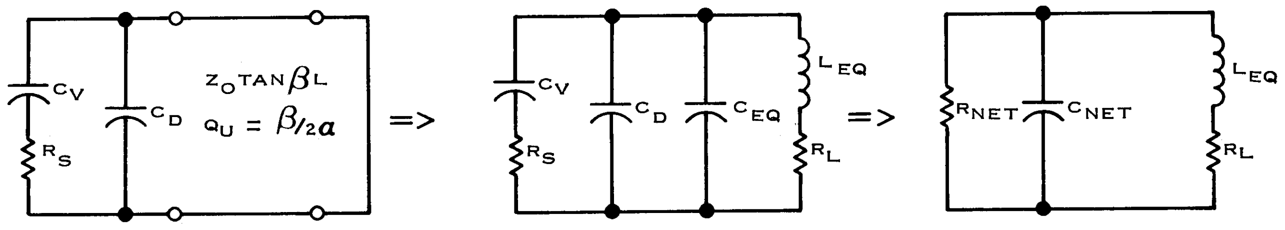

Figure 3-6. Transmission line resonator circuit.

$$Z_R = j\,Z_O\,\mathrm{TAN}\frac{\pi}{2}\,\frac{F_O}{F_{1/4}} \qquad Z_O = \sqrt{\frac{\frac{L}{\mathrm{INCH}}}{\frac{C}{\mathrm{INCH}}}}$$

$$Y_R = -j\,Y_O\,\mathrm{COT}\frac{\pi}{2}\,\frac{F_O}{F_{1/4}} \qquad Y_O = \frac{1}{Z_O}$$

$$Q_{1/4} = \omega_O\left(\frac{\frac{L}{\mathrm{INCH}}}{\frac{R}{\mathrm{INCH}}}\right)$$ assumes series ohmic losses only.

$$C_T = C_V + C_D \qquad Y = G(\omega) + j\,B(\omega)$$

$$C_{NET} = C_{EQ} + C_T$$

$$\theta_O = \frac{\pi}{2}\,\frac{F_O}{F_{1/4}}$$

EQUAL SLOPE CRITERIA

TRANSMISSION LINE	LUMPED EQUIVALENT
$B(\omega) = \omega C_T - Y_O \,\mathrm{COT}\,\theta_O$	$B(\omega) = \omega_O\, C_{NET}\left(\frac{\omega}{\omega_O} - \frac{\omega_O}{\omega}\right)$
$\frac{db}{d\omega} = C_T + \frac{Y_O\,\theta_O}{\omega\,\mathrm{SIN}^2\,\theta_O}$	$\frac{db}{d\omega} = C_{NET}\left(1 + \left(\frac{\omega_O}{\omega}\right)^2\right)$

AT RESONANCE

$$\omega_O C_T = Y_O \text{ COT } \theta_O$$

$$\left.\frac{db}{d\omega}\right|_{\omega_O} = \frac{Y_O}{\omega_O}\left[\text{COT}\,\theta_O + \frac{\theta_O}{\text{SIN}^2\,\theta_O}\right]$$

AT RESONANCE, $\omega = \omega_O$

$$\left.\frac{db}{d\omega}\right|_{\omega_O} = 2\,C_{NET}$$

using the identity $2 \sin\theta \cos\theta = \sin 2\theta$

$$\omega_O C_{NET} = \frac{Y_O}{2}\left(\text{COT }\theta_O + \frac{\theta_O}{\text{SIN}^2\,\theta_O}\right) = Y_O \text{ COT }\theta_O\left(\frac{1}{2} + \frac{\theta_O}{\text{SIN}^2\,\theta_O}\right)$$

$$C_T = \frac{Y_O}{\omega_O}\text{ COT }\theta_O$$

It is necessary to manipulate the equations so that the total circuit Q can be expressed in terms of the tuning parameters and the transmission line parameters. The following manipulations provide the relationships between C_T, C_{NET}, and C_{EQ} to obtain the net capacitive Q on an equal slope basis.

Now

$$\frac{C_{NET}}{C_T} = \frac{1}{2} + \frac{\theta_O}{\text{SIN } 2\theta_O}$$

also,

$$C_{NET} = (C_V + C_D)\left(\frac{1}{2} + \frac{\theta_O}{\text{SIN } 2\theta_O}\right)$$

Also at resonance,

$$\frac{1}{\omega_O C_T} = Z_O \text{ TAN }\theta_O$$

and

$$\frac{1}{\omega_O C_{NET}} = X_{L_{EQ}} = \frac{Z_O \text{ TAN }\theta_O}{\left(\frac{1}{2} + \frac{\theta_O}{\text{SIN } 2\theta_O}\right)}$$

With these equations we can obtain $X_{C_{EQ}}$ as:

$$C_{EQ} = C_{NET} - C_T = C_T \left(\frac{1}{2} + \frac{\theta_O}{\mathrm{SIN}\ 2\ \theta_O}\right) - C_T$$

$$C_{EQ} = \left(\frac{\theta_O}{\mathrm{SIN}\ 2\ \theta_O} - \frac{1}{2}\right) C_T$$

$$\frac{1}{\omega_O} = C_T Z_O \ \mathrm{TAN}\ \theta_O = C_{EQ} Z_O \frac{\mathrm{TAN}\ \theta_O}{\left(\frac{\theta_O}{\mathrm{SIN}\ 2\ \theta_O} - \frac{1}{2}\right)}$$

$$X_{C_{EQ}} = \frac{1}{\omega_O C_{EQ}}$$

And we finally have the expressions for the equivalent reactances contributed by the transmission line as:

$$X_{L_{EQ}} = Z_O \frac{\mathrm{TAN}\ \theta_O}{\frac{1}{2} + \frac{\theta_O}{\mathrm{SIN}\ 2\ \theta_O}}$$

$$X_{C_{EQ}} = -Z_O \frac{\mathrm{TAN}\ \theta_O}{\frac{1}{2} - \frac{\theta_O}{\mathrm{SIN}\ 2\ \theta_O}}$$

$$Y_{L_{EQ}} = -Y_O \ \mathrm{COT}\ \theta_O \left(\frac{1}{2} + \frac{\theta_O}{\mathrm{SIN}\ 2\ \theta_O}\right)$$

$$Y_{C_{EQ}} = Y_O \ \mathrm{COT}\ \theta_O \left(\frac{\theta_O}{\mathrm{SIN}\ 2\ \theta_O} - \frac{1}{2}\right)$$

At quarter-wave resonance the values are:

$$Y_{C_{EQ}}\Big|_{\theta_O = \pi/2} = \pi/4 \ Y_O \qquad X_{C_{EQ}}\Big|_{\theta_O = \pi/2} = -\frac{4}{\pi} Z_O$$

$$Y_{L_{EQ}}\Big|_{\theta_O = \frac{\pi}{2}} = -\frac{\pi}{4}\, Y_O \qquad\qquad X_{L_{EQ}}\Big|_{\theta_O = \frac{\pi}{2}} = \frac{4}{\pi}\, Z_O$$

where

$$\lim_{\theta_O \to \frac{\pi}{2}} \frac{\text{TAN } \theta_O}{\frac{1}{2} - \frac{\theta_O}{\text{SIN } 2\, \theta_O}} \cong \lim_{\theta_O \to \frac{\pi}{2}} \frac{2 \text{ TAN } \theta_O \text{ SIN } \theta_O \text{ COS } \theta_O}{-\theta_O} \cong \frac{2 \text{ SIN}^2\, \theta_O}{-\theta_O} \cong -\frac{4}{\pi}$$

Before continuing the derivation it will be necessary to justify the assumption that transmission line losses are primarily due to conductor losses, and also to present the Q-frequency relationship for the transmission line. The October 3 interim report section 3.3.1 shows that the unloaded Q for a transmission line resonator is primarily a function of the conductor losses and is proportional to the square root of frequency. The equations simply stated are:

$$Q_U = \frac{\beta}{2\alpha}$$

where

$$\beta = K_1 F$$

$$\alpha = K_2 \sqrt{F}$$

and finally,

$$\frac{Q_L}{Q_{L\ MAX}} = \left(\frac{F_O}{F_{MAX}}\right)^{1/2}$$

Note that for the lumped inductor resonator it was necessary to include an exponential factor B. For this report B = 1/2 has been used in both cases.

It is possible to normalize X_{LEQ} and R_L to their respective values at quarter-wave frequency

$$\frac{X_{L_{EQ}}}{X_{L_{EQ\,1/4}}} = \overline{X}_{L_{EQ}} = \frac{\pi}{4}\; \frac{\text{TAN } \theta_O}{\frac{1}{2} + \frac{\theta_O}{\text{SIN } 2\, \theta_O}}$$

R_L is normalized to make the transmission line Q obey the $(F_O/F_{1/4})^{1/2}$ law as follows.

$$\frac{Q_R}{Q_{R\ 1/4}} = \left(\frac{X_{L_{EQ}}}{R_L}\right)\Bigg|_{\omega_O} \cdot \left(\frac{R_L}{X_{L_{EQ}}}\right)\Bigg|_{\omega_{1/4}} = \left(\frac{F_O}{F_{1/4}}\right)^{1/2}$$

$$\frac{R_L}{R_{L\,1/4}} = \bar{R}_L = \left(\frac{F_{1/4}}{F_O}\right)^{1/2} \frac{\pi}{4} \quad \frac{\text{TAN } \theta_O}{1/2 + \theta_O/\text{SIN } 2\theta_O}$$

The equations have now been developed for the final derivation to obtain total circuit Q.

The basic equivalent circuit has the following form (figure 3-7).

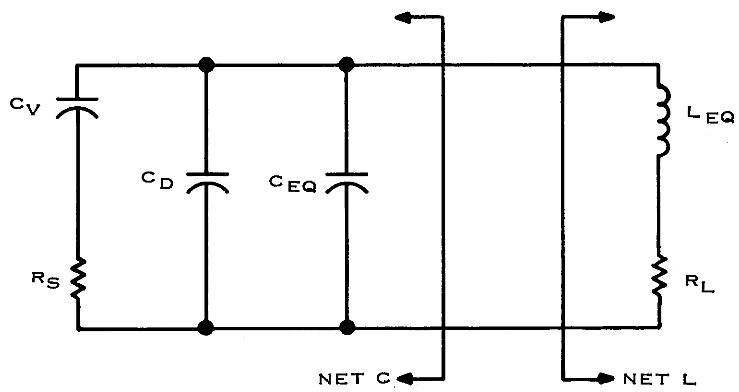

$$Q_L = \frac{X_{LEQ}}{R_L} \qquad Q_L = Q_{LMAX}\,(F_O/F_{MAX})^{1/2} \qquad B = 1/2 \text{ FOR CONDUCTOR LOSS ONLY}$$

$$Q_C = \frac{Q_V^2 R_S}{X_{CNET}} \qquad Q_T = \frac{1}{1/Q_C + 1/Q_L}$$

Figure 3-7. Reactance separation circuit for transmission line.

Q_C must now be derived in terms of $Q_{V\,MAX}$ to obtain the desirable form for the net capacitor Q. The derivation must keep in mind that R_S, Q_V and $X_{C\,NET}$ are all functions of frequency hence:

$$Q_C = \frac{\left(\frac{X_{CV}}{RS}\right)^2 RS}{X_{C_{NET}}} = \left(\frac{1}{\omega C_V R_S}\right)^2 S \left(\omega C_{NET}\right)$$

$$Q_V = \left(\frac{1}{\omega C_V R_S}\right)\Bigg|_{\omega_O} \qquad Q_{V\,MAX} = \left(\frac{1}{\omega C_V R_S}\right)_{\omega\,MAX}$$

$$Q_C = Q_V^2 \cdot \left(R_S\right)\Big|_{\omega_O} \left(\omega C_{NET}\right)\Big|_{\omega_O}$$

From section 6 we can repeat the expression for variable capacitor Q for the transmission line resonator as:

$$Q_V = Q_{V_{MAX}} \left(\frac{X_{C_V}}{X_{C_{V\ MIN}}} \right)^A = Q_{V\ MAX} \left(\frac{\mathrm{TAN}\ \theta_O}{\mathrm{TAN}\ \theta_{MAX}} \right)^A$$

Substituting

$$Q_C = Q_{V\ MAX} \left(\frac{\mathrm{TAN}\ \theta_O}{\mathrm{TAN}\ \theta_{MAX}} \right)^A \cdot \left(\frac{1}{\omega C_V R_S} \right) \Bigg|_{\omega_O} \cdot \left(R_S \right) \Bigg|_{\omega_O} \cdot \left(\omega C_{NET} \right) \Bigg|_{\omega_O}$$

$$\frac{Q_C}{Q_{V\ MAX}} = \left(\frac{\mathrm{TAN}\ \theta_O}{\mathrm{TAN}\ \theta_{MAX}} \right)^A \left(\frac{C_{NET}}{C_V} \right) \Bigg|_{\omega_O} = \left(\frac{\mathrm{TAN}\ \theta_O}{\mathrm{TAN}\ \theta_{MAX}} \right)^A \left(\frac{(C_V + C_D)(1/2 + \frac{\theta_O}{\mathrm{SIN}\ 2\ \theta_O})}{C_V} \right) \Bigg|_{\omega_O}$$

$$\frac{Q_C}{Q_{V\ MAX}} = \left(\frac{\mathrm{TAN}\ \theta_O}{\mathrm{TAN}\ \theta_{MAX}} \right)^A \left(\frac{1}{2} + \frac{\theta_O}{\mathrm{SIN}\ 2\ \theta_O} \right) \left(\frac{C_V + C_D}{C_V} \right) \Bigg|_{\omega_O}$$

which can be simplified by applying the resonance equation

$$\omega_O C_V + \omega_O C_D = Y_O \mathrm{COT}\ \theta_O$$

$$C_V + C_D = \frac{Y_O}{\omega_O}\ \mathrm{COT}\ \theta_O$$

$$C_V = \frac{Y_O}{\omega_O}\ \mathrm{COT}\ \theta_O - C_D$$

Then,

$$\left(\frac{C_V + C_D}{C_V} \right) \Bigg|_{\omega_O} = \frac{\frac{Y_O}{\omega_O}\ \mathrm{COT}\ \theta_O}{\frac{Y_O}{\omega_O}\ \mathrm{COT}\ \theta_O - C_D} = \frac{1}{1 - \omega_O C_D Z_O \mathrm{TAN}\ \theta_O}$$

where

$\omega_O C_D Z_O \mathrm{TAN}\ \theta_O \leq 1$, finally

where

$$\frac{Q_C}{Q_{V\ MAX}} = \left(\frac{\text{TAN}\ \theta_O}{\text{TAN}\ \theta_{MAX}}\right)^A \left(\frac{1}{2} + \frac{\theta_O}{\text{SIN}\ 2\ \theta_O}\right)\left(\frac{1}{1 - \omega_O\ C_D\ Z_O\ \text{TAN}\ \theta_O}\right)$$

when $C_D \equiv 0$ we get the expression

$$\frac{Q_C}{Q_{V\ MAX}} = \left(\frac{\text{TAN}\ \theta_O}{\text{TAN}\ \theta_{MAX}}\right)^A \left(\frac{1}{2} + \frac{\theta_O}{\text{SIN}\ 2\ \theta_O}\right)$$

For the uhf band it is possible to simplify the equation as follows:

$$\omega_O\ C_d\ Z_O\ \text{TAN}\ \theta_O = \left({}^{F_O}/_{F_{MAX}}\right)\ \omega\,\text{MAX}\ C_d\ Z_O\ \text{TAN}\ \theta_O$$

$$= \left(\frac{F_O}{F_{MAX}}\right) 8\,\pi\ \text{X}\ 10^{-4}\ C_D\ Z_O\ \text{TAN}\ \theta_O$$

C_D in picofarads

Z_O in ohms

$F_{MAX} = 400$ MHZ

The $Q_C/Q_{V\ MAX}$ ratio is expressed in terms of the tuning parameters by expressing θ_O in the same terms.

$$\theta_O = \frac{\pi}{2}\frac{F_O}{F_{1/4}} = \frac{\pi}{2}\frac{F_O}{F_{MAX}}\cdot\frac{F_{MAX}}{F_{1/4}} = \frac{\pi}{2}\frac{F_O}{F_{MAX}}\ \frac{1}{\overline{F}}$$

The total nodal Q is now obtained by combining the net Q's of capacitor and inductor.

$$\frac{1}{Q_T} = \frac{1}{Q_L} + \frac{1}{Q_C} \qquad Q_T = \frac{1}{\frac{1}{Q_L} + \frac{1}{Q_C}}$$

$$Q_T = \frac{1}{\dfrac{1}{Q_{L\ MAX}\left(\dfrac{F_O}{F_{MAX}}\right)^{1/2}} + \dfrac{1}{Q_{V\ MAX}\left(\dfrac{\text{TAN}\ \theta_{MAX}}{\text{TAN}\ \theta_O}\right)^A \left(\dfrac{1}{2} + \dfrac{\theta_O}{\text{SIN}\ 2\ \theta_O}\right)\left(\dfrac{1}{1 - \omega_O C_D Z_O \text{TAN}\,\theta_O}\right)}}$$

$$Q_T = Q_{V\,MAX} \frac{1}{\left(\frac{F_{MAX}}{F_O}\right)^{1/2} \frac{Q_{V\,MAX}}{Q_{L\,MAX}} + \left(\frac{\tan\theta_{MAX}}{\tan\theta_O}\right)^{A} \frac{1 - \omega_O C_D Z_O \tan\theta_O}{\left(\frac{1}{2} + \frac{\theta_O}{\sin 2\theta_O}\right)}}$$

The variation of total Q as the resonator is tuned across a band of frequencies is

$$\frac{Q_T}{Q_{T\,MAX}} = \frac{\frac{Q_{V\,MAX}}{Q_{L\,MAX}} + \frac{1 - \omega_{MAX} C_D Z_O \tan\theta_{MAX}}{\frac{1}{2} + \frac{\theta_{MAX}}{\sin 2\theta_{MAX}}}}{\left(\frac{F_{MAX}}{F_O}\right)^{1/2} \frac{Q_{V\,MAX}}{Q_{L\,MAX}} + \left(\frac{\tan\theta_{MAX}}{\tan\theta_O}\right)^{A} \frac{1 - \omega_O C_D Z_O \tan\theta_O}{\left(\frac{1}{2} + \frac{\theta_O}{\sin 2\theta_O}\right)}}$$

$$\theta_O = \frac{\pi}{2} \frac{F_O}{F_{1/4}}$$

$$\theta_{MAX} = \frac{\pi}{2} \frac{F_{MAX}}{F_{1/4}}$$

When $C_D \equiv 0$

$$\frac{Q_T}{Q_{T\,MAX}} = \frac{\frac{Q_{V\,MAX}}{Q_{L\,MAX}} + \left(\frac{1}{2} + \frac{\theta_{MAX}}{\sin 2\theta_{MAX}}\right)^{-1}}{\left(\frac{F_{MAX}}{F_O}\right)^{1/2} \frac{Q_{V\,MAX}}{Q_{L\,MAX}} + \left(\frac{\tan\theta_{MAX}}{\tan\theta_O}\right)^{A} \left(\frac{1}{2} + \frac{\theta_O}{\sin 2\theta_O}\right)^{-1}}$$

8. DERIVATION OF VARACTOR CROSS MODULATION FORMULA

Consider a parallel RLC circuit in which the capacitance has two parallel components, C_B due to the varactor at bias V_B and a fixed capacitance. The total capacitance is C. The Q of the circuit is R/X. The expression for the frequency response is

$$A = \left|\frac{E}{E_O}\right| = \frac{1}{\sqrt{1 + V^2}}$$

where E is the nodal voltage, E_O is the nodal voltage at $\omega_O{}^2 = 1/LC$ and V is the normalized frequency, Q BW/F_O. Taking two derivatives yields

$$\frac{dA}{dV} = -V(1 + V^2)^{-3/2}$$

and

$$\frac{d^2A}{dV^2} = -(1 + V^2)^{-5/2}\,(1 - 2V^2)$$

Setting the second derivative equal to zero and solving for V gives the bandwidth having maximum slope:

$$0 = 1-2V^2$$

$$V = \frac{1}{\sqrt{2}}$$

Substituting this in the original expression gives

$$A = \sqrt{2/3}$$

at the maximum slope bandwidth. Noting that

$$Q = \frac{F_O}{BW_3}$$

where BW_3 is the half-power (3 db) bandwidth gives

$$V = \frac{1}{\sqrt{2}} = Q\,\frac{BW}{F_O}$$

$$= \frac{F_O}{BW_3} \cdot \frac{BW}{F_O}$$

$$BW = \frac{BW_3}{\sqrt{2}}$$

where BW is the bandwidth of maximum dA/dV.

Now,

$$\frac{dV}{dBW} = \frac{Q}{F_O}$$

and

$$\frac{dA}{dV} = -V(1 + V^2)^{3/2}$$

so that

$$\frac{dA}{dBW} = -\frac{Q}{F_O} V(1 + V^2)^{3/2}$$

which, at the maximum slope point ($V=1/\sqrt{2}$) is

$$\frac{dA}{dBW} = -\frac{Q}{F_O} \cdot \frac{1}{\sqrt{2}} (1 + \frac{1}{2})^{-3/2}$$

$$= -\frac{2}{3\sqrt{3}} \cdot \frac{Q}{F_O}$$

For small changes in A

$$\Delta A \cong -\frac{2}{3\sqrt{3}} \cdot \frac{Q}{F_O} \Delta BW$$

Likewise, for small ΔBW, $\Delta BW \cong 2\Delta F$

$$\Delta A \cong -\frac{4}{3\sqrt{3}} \cdot \frac{Q}{F_O} \Delta F$$

From

$$\omega^2 = \frac{1}{LC}$$

$$2\omega\, d\omega = -\frac{1}{LC^2} dC$$

$$d\omega = -\frac{\omega_O}{2C} dC$$

$$\Delta F \cong -\frac{F_O}{2C} \Delta C$$

Substituting:

$$\Delta A \cong -\frac{2}{3\sqrt{3}} \cdot \frac{Q}{C} \Delta C$$

The ΔC in this expression comes from the change in average varactor capacitance, C_{AVE}, due to modulation of an undesired carrier E_U. Letting

$$\overline{V} = \frac{E_U \text{ (PEAK)}}{V_B + \phi}$$

We have, from Strickholm[26]

$$\frac{C_{AVG}}{C_B} = \frac{1}{2\pi} \int_{-\pi}^{\pi} (1 + \overline{V} \text{ SIN } \theta)^{-N} \, d\theta = F(\overline{V})$$

which function has been plotted in figure 1-10 of the IDR. The ΔC in the above expression for ΔA is about an operating point V_U illustrated in figure 3-8.

Figure 3-8. Average varactor capacitance versus ac voltage.

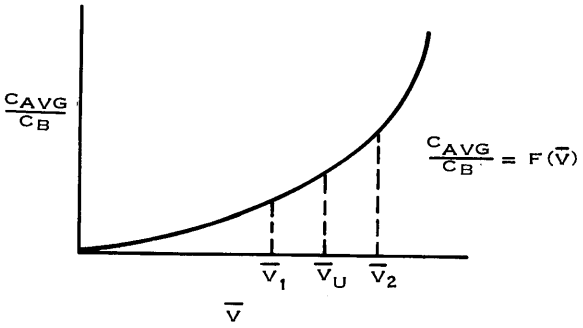

If $\overline{V} << 1$, the decrease in average capacitance to point $\overline{V}_1$ is nearly equal to the increase to point $\overline{V}_2$ so that

$$\Delta C \cong \frac{C_B}{2} \left[F(\overline{V}_2) - F(\overline{V}_1) \right]$$

$$\text{Therefore, } \Delta A \cong -\frac{1}{3\sqrt{3}} \, Q \, \frac{C_b}{C} \left[F(\overline{V}_2) - F(\overline{V}_1) \right]$$

We now need to relate $\overline{V}2$ and $\overline{V}1$ to the carrier amplitude and modulation index of the undesired signal whose envelope is shown in figure 3-9.

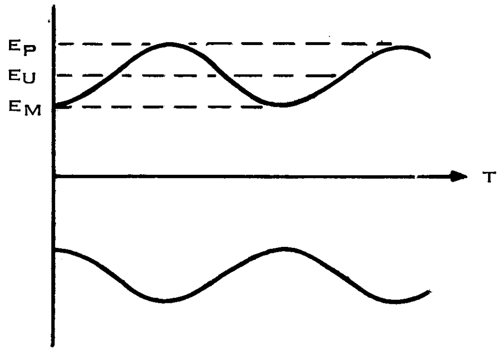

Figure 3-9. Modulated undesired signal envelope.

The modulation index, M_U, is

$$M_U = \frac{E_P - E_M}{2E_U} = \frac{E_P - E_U}{E_U} = \frac{E_P}{E_U} - 1$$

Also,

$$M_U = \frac{E_U - E_M}{E_U} = 1 - \frac{E_M}{E_U}$$

so,

$$E_P = E_U(M_U + 1)$$

and

$$E_M = E_U \, (1 - M_U)$$

Therefore,

$$\overline{V}_2 = \frac{E_P}{V_B + \phi} = \frac{E_U(M_U + 1)}{V_B + \phi}$$

$$\overline{V}_1 = \frac{E_M}{V_B + \phi} = \frac{E_U(1 - M_U)}{V_B + \phi}$$

ΔA can be related to a specified acquired modulation index, M_A, on the small signal by considering the small segment of the selectivity curve in figure 3-10.

Figure 3-10. Worst case operating point.

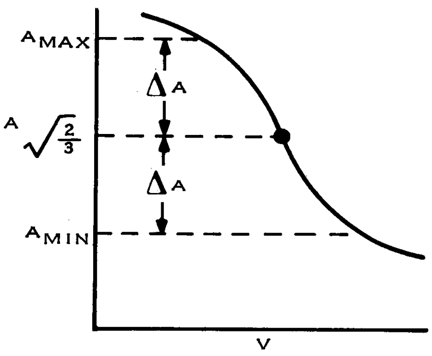

The equation for A was normalized to unity at the response peak so that at the maximum slope point, the amplitude is $\sqrt{2/3}$. For small ΔA the response is symmetrical so that

$$M_A = \frac{A_{MAX}}{\sqrt{\frac{2}{3}}} - 1 = \frac{\sqrt{\frac{2}{3}} + \Delta A}{\sqrt{\frac{2}{3}}} - 1 = \sqrt{\frac{3}{2}}\,\Delta A$$

Since

$$\Delta A = -\frac{}{3\sqrt{3}}\, Q\, \frac{C_B}{C} \left[F(\overline{V}_2) - F(\overline{V}_1)\right]$$

$$M_A = \sqrt{\frac{3}{2}} \cdot \frac{1}{3\sqrt{3}}\, Q\, \frac{C_B}{C} \left[F(\overline{V}_2) - F(\overline{V}_1)\right]$$

$$M_A = \frac{1}{3\sqrt{2}}\, Q\, \frac{C_B}{C} \left[F(\overline{V}_2) - F(\overline{V}_1)\right]$$

where

$$F(\overline{V}) = \frac{1}{2\pi} \int_{-\pi}^{\pi} (1 + \overline{V}\,\mathrm{SIN}\,\phi)^{-N}\, d\theta$$

and

$$\overline{V}_2 = \frac{E_U}{V_B + \phi} (M_U + 1)$$

$$\overline{V}_1 = \frac{E_U}{\overline{V}_B + \phi} (1 - M_U)$$

To obtain a closed form solution, the integrand must be expanded into a binomial series which is then truncated to a quadratic.

$$(1 + \overline{V} \text{ SIN } \theta)^{-N} = 1 - N \overline{V} \text{ SIN } \theta \ - \frac{N(-N-1)}{2!} \overline{V}^2 \text{ SIN}^2 \theta \ + \ . \ . \ .$$

$$2\pi \frac{C_{AVG}}{C} \cong \int_{-\pi}^{\pi} d\theta \ - \int_{-\pi}^{\pi} N \overline{V} \text{ SIN } \theta \ d\theta + \int_{-\pi}^{\pi} \frac{N(N+1)}{2!} \overline{V}^2 \text{ SIN}^2 \theta \ d\theta \ + \ . \ . \ .$$

$$= \theta \Big|_{-\pi}^{\pi} + N \overline{V} \text{ COS}\theta \Big|_{-\pi}^{\pi} + \frac{N(N+1)}{2!} \overline{V}^2 \ \frac{\theta}{2} \Big|_{-\pi}^{\pi} - \frac{N(N+1)}{2!} \overline{V}^2 \ \frac{1}{2} \sin \theta \cos \theta \Big|_{-\pi}^{\pi} + \ . \ . \ .$$

$$= \pi + \pi + \quad N\overline{V} \ (-1+1) + \frac{N(N+1)}{2!} \overline{V}^2 \left(\frac{\pi}{2} + \frac{\pi}{2}\right) - \frac{N(N+1)}{2!} \overline{V}^2 \ \frac{1}{2} \ (0-0) + \ . \ . \ .$$

$$F(\overline{V}) = \frac{C_{AVG}}{C} \cong 1 + \frac{N(N+1)}{4} \overline{V}^2$$

Substituting this in the expression for M_A gives

$$M_A = \frac{1}{3\sqrt{2}} \ Q \frac{C_B}{C} \left[1 + \frac{N(N+1)}{4} \overline{V}_2^2 - 1 - \frac{N(N+1)}{4} \overline{V}_1^2\right]$$

$$= \frac{1}{3\sqrt{2}} \cdot \frac{N(N+1)}{4} Q \ \frac{C_B}{C} \left[\overline{V}_2^2 - \overline{V}_1^2\right]$$

$$= \frac{1}{3\sqrt{2}} \cdot \frac{N(N+1)}{4} Q \ \frac{C_B}{C} \left[\overline{V}^2 (M_U + 1)^2 \ \ - \overline{V}^2 \ (1 - M_U)^2\right]$$

$$= \frac{1}{3\sqrt{2}} \cdot \frac{N(N+1)}{4} Q \ \frac{C_B}{C} \ \overline{V}^2 \ (4 \ M_U)$$

$$\frac{M_A}{M_U} = \frac{1}{3\sqrt{2}} \ N(N+1) \ Q \ \frac{C_B}{C} \ \overline{V}^2$$

Finally, solving for $\overline{V}^2$, gives

$$\overline{V}^2 = 3\sqrt{2} \; \frac{1}{N(N+1)Q} \cdot \frac{C}{C_B} \cdot \frac{M_A}{M_U}$$

Since this derivation depends upon truncation of a series, it is necessary to formulate an estimate of the range of $\overline{V} = E_U \text{ (peak)}/(V_B + \phi)$, which allows engineering accuracy. The neglected fourth and fifth terms of the series are

$$-\frac{N(N+1)(N+2)}{3!}\overline{V}^3 \, \text{SIN}^3\theta + \frac{N(N+1)(N+2)(N+3)}{4!}\overline{V}^4 \, \text{SIN}^4\theta$$

When these are integrated from $-\pi = \theta = \pi$ and added to the previous result, the following is obtained:

$$\frac{C_{AVG}}{C} \cong 1 + \frac{N(N+1)}{4}\overline{V}^2 + \frac{N(N+1)(N+2)(N+3)}{64}\overline{V}^4 + \ldots$$

For a theoretical abrupt junction varactor N = 1/2 and

$$\frac{C_{AVG}}{C} \cong 1 + \frac{3}{16}\overline{V}^2 + \frac{105}{512}\overline{V}^4$$

For a 10-percent error in C_{AVG}/C due to truncation of the third term we set

$$1.1 = \frac{1 + \frac{3}{16}\overline{V}^2 + \frac{105}{512}\overline{V}^4}{1 + \frac{3}{16}\overline{V}^2}$$

and obtain

$$\overline{V} = .83$$

Since experimental and theoretically calculated $\overline{V}$ is usually smaller than 0.83 for -20 and -10 db cross modulation, the quadratic truncation is justified. For N less than 1/2, the error becomes smaller.

9. DERIVATION OF IMAGE BANDWIDTH AS A FUNCTION OF INTERMEDIATE FREQUENCY

9.1 High Side Injection (Local Oscillator Above the Signal Frequency)

Let f_s be the signal frequency and if be the intermediate frequency. The image frequency, f_i, is

$$f_i = f_o + 2if$$

The image bandwidth, BW_i, is

$$BW_i = f_i - f_i'$$

where

$$f_i' = \frac{f_o^2}{f_i}$$

$$BW_i = f_i - \frac{f_o^2}{f_i}$$

$$\frac{BW_i}{f_o} = \frac{f_i}{f_o} - \frac{f_o}{f_i}$$

$$\frac{BW_i}{f_o} = \frac{f_o + 2if}{f_o} - \frac{f_o}{f_o + 2if}$$

$$\frac{BW_i}{f_o} = 1 + 2\frac{if}{f_o} - \frac{1}{1 + 2\frac{if}{f_o}}$$

9.2 Low Side Injection (Local Oscillator Below the Signal Frequency)

$$f_i = f_o - 2if$$

$$BW_i = f_i' - f_i$$

$$f_i' = \frac{f_o^2}{f_i}$$

$$\frac{BW_i}{f_o} = \frac{1}{1 - 2\frac{if}{f_o}} - \left(1 - 2\frac{if}{f_o}\right)$$

10. RELATIVE STOPBAND ATTENUATION OF COHN FILTER

Consider the Cohn filter symbolized in the following block diagram (figure 3-11):

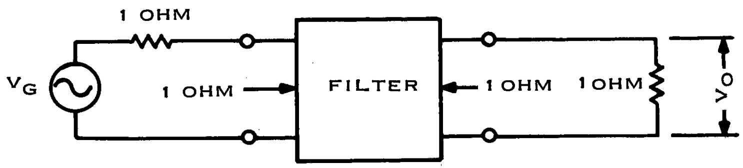

Figure 3-11. Cohn filter defining network.

The passband insertion gain, G_O, is numerically

$$G_O = \frac{P_{OUT}}{P_{IN}} = \frac{V_O^{\,2}}{\left(\frac{V_G}{2}\right)^2} = 4\left(\frac{V_O}{V_G}\right)^2$$

since the input resistance of the filter is assumed to be 1 ohm. Rearranging

$$\frac{V_O}{V_G} = \frac{\sqrt{G_O}}{2}$$

Cohn[19] shows (equation 19) that in the stopband

$$\left|\frac{V_O}{V_G}\right|_S = \frac{R}{\left(\omega_S'\right)^N G_1 G_2 G_3 \cdots G_N}$$

where R is the terminating resistance (equal to 1 ohm) ω_S' is the prototype stopband frequency, N is the number of bandpass filter resonators, and G_i is the prototype element values. Cohn shows that all the G_i are equal so that

$$\left|\frac{V_O}{V_G}\right|_S = \frac{1}{\left(\omega_S' G\right)^N}$$

The attenuation at $\omega_S{}'$ relative to that at zero for the prototype is therefore

$$L_R = \frac{\left|\frac{V_O}{V_G}\right|_S}{\frac{V_O}{V_G}} = \frac{2}{\sqrt{G_O}\left(\omega_S{}' G\right)^N}$$

But from Cohn's equation (1),

$$L_O = 4.343\,\frac{NG}{Q_U}$$

where L_O is the passband insertion loss in decibels for a minimum-loss filter having equal resonator Q_U.

$$G = \frac{L_O\,Q_U}{4.343\,N}$$

Further note that $G_O = \dfrac{1}{10^{\frac{L_O}{10}}}$

Substituting in the L_R expression

$$L_R = \frac{2\sqrt{10^{\frac{L_O}{10}}}}{\left(\omega_S{}'\,\frac{L_O\,Q_U}{4.343\,N}\right)^N}$$

$\omega_S{}'$ of the prototype maps to BW/f_o of the bandpass giving

$$L_R = \frac{2\cdot 10^{\frac{L_O}{20}}}{\left(\frac{L_O}{4.343N}\,Q_U\,\frac{BW}{f_o}\right)^N}$$

for the bandpass filter. Letting

$$\alpha_R = -20\log L_R$$

$$\alpha R = -6 - L_O + 20N\,\mathrm{LOG}\left(\frac{L_O}{4.343N}\,Q_U\,\frac{BW}{f_o}\right),\ \mathrm{DB}$$

in which L_O is now expressed as the center frequency loss in decibels.

11. DERIVATION OF THE LAW OF VARIATION OF A SPIRAL COIL

Consider the spiral coil shown in figure 1-45. The inductance is given as

$$L = \frac{A^2 N^2}{8A + 11C}$$

where

$$A = \frac{D_O + D_I}{4} \quad \text{and} \quad C = \frac{D_O - D_I}{2}$$

Caulton and Poole[27] state that Q is optimized when $D_O/D_I = 5$; consequently,

$$A = \frac{D_O}{4}\left(1 + \frac{D_I}{D_O}\right) = K_1 D_O \quad \text{and} \quad C = \frac{D_O}{2}\left(1 - \frac{D_I}{D_O}\right) = K_2 D_O$$

From Daly et al[15]

$$Q = K_3 \frac{LW}{NA} = \frac{K_3 \cdot K_1 \cdot D_O \cdot N \cdot W}{8K_1 D_O + 11 K_2 D_O} = K_4 N W$$

If parasitic capacitance is neglected,

$$K_5 N W = D_O - D_I = D_O\left(1 - \frac{D_I}{D_O}\right)$$

and

$$Q = K_4 \cdot \frac{D_O}{K_5}\left(1 - \frac{D_I}{D_O}\right) = K_6 D_O$$

The volume of the coil,

$$V = \frac{\pi D_O^2}{4} \cdot H = \frac{\pi}{4} \cdot H \cdot \frac{Q^2}{K_6^2} = C_1 Q^2$$

The law of variation, p, is equal to 2.

12. GLOSSARY

The following is a list of terms and their definitions used in the equations of this report.

A - The constant exponent associated with the frequency dependency of tuning capacitor Q. "A" is empirically obtained and a specific value is applicable only to the specific class of resonators from which it is obtained.

B - The constant exponent associated with the frequency dependency of inductor Q. "B" may be empirically derived, but for inductors where skin loss is the primary loss factor the value $B = 1/2$ is obtained from theoretical considerations.

C_D - A capacitor associated with the nodal resonator circuits, which is used to account for additional capacity due to stray capacity, trimmer capacity, and, in the lumped inductor resonator, it also accounts for the parasitic capacity.

C_I - Minimum tuning capacity factor equal to $(1 + \overline{C}_D)$.

$F_O \rightarrow \omega_O$ - The specific frequency of resonance between F_{MAX} and F_{MIN}.

$F_P \rightarrow \omega_P$ - This is the resonate combination of C_D and L_{EQ} referred to as the pole frequency. F_P was defined to provide a method of compensating for parasitic capacity in an actual resonator circuit where C_D may not be known but F_P can be measured.

$F_{1/4} \rightarrow \omega_{1/4}$ - Quarter-wave frequency of the transmission line.

Q_C - The quality factor of the capacitive part of a resonant circuit.

$C_{T\ MAX}$ - The maximum value of total tuning capacity required to tune the resonator to minimum frequency. The value is the sum of C_D and $C_{V\ MAX}$.

$C_{T\ MIN}$ - The minimum value of total tuning capacity required to tune the resonator to maximum frequency. The value is the sum of C_D and $C_{V\ MIN}$.

C_{NET} - Total nodal capacity for a transmission line resonator. Includes C_V, C_D, and C_{EQ}.

C_V - The capacity of the voltage variable capacitor required to tune the resonator to F_O. C_V contains only the capacity actually being controlled with voltage.

$C_{V\ MAX}$ - The maximum value of C_V at F_{MIN}.

$C_{V\ MIN}$ - The minimum value of C_V at F_{MAX}.

$F_{MAX} \rightarrow \omega_{MAX}$	-	The maximum operating frequency of the resonator.
$F_{MIN} \rightarrow \omega_{MIN}$	-	The minimum operating frequency of the resonator.
Q_L	-	The quality factor of the inductive part of a resonant circuit.
Q_T	-	The total quality factor of a resonator circuit composed of all the loss elements. Q_T is referred to as nodal Q.
$Q_{T\ MAX}$	-	The maximum value of Q_T within the tuning range. $Q_{T\ MAX}$ usually occurs at F_{MAX}.
Q_V	-	The Q of the voltage controlled capacitor at F_O.
$Q_{V\ MAX}$	-	The maximum value of Q_V.
$Q_{1/4}$	-	The Q of a transmission line at quarter-wave resonance.
$X_{C_{EQ}}$	-	The equivalent capacitive reactance of a transmission line for the equal slope selectivity criteria.
X_{CT}	-	The total tuning capacity reactance composed of C_D and C_V.
$X_{L_{EQ}}$	-	The equivalent inductive reactance of a transmission line for the equal slope selectivity criteria.
Y_R	-	Driving point admittance of a shorted transmission line.
Z_O	-	Characteristic impedance of a transmission line.
Z_R	-	Driving point impedance of a shorted transmission line.
$\overline{C}_D = C_D/C_{V\ MIN}$	-	Stray capacity C_D normalized to the minimum value of voltage-controlled tuning capacity.
$\overline{C}_T$	-	Tuning ratio of total nodal capacity including C_D and C_V.
$\overline{C}_V$	-	Tuning ratio of voltage-controlled tuning capacitor.
$\overline{F}_T = F_{MAX}/F_{MIN}$	-	Frequency ratio of maximum to minimum operating frequencies.
θ_{MAX}	-	Electrical length of the transmission line at F_{MAX}.
θ_O	-	Electrical length of the transmission line at F_O.

UNCLASSIFIED
Security Classification

DOCUMENT CONTROL DATA - R & D

(Security classification of title, body of abstract and indexing annotation must be entered when the overall report is classified)

1. ORIGINATING ACTIVITY *(Corporate author)* COLLINS RADIO COMPANY TUNER FUNCTIONAL GROUP CEDAR RAPIDS, IOWA 52406	2a. REPORT SECURITY CLASSIFICATION UNCLASSIFIED 2b. GROUP NA

3. REPORT TITLE

UHF SOLID-STATE PRESELECTOR
DESIGN STUDY

4. DESCRIPTIVE NOTES *(Type of report and inclusive dates)*
FINAL REPORT, 15 SEPTEMBER 1969 TO 3 JANUARY 1970

5. AUTHOR(S) *(First name, middle initial, last name)*
RUSSELL W. HANSON
STEVE F. RUSSELL
DAVID B. HALLOCK

6. REPORT DATE	7a. TOTAL NO. OF PAGES	7b. NO. OF REFS
3 JANUARY 1969	148	27

8a. CONTRACT OR GRANT NO. N00039-69-C-2602	9a. ORIGINATOR'S REPORT NUMBER(S) 523-0762599-00111M
b. PROJECT NO. 62105N XF 52545 001	
c.	9b. OTHER REPORT NO(S) *(Any other numbers that may be assigned this report)*
d.	

10. DISTRIBUTION STATEMENT

11. SUPPLEMENTARY NOTES	12. SPONSORING MILITARY ACTIVITY DEPARTMENT OF THE NAVY NAVAL ELECTRONIC SYSTEMS COMMAND

13. ABSTRACT

A theoretical analysis is presented relating the best method of resonator distribution when considering image, noise figure, and cross modulation specifications.

Methods of uhf preselection are discussed including capacitance-tuned resonators, switched bandpass filters, and the parametric up-converter.

The relative capabilities of amplifiers and discrete inductors as components for microminiature uhf preselector design are presented.

Block diagram and component trade-offs are presented, which in turn lead to a recommended design. Also specified are component areas where further investigation is deemed necessary.

14. KEY WORDS	LINK A		LINK B		LINK C	
	ROLE	WT	ROLE	WT	ROLE	WT
1. PRESELECTORS 2. RECEIVERS 3. UHF AMPLIFIERS 4. MIXERS 5. NOISE FIGURE 6. IMAGE SUPPRESSION 7. DYNAMIC RANGE 8. VARACTOR TUNING						

INSTRUCTIONS TO FILL OUT DD FORM 1473 - DOCUMENT CONTROL DATA

(See ASPR 4-211)

1. ORIGINATING ACTIVITY: Enter the name and address of the contractor, subcontractor, grantee, Department of Defense activity or other organization *(corporate author)* issuing the report.

2a. REPORT SECURITY CLASSIFICATION: Enter the overall security classification of the report. Indicate whether "Restricted Data" is included. Marking is to be in accordance with appropriate security regulations.

2b. GROUP: Automatic downgrading is specified in DoD directive 5200.10 and Armed Forces Industrial Security Manual. Enter the group number. Also, when applicable, show that optional markings have been used for Group 3 and Group 4 as authorized.

3. REPORT TITLE: Enter the complete report title in all capital letters. Titles in all cases should be unclassified. If a meaningful title cannot be selected without classification, show title classification in all capitals in parenthesis immediately following the title.

4. DESCRIPTIVE NOTES: If appropriate, enter the type of report, e.g., interim, progress, summary, annual, or final. Give the inclusive dates when a specific reporting period is covered.

5. AUTHOR(S): Enter the name(s) of the author(s) in normal order, e.g., full first name, middle initial, last name. If military, show grade and branch of service. The name of the principal author is a minimum requirement.

6. REPORT DATE: Enter the date of the report as day, month, year; or month, year. If more than one date appears on the report, use date of publication.

7a. TOTAL NUMBER OF PAGES: The total page count should follow normal pagination procedures, i.e., enter the number of pages containing information.

7b. NUMBER OF REFERENCES: Enter the total number of references cited in the report.

8a. CONTRACT OR GRANT NUMBER: If appropriate, enter the applicable number of the contract or grant under which the report was written.

8b, 8c, and 8d. PROJECT NUMBER: Enter the appropriate military department identification, such as project number, task area number, systems numbers, work unit number, etc.

9a. ORIGINATOR'S REPORT NUMBER(S): Enter the official report number by which the document will be identified and controlled by the originating activity. This number must be unique to this report.

9b. OTHER REPORT NUMBER(S): If the report has been assigned any other report numbers *(either by the originator or by the sponsor)*, also enter this number(s).

10. DISTRIBUTION STATEMENT: Enter the one distribution statement pertaining to the report.

Contractor-Imposed Distribution Statement

The Armed Services Procurement Regulations *(ASPR), para 9-203* stipulates that each piece of data to which limited rights are to be asserted must be marked with the following legend:

"Furnished under United States Government Contract No.________. Shall not be either released outside the Government, or used, duplicated, or disclosed in whole or in part for manufacture or procurement, without the written permission of __________, except for: (i) emergency repair or overhaul work by or for the Government, where the item or process concerned is not otherwise reasonably available to enable timely performance of the work; or (ii) release to a foreign government, as the interests of the United States may require; provided that in either case the release, use, duplication or disclosure hereof shall be subject to the foregoing limitations. This legend shall be marked on any reproduction hereof in whole or in part."

If the above statement is to be used on this form, enter the following abbreviated statement:

"Furnished under U. S. Government Contract No.______. Shall not be either released outside the Government, or used, duplicated, or disclosed in whole or in part for manufacture or procurement, without the written permission of_________, per ASPR 9-203."

DoD Imposed Distribution Statements *(reference DoD Directive 5200.20)* "Distribution Statements *(Other than Security)* on Technical Documents," March 29, 1965.

STATEMENT NO. 1 - Distribution of this document is unlimited.

STATEMENT NO. 2 (UNCLASSIFIED document) - This document is subject to special export controls and each transmittal to foreign governments or foreign nationals may be made only with prior approval of *(fill in controlling DoD office)*.

(CLASSIFIED document) - In addition to security requirements which must be met, this document is subject to special export controls and each transmittal to foreign governments or foreign nationals may be made only with prior approval *(fill in controlling DoD Office)*.

STATEMENT NO. 3 (UNCLASSIFIED document) - Each transmittal of this document outside the agencies of the U. S. Government must have prior approval of *(fill in controlling DoD Office)*.

(CLASSIFIED document) - In addition to security requirements which apply to this document and must be met, each transmittal outside the agencies of the U. S. Government must have prior approval of *(fill in controlling DoD Office)*.

STATEMENT NO. 4 (UNCLASSIFIED document) - Each transmittal of this document outside the Department of Defense must have prior approval of *(fill in controlling DoD Office)*.

(CLASSIFIED document) - In addition to security requirements which apply to this document and must be met, each transmittal outside the Department of Defense must have prior approval of *(fill in controlling DoD Office)*.

STATEMENT NO. 5 (UNCLASSIFIED document) - This document may be further distributed by any holder only with specific prior approval of *(fill in controlling DoD Office)*.

(CLASSIFIED document) - In addition to security requirements which apply to this document and must be met, it may be further distributed by the holder ONLY with specific prior approval of *(fill in controlling DoD Office)*.

11. SUPPLEMENTARY NOTES: Use for additional explanatory notes.

12. SPONSORING MILITARY ACTIVITY: Enter the name of the departmental project office or laboratory sponsoring *(paying for)* the research and development. Include address.

13. ABSTRACT: Enter an abstract giving a brief and factual summary of the document indicative of the report, even though it may also appear elsewhere in the body of the technical report. If additional space is required, a continuation sheet shall be attached.

It is highly desirable that the abstract of classified reports be unclassified. Each paragraph of the abstract shall end with an indication of the military security classification of the information in the paragraph, represented as *(TS)*, *(S)*, *(C)*, or *(U)*.

There is no limitation on the length of the abstract. However, the suggested length is from 150 to 225 words.

14. KEY WORDS: Key words are technically meaningful terms or short phrases that characterize a report and may be used as index entries for cataloging the report. Key words must be selected so that no security classification is required. Identifiers, such as equipment model designation, trade name, military project code name, geographic location, may be used as key words but will be followed by an indication of technical context. The assignment of links, roles, and weights is optional.

★ U.S. GOVERNMENT PRINTING OFFICE : 1966 O—236-690